Internal Tidal Hydrodynamics and Ambient Characteristics of the Adriatic (ITHACA)

Report on the second year of work

Principal investigator:

Mirko Orlic[1]

Co-principal investigators:

Gordana Beg Paklar[2]

Vlado Dadic[2]

Nenad Leder[3]

Participants:

Zvjezdana Bencetic Klaic[1]

Branka Grbec[2]

Frano Matic[2]

Hrvoje Mihanovic[3]

Mira Morovic[2]

Miroslava Pasaric[1]

Zoran Pasaric[1]

Ivica Vilibic[2]

[1]Andrija Mohorovicic Geophysical Institute, Faculty of Science, University of Zagreb, Croatia

[2]Institute of Oceanography and Fisheries, Split, Croatia

[3]Hydrographic Institute of the Republic of Croatia, Split, Croatia

Zagreb – Split, December 2006

Table of contents

1. Introduction 4

2. Meteorological data 5

2.1. Measuring sites 5

2.2. Air temperature 6

2.3. Air flow 7

2.3.1. Etesians vs. sea-land breeze 8

2.3.2. Bora episode, 5-7 February 2006 10

2.3.3. Sirocco episode, 14-15 September 2006 11

2.3.4. Running spectra 16

2.3.5. Divergence episodes 16

2.4. Air pressure 19

2.4.1. Rossby waves 19

2.4.2. Cyclogenesis 22

2.5. Conclusion 22

3. Optical properties of the Bisevo, Susac and Lastovo area 26

3.1. Introduction 26

3.2. Data and methods 26

3.3. Results and discussion 28

3.4. Concluding remarks 35

4. CTD measurements and thermohaline properties 38

4.1. Data acquisition 38

4.2. Ambient characteristics 39

4.3. Internal waves 47

5. Thermistor time series 52

5.1. Data acquisition 52

5.2. Comparison between TidbiT measurements at Cape Struga and Aanderaa thermistor string measurements off Cape Struga 54

5.3. Stationary spectral analysis of thermistor data collected at Bisevo, Susac and Lastovo 56

5.4. Wavelet analysis of thermistor data collected at Bisevo, Susac and Lastovo 56

6. Results of ADCP measurements 68

6.1. Data acquisition 68

6.2. Main statistical features 69

6.3. Time series analysis 71

6.3.1. Monthly mean currents 71

6.3.2. Daily currents 71

6.3.3. Variability at diurnal and shorter time scales 74

7. Sea-level and bottom-pressure time series 87

7.1. Adriatic sea-level oscillations – short overview 87

7.2. Data acquisition and processing 88

7.3. Results 89

7.3.1. Harmonic analysis 89

7.3.2. Spectral and wavelet analysis 90

8. Summary and conclusion 101

Acknowledgements 102

References 103

1. Introduction

Project "Internal Tidal Hydrodynamics and Ambient Characteristics of the Adriatic (ITHACA)" concentrates on diurnal internal tides – their generation at the Adriatic shelf break, propagation across the Palagruza Sill and dependence on stratification and currents in the area. Systematic oceanographic measurements started in 1950s at the Split-Gargano transect by the Institute of Oceanography and Fisheries (Split) and in 1960s in a wider area by the Hydrographic Institute (Split). It was found that the area is under the strong influence of seasonal and interannual variability. Early short-term current measurements revealed a pronounced seasonal signal, with oppositely directed alongshore flow in the winter and summer seasons. Seasonally dependent circulation contributes to a strong temporal variability of thermohaline properties. Since the beginning of 1980s long-term current measurements were occasionally performed, showing barotropic-like current reversals on scales of a few days. More recently, higher-frequency phenomena attracted some interest. In particular, it has been found that during the stratified season, diurnal internal tides are generated by the interaction of diurnal barotropic tides with topography and that they result in thermocline variability with amplitudes reaching 3 m. No indications were found of semidiurnal internal tides, probably because the semidiurnal tidal currents have a minimum at the shelf break. As the detection of internal tides was based solely on data collected by three thermistors on the island of Lastovo, and there were no current measurements to support the finding, an intention of the present project is to provide a more complete data set, which would enable propagation characteristics of internal waves to be determined, not just their amplitudes. Attention is also paid to the way changes of background stratification and currents modify internal waves, and vice versa – to a possible influence of internal waves on deductions based on measurements that are scattered in space and time. Thus, observations and modeling are planned so as to enable the following hypotheses to be tested:

- Diurnal surface tides generate internal tidal waves at the Adriatic shelf break.
- Internal tidal energy radiates away from the shelf break. Some waves travel towards the northwest, thus crossing the Palagruza Sill.
- Generation and propagation of baroclinic waves is influenced by stratification and currents prevailing in the area.

The project started on 12 April 2005 with the financial support of the USA Office of Naval Research (award No. N00014-05-1-0698) and the Croatian Ministry of Science, Education and Sports (contract No. 3/2005) and is expected to last until 30 September 2007. Field work was prepared during the first year, experiment was executed during the second year, whereas a thorough analysis of the data and model results is planned for the third year.

This is report on the second year of work on the project, which – following the project proposal – concentrated on the collection of data. These comprised meteorological time series as well as optical and CTD measurements and time series of temperature, currents, sea level and bottom pressure collected at a number of locations. The report is structured accordingly.

2. Meteorological data

During the ITHACA field work meteorological data were routinely collected at five stations in the area: Split-Marjan, Dubrovnik, Komiza, Hvar and Palagruza. These were used to document atmospheric conditions along the line extending from the coast to the open sea.

2.1. Measuring sites

Position of meteorological measuring sites is illustrated in Figure 2.1. Hourly means of air temperature, pressure and wind speed and direction were available for the period 1 February – 30 September 2006, i.e. for the whole warm part of the year and some months of transition seasons. Measurements were performed by the Meteorological and Hydrological Service of the Republic of Croatia (hereafter MHS), and they are related to the local standard time (LST). Occasionally, some wind data for Split-Marjan and Komiza were missing. These were linearly interpolated from winds recorded in Dubrovnik and Hvar, respectively.

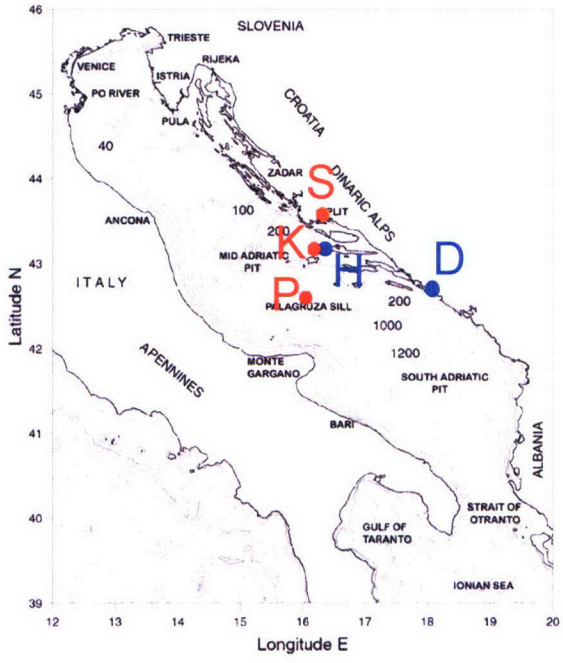

Figure 2.1 Position of the meteorological measuring sites: Split-Marjan (S, coastal station), Komiza (K, offshore station) and Palagruza (P, open-sea station). Some wind data for Split-Marjan and Komiza were missing. Therefore, they were interpolated from Dubrovnik (D, coastal station) and Hvar (H, offshore station) data, respectively. The bathymetry of the Adriatic Sea is also shown.

The measuring sites were selected so as to capture gradual changes from coastal to open-sea conditions, where Split-Marjan (S), Komiza (K) and Palagruza (P) are taken as representative for coastal, offshore and open-sea locations. The influence of coastal and/or mainland environment can be seen in annual variations of some of the meteorological elements, among which are the air temperature and wind.

2.2. Air temperature

Due to different thermal properties, the land, which has a low specific heat, heats and cools more quickly than the sea. Consequently, during the warm part of the year, the air close to the land heats more quickly compared to the air above the sea. On the contrary, during the winter, the air above the land cools quicker than the air over the sea. Therefore, for the midsummer we expect the highest and the lowest temperatures at the sites S and P, respectively. During the midwinter, temperatures should exhibit opposite behavior (highest values for P and lowest for S). Further, temperatures at K should generally have values between those recorded at S and P during both seasons. On the other hand, for the transition seasons (spring and fall) we expect similar temperatures at all three measuring sites.

The above is confirmed by results shown in Figure 2.2 and Figure 2.3, where Figure 2.3 is given in order to illustrate the temperature differences at three sites more clearly. During the period from mid-June to mid-August sites S and P generally have the highest and the lowest temperatures respectively, while temperatures at K lie between the above values. On the other hand, during transition months (February, March and September) daily mean temperatures at all three sites are similar.

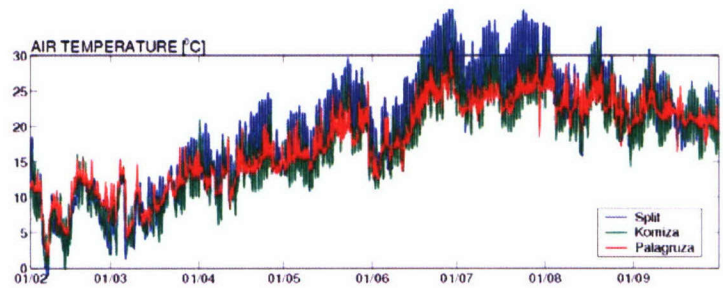

Figure 2.2 Temporal variations of the hourly mean air temperature at the coastal (Split-Marjan, S), offshore (Komiza, K) and open-sea (Palagruza, P) measuring sites in the year 2006.

Additionally, maritime and continental influences are also visible in daily amplitudes. Thus, under synoptically undisturbed summertime conditions (without frontal passages), the coastal site (S) has larger daily temperature amplitude compared to the open-sea (P) site (Figure 2.3, center).

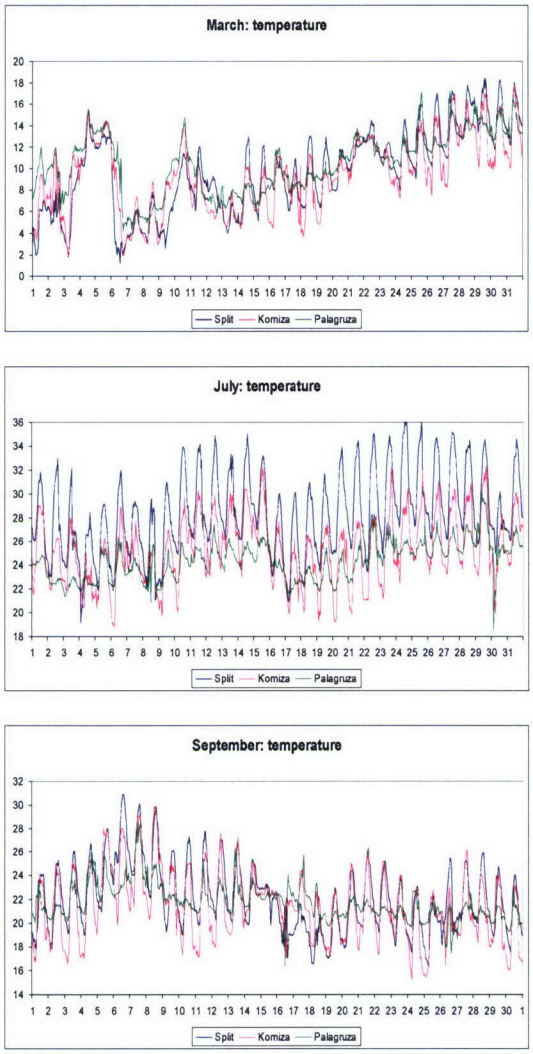

Figure 2.3 Hourly mean air temperatures at the coastal (Split-Marjan, S), offshore (Komiza, K) and open-sea (Palagruza, P) measuring sites for March (top), July (center) and September 2006 (bottom).

2.3. Air flow

In this section persistent summertime (etesians and sea-land breezes) as well as transient (bora and sirocco) winds over the Adriatic are discussed. The latter are well known as being important for the mechanical forcing of the sea (e.g. Pasaric and Orlic, 2004). Additionally, two cases of the low-level airflow divergence are also described. In the representation of the wind directions the oceanographic convention, indicating where the wind blows to, is used.

2.3.1. Etesians vs. sea-land breeze

During the warm part of the year, the etesian winds blow over the Mediterranean. They are more pronounced over its eastern parts. Etesians are dynamically generated by both deep Asiatic low (known as the Karachi depression), which extends far west, sometimes even reaching the Cyprus (e.g. Poulos et al., 1997), and the high pressure system of the Azores, which in summer moves northward and extends to the southeastern Europe. Over the Adriatic the etesians start to develop in the second part of June and they last until September. Since they are rather weak, the corresponding southeastward air flow is clearly seen only at distant islands, while along the coast it is dominated by the local, thermally induced sea-land breezes (SLB) (Makjanic, 1978).

Local SLB are caused by the different thermal properties of the land and the sea. In idealized case, they are perpendicular to the straight shoreline. However, along the eastern Adriatic irregularly shaped coast there is a number of islands, islets and cliffs. In addition, close to the sea a long mountain range (the edge of Dinaric Alps) stretches in NW-SE direction, with some of the tips almost 2 km high. Thus, a complex wind regime resulting from interaction of SLB induced by both mainland and islands, and slope winds, establishes during the synoptically undisturbed, summertime anticyclonic conditions (Orlic et al., 1988; Prtenjak, 2003; Nitis et al., 2005: Prtenjak et al., 2006). Certainly, the level of the SLB regime complexity differs from one locality to another, depending on the complexity of the local topographical and surface conditions.

Based on the above considerations we expect different summertime airflow patterns at three measuring sites. Namely, at the open-sea (P) and the coastal site (S) we expect the domination of etesians and SLB, respectively, where the latter is additionally modified by up- and down-slope winds. In order to confirm the above hypothesis, we inspected periods favorable for the well developed etesian air flow and SLB (Makjanic, 1978). Based on the synoptic conditions (MHS, 2006), these were 9 – 15 and 21 – 27 July 2006 (Figure 2.4 and Figure 2.5). During the first period the atmospheric conditions over the greater Adriatic area were driven by anticyclone extending over the major part of Europe. On the other hand, during the second period the area of interest was influenced by a weak high pressure field accompanied by the weak winds aloft.

Here we focus on the wind directions shown in Figure 2.4, while Figure 2.5 is given in order to further illustrate atmospheric conditions at selected measuring sites. The establishment of the daytime sea-breeze may be clearly seen at Split-Marjan from 9 to 14 and from 21 to 27 July (wind directions of about 45°). On the other hand, the nighttime land-breezes, which are generally weaker than their daytime counterpart (Orlic et al., 1988), are in Split-Marjan present during the nights from 10/11 to 15/16, from 22/23 to 23/24, and from 25/26 to 28/29 July, and during the early morning hours of 25 July (wind directions of about 225°). At the other two sites, the effects of SLB are found only in Komiza for the nights of 13/14 and 14/15 July.

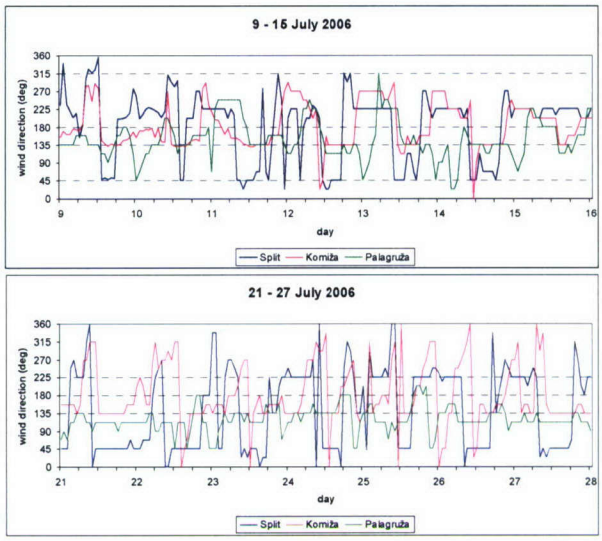

Figure 2.4 Hourly mean wind directions for periods favorable for establishment of the etesian and SLB air flow. Upper and lower panels correspond to 9-15 and 21-27 July 2006, respectively.

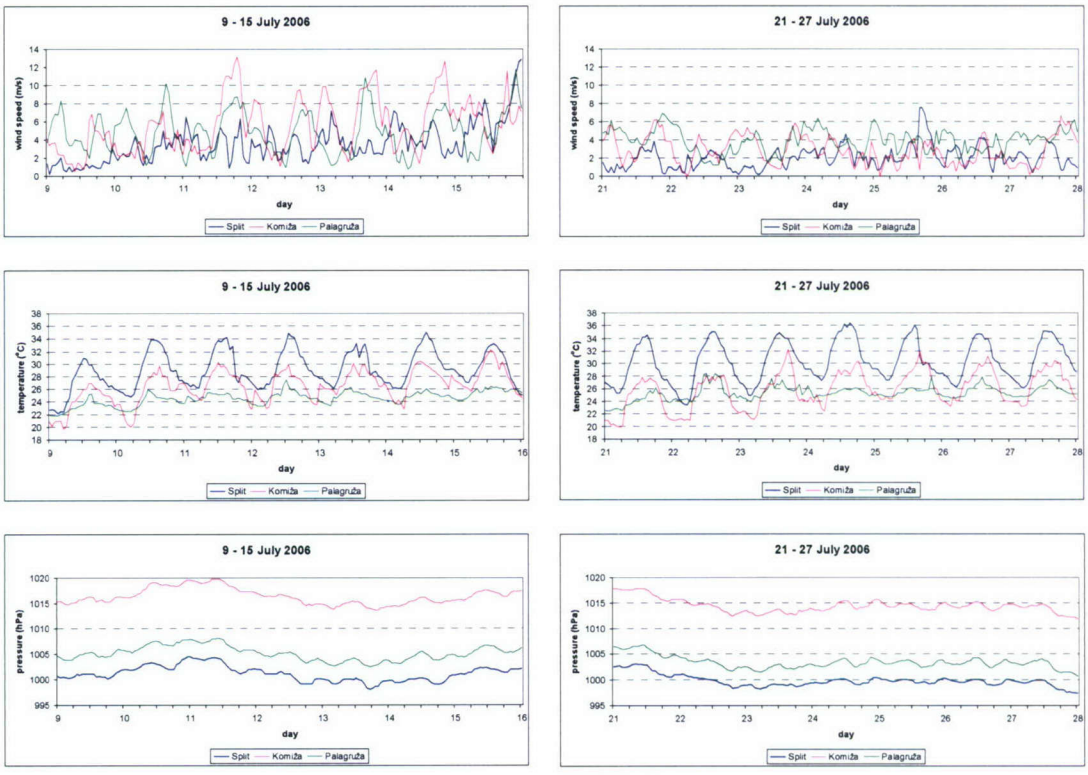

Figure 2.5 Hourly mean wind speed, air temperature and pressure data for periods favorable for establishment of the etesian and SLB air flow. Left and right panels correspond to 9-15 and 21-27 July 2006, respectively. High-pressure synoptic conditions are confirmed by the regular, bell-shaped diurnal variations of temperature at Split. Small temperature disturbances during the afternoon hours (e.g. Komiza and Split on 11 and 13 July) can be attributed to the development of the local convective cloudiness.

At Komiza and Palagruza (Figure 2.6) air flow was substantially affected by etesians, with departures from wind directions of about 135° being larger at Komiza. At the same time, the Split-Marjan data did not exhibit any influence of the southeastward, etesian flow, which is in accordance with previous findings (Makjanic, 1978).

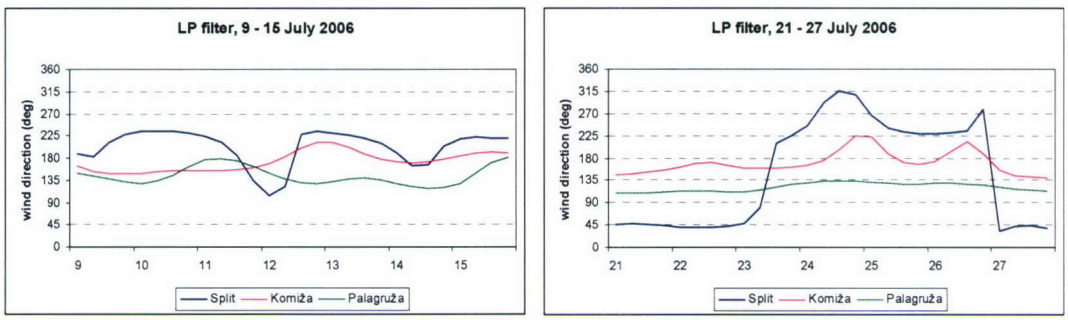

Figure 2.6 Low-pass filtered wind direction data for two periods favorable for the establishment of both the etesians and the SLB.

2.3.2. Bora episode, 5-7 February 2006

Bora (*bura* locally) is a cold, gusty (e.g Petkovsek, 1987; Cvitan, 2003; Belusic et al., 2004; Belusic and Klaic, 2004, 2006), southwestward, downslope windstorm, which frequently blows over the Adriatic during the cold part of the year. It exerts a strong mechanical forcing on the Adriatic thus inducing a rather complex response of the sea (e.g. Beg Paklar et al., 2001a; Pasaric and Orlic , 2004). Due to its violent gusts, it may also be hazardous to traffic and may cause damage to economy and infrastructure (Figure 2.7).

Among several bora episodes that occurred during the period of study, and that were recorded at all three sites, the episode from 5-7 February (Figure 2.8) was characterized by rather high wind speeds, where averages over the entire episode for Split-Marjan, Komiza and Palagruza were 9.1, 8.7 and 9.1 m/s, respectively. Corresponding figures for the maximum hourly means were 15.3, 19.4 and 16.2 m/s. (Note that the episode from 11-15 February was accompanied by substantially weaker wind speeds.) The event was caused by a cyclone which, according to diagnostic charts of Deutscher Wetterdienst (hereafter DWD), started to develop in Genoa Bay on 3 February. In time, the Genoa cyclone shifted southeastward. Thus, on 5 February it was centered above the southeastern Italy at the sea surface (Figure 2.9). Southwestward airflow was additionally intensified due to a high-pressure field found at the surface over the northern and northwestern Europe. Intrusion of the cold air from the northeastern Europe resulted in a noticeable temperature drop (Figure 2.8 top). At Split-Marjan, for example, the temperature decreased by about 10°C during the 48 hour period starting at midnight of 5 February.

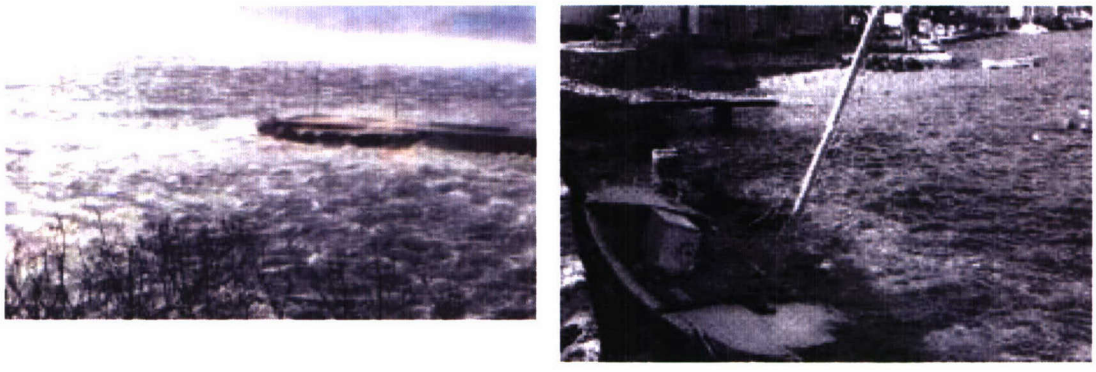

Figure 2.7 Bora over the Adriatic on 5 February 2006. Typical appearance of the sea surface (left). As seen from the picture taken in Velebit Channel, bora tears up the wave crests which bubble up like a boiling water, spraying small particles of foam and water into air. Thus, visibility above the sea is reduced. On the island of Vis (right) a boat (*gajeta* locally) was sank in the Vis harbor (source: MHS, 2006).

2.3.3. Sirocco episode, 14-15 September 2006

Sirocco (*jugo* locally) may also play an important role in the forcing of the Adriatic Sea (e.g. Pasaric and Orlic, 2004). It often produces high waves and consequently causes problems in the sea traffic. Most frequently sirocco is related to a deep cyclone or trough over the Europe approaching from the west, or smaller-scale low pressure vortex over the Adriatic Sea (rainy sirocco), while anticyclonic (dry) sirocco is rather infrequent (Penzar et al., 2001). The above is further confirmed by a recent analysis of the severe sirocco at Split-Marjan (Vecenaj, 2005) (Figure 2.10). The above analysis also suggests that a cyclogenesis in Genoa Bay plays the mayor role in the establishment of the strongest sirocco conditions over the Adriatic.

One among the sirocco episodes that were apparent at all three measuring sites is illustrated in Figure 2.11. The establishment of northwestward airflow at all three measuring sites (directions of about 315° on 14 September) was accompanied by the pressure decrease and simultaneous increase of the wind speed. Thus, the mean speeds for Split-Marjan, Komiza and Palagruza averaged over the entire sirocco period where 7.0, 8.6 and 10.4 m/s, while maximum hourly speeds were 12.3, 11.6 and 16.0 m/s, respectively.

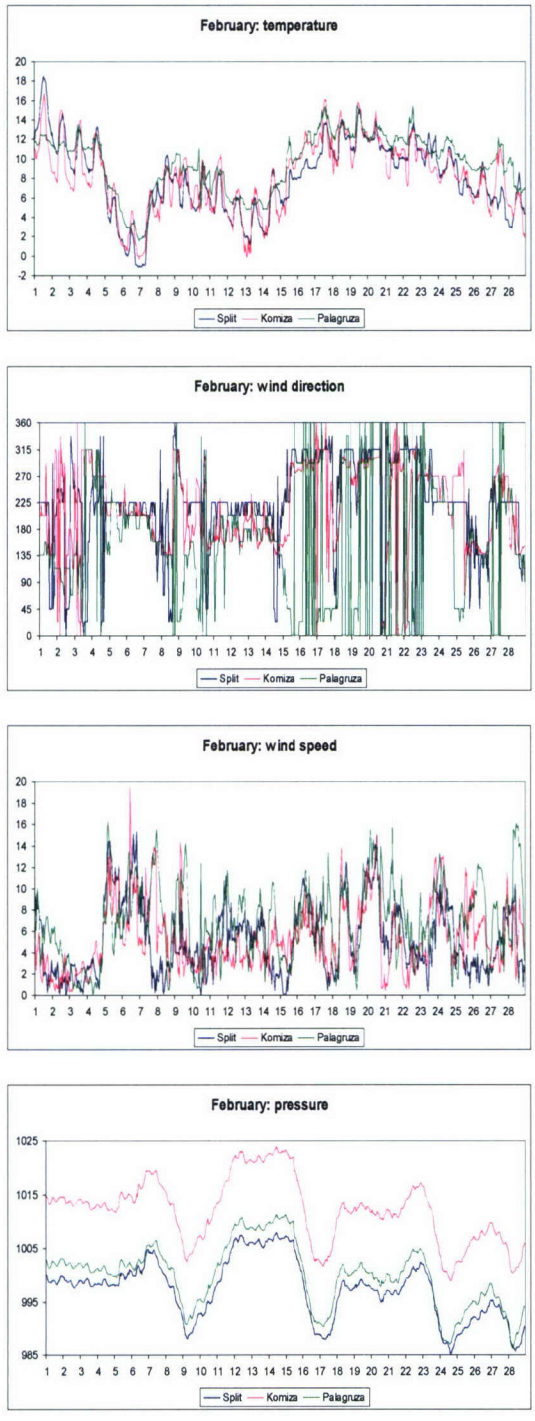

Figure 2.8 Hourly mean air temperature, wind and pressure data for February 2006.

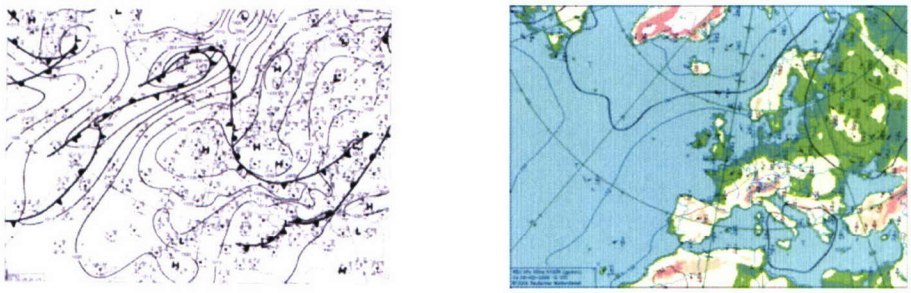

Figure 2.9 Surface (left, 00 UTC) and 850 hPa (right, 12 UTC) diagnostic charts for Europe and for 5 February 2006, where former roughly corresponds to bora onset recorded at three measuring sites (source: DWD).

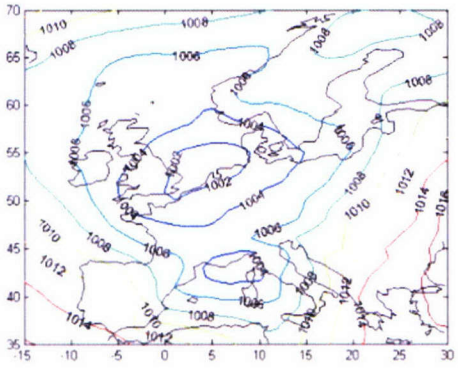

Figure 2.10 Mean sea level air pressure field (hPa) averaged over the severe sirocco episodes recorded at Split-Marjan during the 1991-2000 period (source: Vecenaj, 2005).

Compared to the previous days, when the regular, bell-shaped diurnal variation of the temperature with the lowest values around the sunrise was found at Split-Marjan, on 14 September the temperature pattern reflecting the effects of the mainland started to distort. The departure from bell-shaped variation is particularly noticeable for the almost isothermal period between the evening hours of 14 September and the noon of 15 September. It reveals the effects of cloud cover, which then affected the energy budget. Thus, the net nighttime radiative cooling (and consequent air temperature decrease) was reduced due to both reflection and re-emission of infrared radiation by the clouds.

Synoptic conditions responsible for the sirocco occurrence are documented in Figure 2.12. One may see that the onset of northwestward flow (14 September at 00 UTC) was supported by both a cyclone over the Atlantic centered aloft between the Greenland and the British Isles and a high pressure field stretching from eastern Europe to north Africa. In time, the low pressure trough of the Atlantic cyclone elongated in southeastward direction and eventually a new cyclone was formed over western Europe. On 15 September at 12 UTC it was centered above France at 850 hPa and it extended over the big portion of Europe, including the Adriatic. Simultaneously, the high pressure field

was pushed northeastward and finally, on 15 September, it resulted in an anticyclone centered aloft above the Scandinavia. The above dipole structure with the anticyclone over Scandinavia and the cyclone over the major part of Europe, which further supported sirocco flow at Split and Komiza, was also found on some latter occasions (not shown).

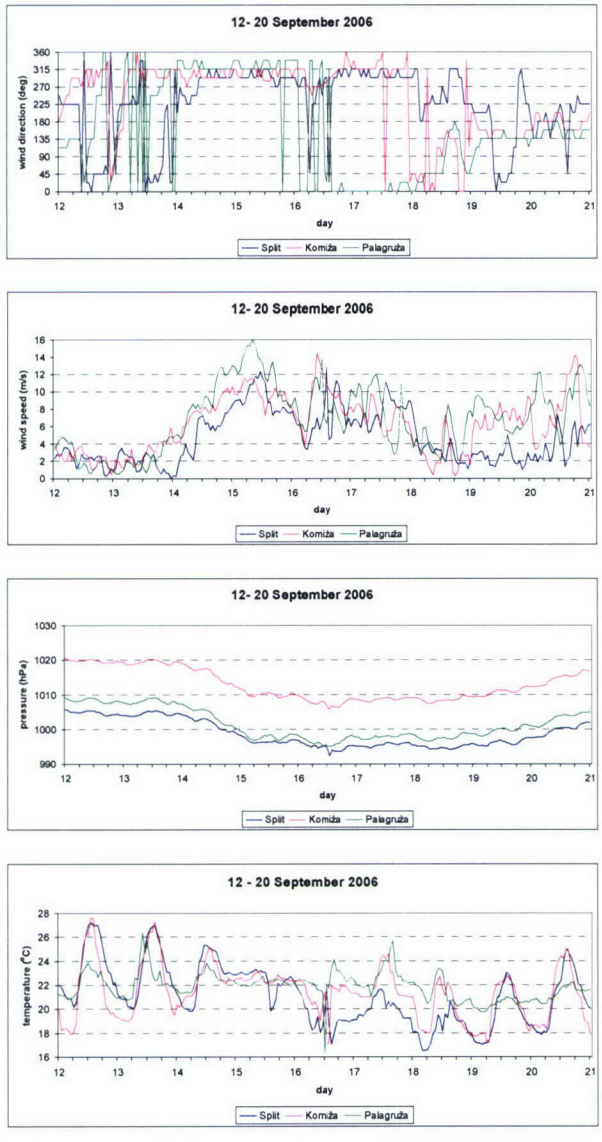

Figure 2.11 Hourly mean wind, air pressure and temperature data for 12-20 September 2006.

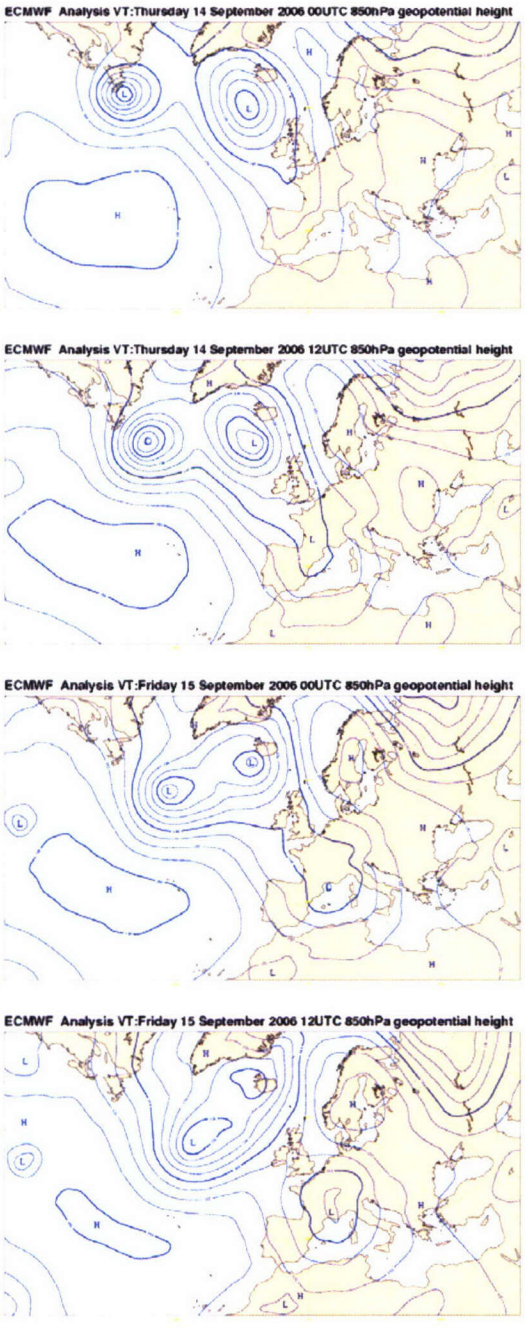

Figure 2.12 850 hPa charts for Europe and for 14 and 15 September 2006 according to ECMWF analysis.

2.3.4. Running spectra

Figure 2.13 shows the running spectra for the wind components perpendicular (NE-SW) and parallel (NW-SE) to the shoreline. Thus, the former incorporates all air flows across the Adriatic (including among other SLB and bora) while the latter corresponds to the along-Adriatic flows (such as sirocco and etesians).

For Split-Marjan a strong signal on a daily scale is found for the NE-SW component throughout the warm part of the year (Figure 2.13 top, frequency of about 0.04 cph). This further confirms the importance of SLB, which was already discussed in section 2.3.1. On the other hand, for the along-Adriatic wind component, the signal is shifted towards the larger timescales. For frequencies of about 0.03 cph (timescale of about 33 h), three episodes with increased signals are found between mid-February and mid-March, which correspond to sirocco winds (note that the three energy peaks at 0.03 cph roughly coincide with the maximum northwestward speeds, i.e. positive wind speeds shown on the left side of the panel).

For Komiza slightly increased energy signal at daily scale (frequency of about 0.04 cph) for the across-Adriatic wind component is found in July (Figure 2.13 center). However, the signal at the same timescale in July is much stronger for the along-Adriatic wind component. (Somewhat smaller peaks at daily scale are also found for the periods from mid-February to mid-March and from mid-April to mid-June). Furthermore, in July and from mid-February to mid-March the secondary peaks are found at the timescales of about 12 h (frequencies of about 0.08 cph), where the February/March signals were weaker when compared to summertime signals. Similar patterns for the along-Adriatic air flow in July and from mid-February to mid-March, with the peaks at the timescale of about 24 h and the secondary peaks at the timescale of about 12 h, are also found for Palagruza (Figure 2.13 botom).

2.3.5. Divergence episodes

During the period of study some interesting cases of the low-level air flow divergence, which might have affected the Adriatic currents, occurred in the region between Komiza and Palagruza (Figure 2.14).

The first event occurred on 8 June, when wind speeds at Palagruza were almost throughout the day much stronger (even up to about 8 m/s) than at Komiza. In the first part of the day, the wind directions at both sites were rather similar (roughly corresponding to 150°), whereas in early afternoon hours wind at Komiza and Palagruza turned to about 200° and 135°, respectively. Such air flow should result in the low-level divergence and consequent descent of the air.

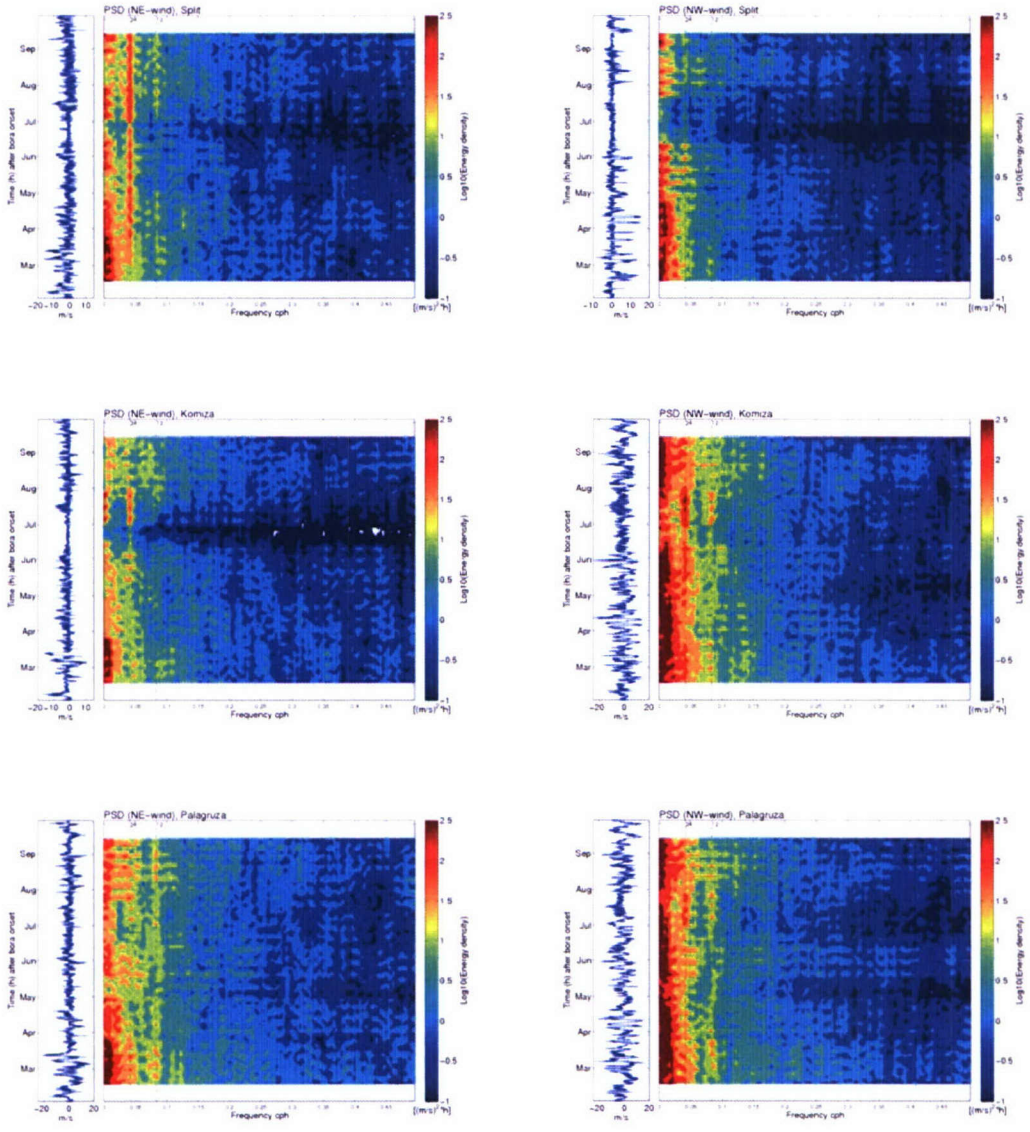

Figure 2.13 Running spectra for NE-SW (i.e. perpendicular to the shoreline, left) and NW-SE (i.e. parallel to the shoreline) air flow for Split (top), Komiza (center) and Palagruza (bottom) and for the year 2006. In each panel the original, hourly mean wind speed time series is shown on the left.

On the other hand, on 14 June from about 9 to 15 LST, the wind speeds at both sites were rather similar, while wind directions differed substantially. Thus, at Palagruza the wind was close to etesians, while at Komiza it was closer to sirocco. Therefore, the low-level divergence, and resulting air descent, again occurred in the region between the two islands.

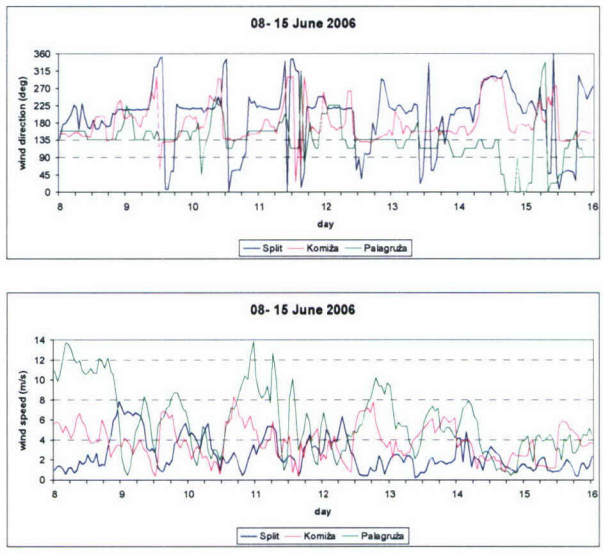

Figure 2.14 Wind direction (top) and speed (bottom) for the 8-15 June 2006 period.

2.4. Air pressure

2.4.1. Rossby waves

The Rossby (planetary) waves are frequently found in the wintertime atmosphere within the layer extending from the middle (pressure of about 500 hPa) to the upper troposphere. As they represent atmospheric disturbances of the planetary scale, they are characterized by long periods, which are measured in days. The north-south undulations in the jet stream produced by Rossby waves create regions of upper-level divergence/convergence, thus initiating and/or maintaining the mid-latitude surface cyclones and anticyclones. (Note that the upper level divergence, which is found at the eastern side of a trough [i.e. western side of a ridge] is accompanied by the air ascent and consequent cyclogenesis or cyclone maintenance. On the contrary, the upper level convergence occurs at the western side of a trough [eastern side of a ridge] and it results in the air descent and consequent development or maintenance of an anticyclone.)

During February and March 2006 the temporal variations of the air pressure field exhibited quasi-periodic behavior at the time scales of about 7 to 11 days (Figure 2.15 and Figure 2.16) thus pointing to the existence of Rossby waves (see intervals from 9 to 17 and from 17 to 24 February and from 12 to 23 March). In order to confirm their existence, the 500 hPa charts were inspected in detail. Here, only a few snapshots which illustrate the link between the surface pressure and conditions aloft are shown (Figure 2.17).

On 11 February, the western part of the Rossby wave trough (i.e eastern part of the ridge) and consequent upper-level convergence is found above the Adriatic. The latter is evident from the isolines of geopotential, which approach one another in along-flow direction. Due to the mass conservation, the upper-level convergence should result in the air subsidence, and accordingly in the surface pressure increase. This is confirmed by the pressure variations recorded at all three measuring sites during 11 February (cf. Figure 2.15 and Figure 2.16). On the following day, similar conditions aloft are also found above the area of interest. Again, they are accompanied by the surface pressure increase at Split-Marjan, Komiza and Palagruza.

On the other hand, on 16 and 23 February the Adriatic was topped by the eastern part of the Rossby wave trough, i.e. by the region of upper-level divergence. This resulted in the surface pressure decrease at the three sites during both days. Note that on the two days, the distance between the isolines of geopotential increased in the along-flow direction above the area of interest.

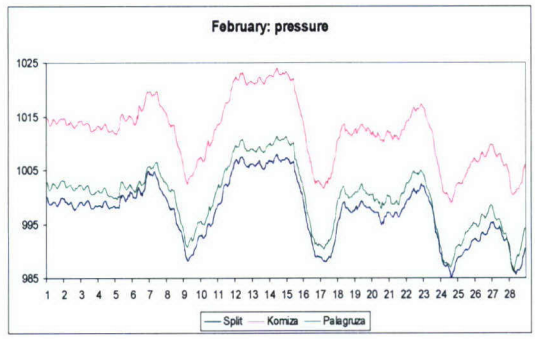

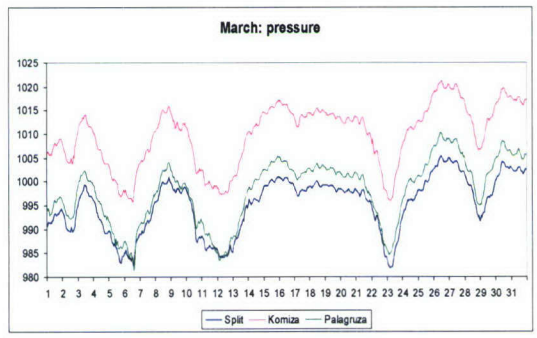

Figure 2.15 Hourly means of air pressure measured in February and March 2006. Note that the Split-Marjan and Palagruza data are not reduced to the sea level.

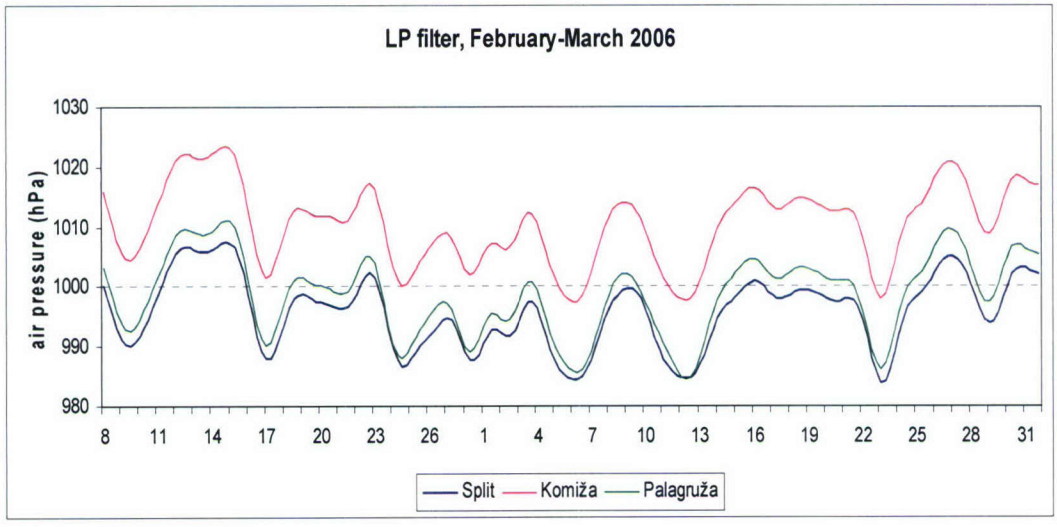

Figure 2.16 Low-pass filtered hourly mean air pressure for February and March 2006.

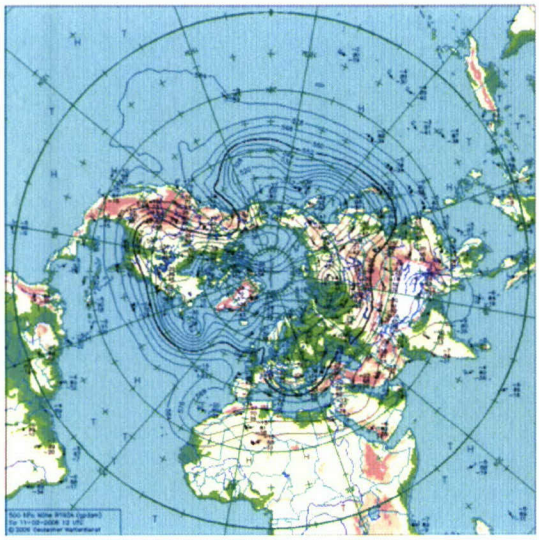

11 February 2006

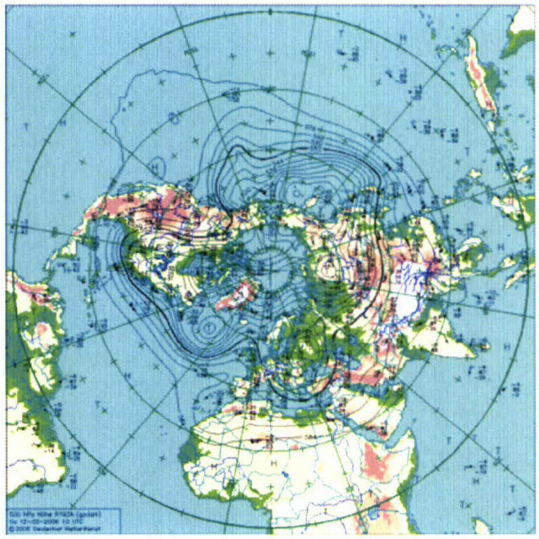

12 February 2006

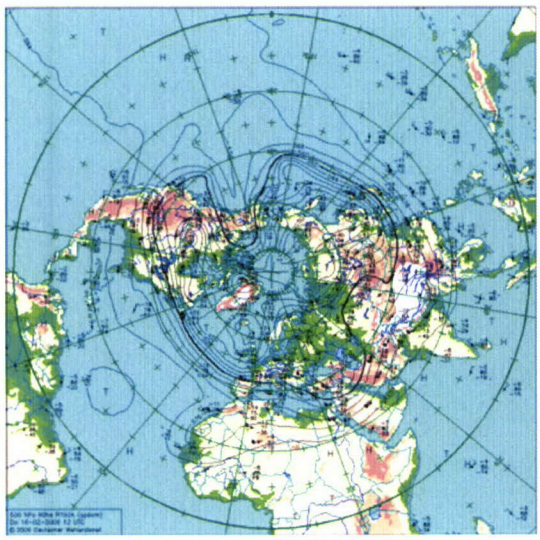

16 February 2006

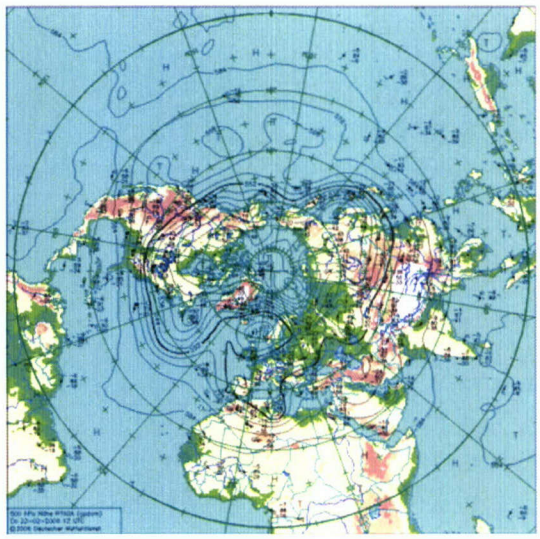

23 February 2006

Figure 2.17 500 hPa hemispheric charts at 12 UTC (source: DWD).

2.4.2. Cyclogenesis

An inspection of the hourly mean data revealed a prominent pressure decrease at the end of May 2006 (Figure 2.18). It was accompanied by a noticeable temperature drop and, in the second part of 30 May, a severe sirocco at Komiza (up to 24.2 m/s) and Palagruza (up to 19.4 m/s). The event was so intense that its signature remained in the low-passed pressure and temperature data (Figure 2.19).

The above was produced by a cyclone formed in the Genoa Bay (Figure 2.20), which in time moved northeastward (Figure 2.21) (MHS, 2006). According to the bulletin of MHS (MHS, 2006) the cyclone caused a stormy weather with a heavy precipitation above the northern Adriatic. Thus, for example, in Porec and Senj 94 liters per square meter were recorded, while in Novalja on the island of Pag hail occurred.

2.5. Conclusion

Hourly mean air pressure, air temperature and wind data for Split-Marjan/Dubrovnik, Komiza/Hvar and Palagruza were investigated for the period extending from 1 February to 30 September 2006. It is shown that the above sites can be taken as representative for the coastal, offshore and open-sea atmospheric conditions, respectively.

A number of various atmospheric processes and events at different spatio-temporal scales (ranging from a few hours to about ten days), that might be relevant for the forcing of the Adriatic, occurred during the period of study. Their inspection should help to interpret the concurrent oceanographic processes.

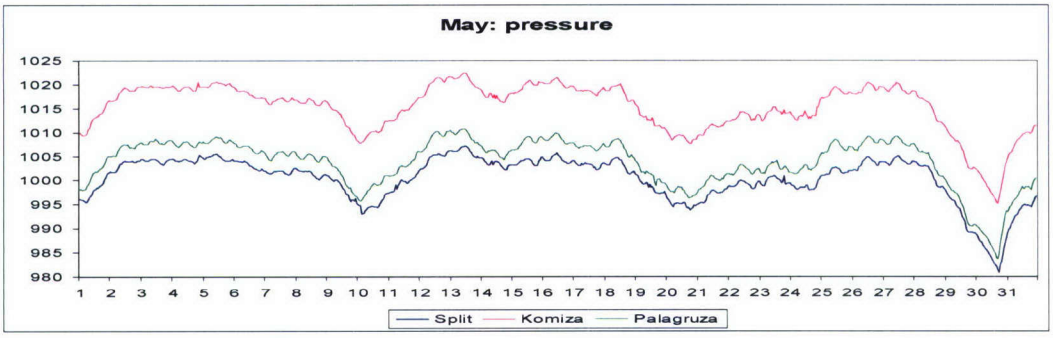

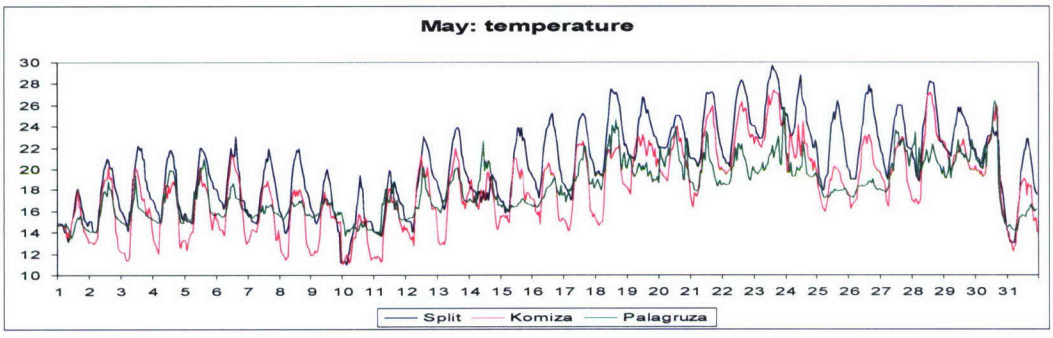

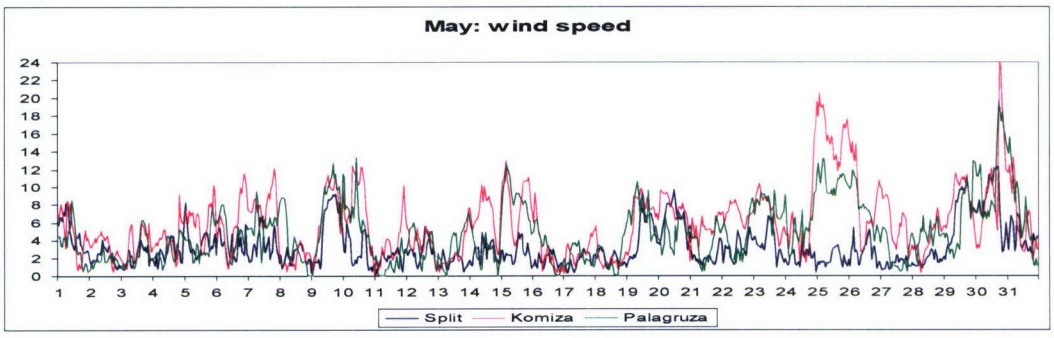

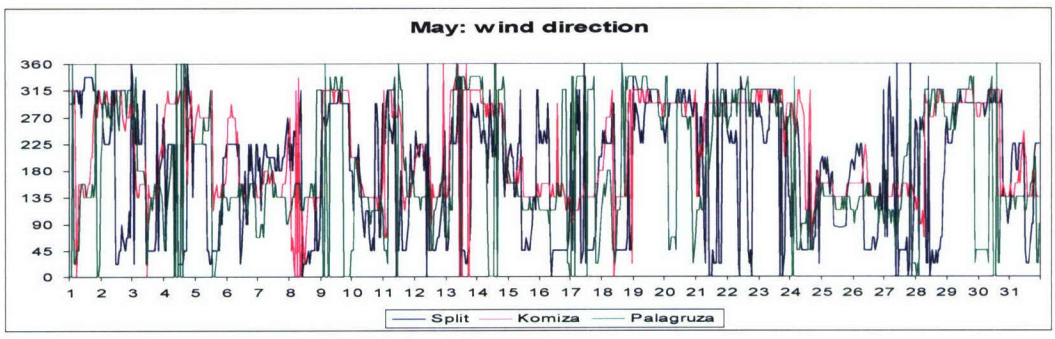

Figure 2.18 Hourly mean air temperature, pressure and wind data for May 2006.

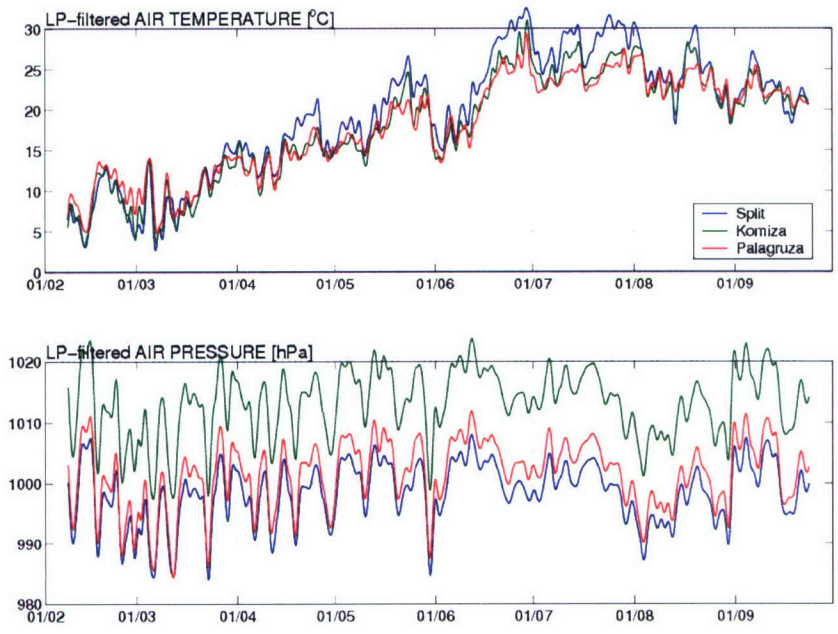

Figure 2.19 Low-pass filtered air temperature and surface pressure data for the whole period of study. Prominent are the temperature and pressure drops at the end of May 2006. The beginning of the each month is indicated on the abscissa.

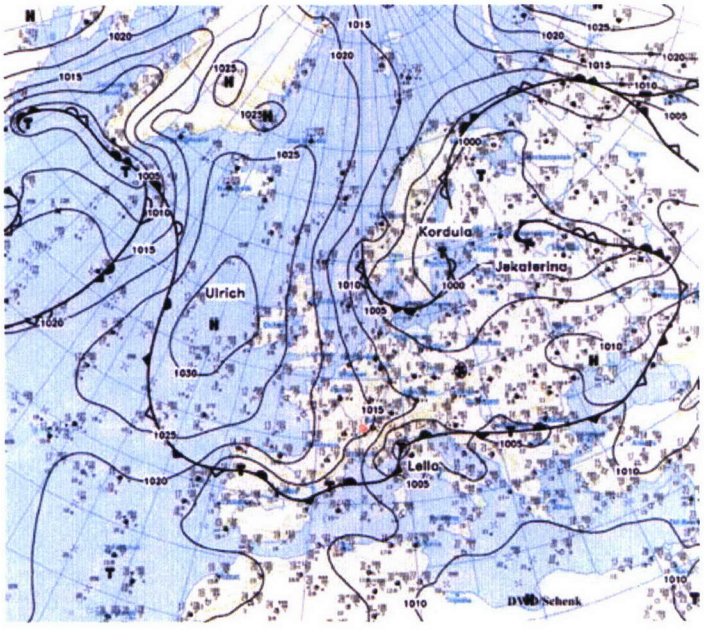

Figure 2.20 Diagnostic chart for 30 May 2006 at 00 UTC (source: MHS, 2006).

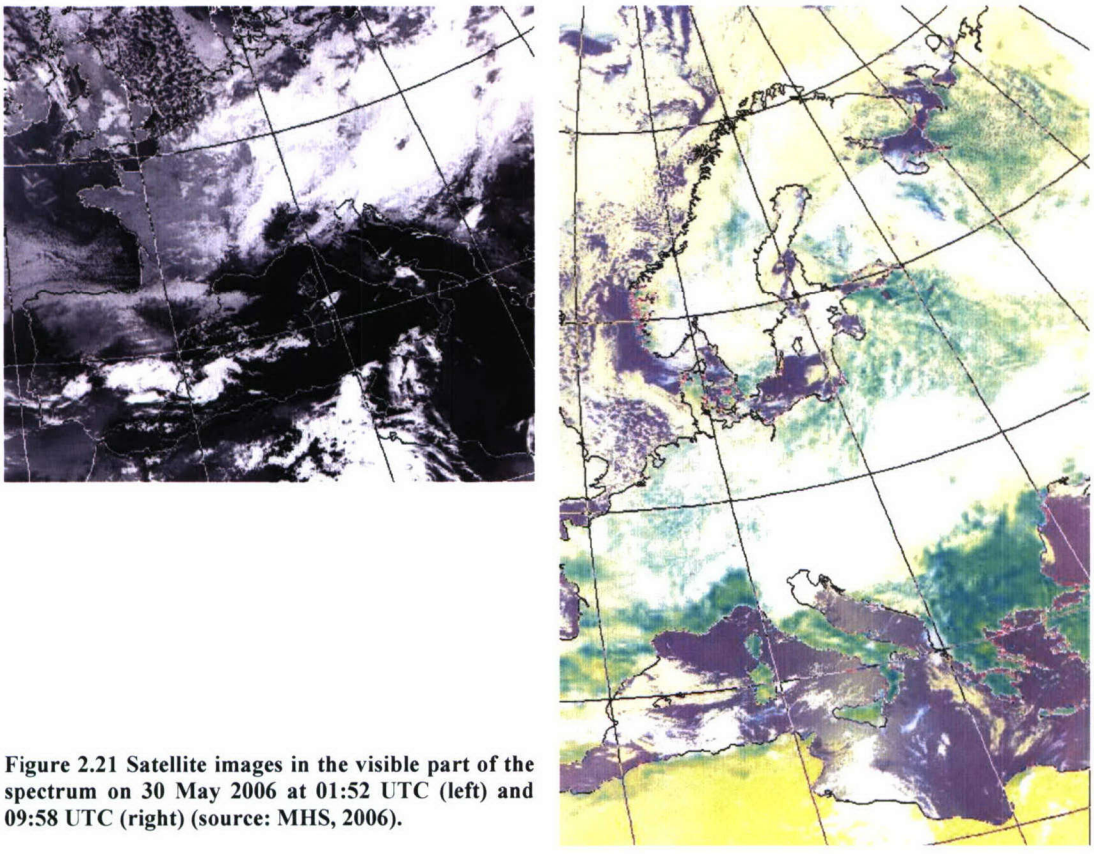

Figure 2.21 Satellite images in the visible part of the spectrum on 30 May 2006 at 01:52 UTC (left) and 09:58 UTC (right) (source: MHS, 2006).

3. Optical properties of the Bisevo, Susac and Lastovo area

During the ITHACA cruises in February and September 2006, the irradiance, radiance and fluorescence were measured through the water column down to about 70 m depth at stations Bisevo, Susac and Lastovo. The investigated region is under the influence of the open sea, and attenuation coefficients calculated for these stations (for different wavelengths and for PAR) have relatively lower values than the coefficients in nearby channel areas.

3.1. Introduction

The scale of optical water types within the Adriatic is considerable in space and also significant seasonal and inter-annual changes occur in time. The investigated area is situated in the open middle Adriatic and optical and thermohaline gradients are lower when compared to the channel area. We expected to find the case 1 waters there, when satellite color images are concerned, pointing to a relatively low biological productivity. The freshwater and nutrient impacts, as well as anthropogenic impact from urban/industrial sources, were not expected.

The motivation for including measurements of optical parameters in the ITHACA experiment was primarily a deficiency of optical data from this area. Sparse PAR attenuation measurements were performed occasionally in the sixties and the eighties of the last century (Morovic and Domijan, 1991), and the only measured optical parameter was transparency (Secchi disk depth) measured monthly to seasonally. The importance of optical data for the investigation of heat transfer in the water column has been demonstrated through several numerical experiments (Morovic et al., 2001, 2006; Beg-Paklar et al., 2001b), and it was shown that change of the optical type (Jerlov, 1969) leads to a different thermal stratification. Another motivation was to allow assessment of methods for the interpretation of satellite data for this area.

3.2. Data and methods

Spectral measurements of light intensity were performed using the Biospherical Profiling Radiometer PRR800 at stations Bisevo, Susac and Lastovo in February and September 2006 (Figure 3.1).

The irradiances and radiances were measured at 14 wavelengths (340, 380, 412, 443, 465, 490, 510, 532, 555, 589, 625, 665, 683 and 710 nm) from the UV to the end of the visible spectrum. PAR attenuation (400-700 nm) and natural fluorescence were also measured. The profiler was lowered manually, from the sunny side of the ship, through the water column to about 70 m depth.

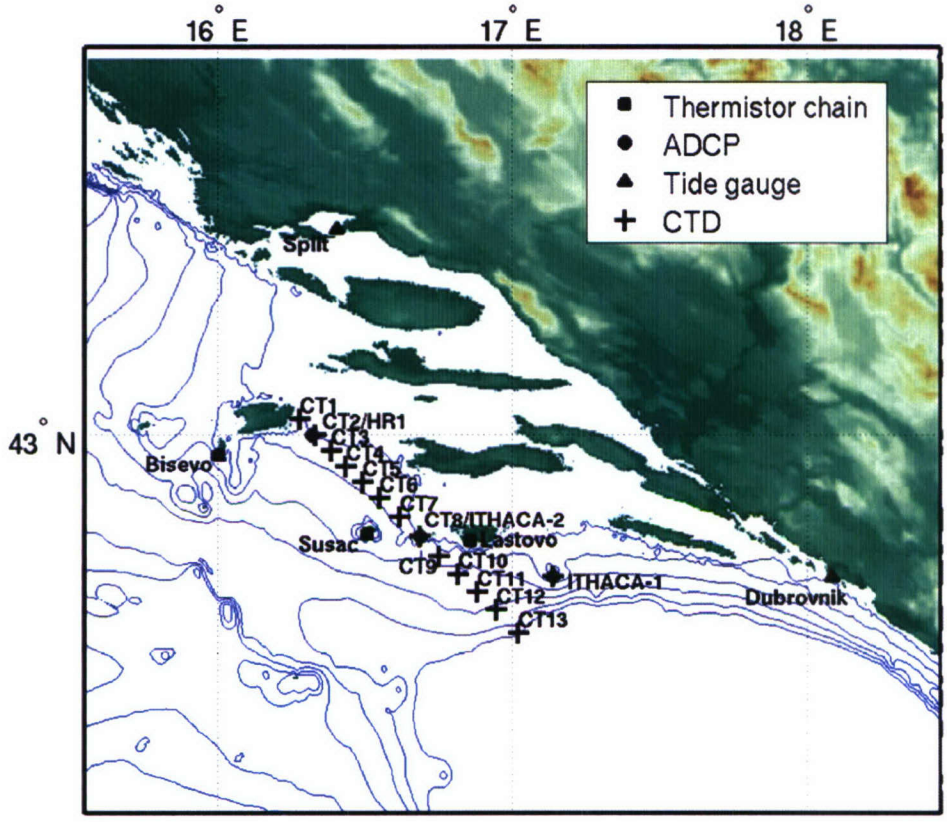

Figure 3.1 Stations at which various oceanographic data were collected between February and September 2006.

Each measurement was accompanied with data for dark calibration. Calibrated data were processed to 1 m depth. Attenuation coefficients were calculated from respective irradiances with the formulae:

$$K_d = \mathrm{d}\ln(E_d(z))/\mathrm{d}z \,,$$

$$K_u = \mathrm{d}\ln(L_u(z))/\mathrm{d}z \,,$$

$$K_{Par} = \mathrm{d}\ln(E_{Par}(z))/\mathrm{d}z \,,$$

where E denotes irradiance, L radiance, d downward and u upward direction for each wavelength and PAR.

Measurements with the SeaBird instrument along the CTD transect included also beam attenuation and fluorescence detection with WetLabs sensors.

3.3. Results and discussion

It is supposed that the offshore waters are rather clear, since the investigated area is distant from anthropogenic/coastal influences. The irradiance spectra for the stations in February (Figure 3.2, upper row) are characterized by the most intense wavelength of 490 nm at all depths. For this wavelength, clear oceanic waters are most transparent, which is an indication, among others, of the clarity of this area. The spectrum became narrower with depth. The shape of the spectral curve is very similar for the three stations.

Upward radiance spectra (Figure 3.2, lower row) are narrower than irradiance spectra and have two orders of magnitude lower intensities than the irradiances for the same depth. Upward spectra become also narrower with depth, but with a peak at 490 nm.

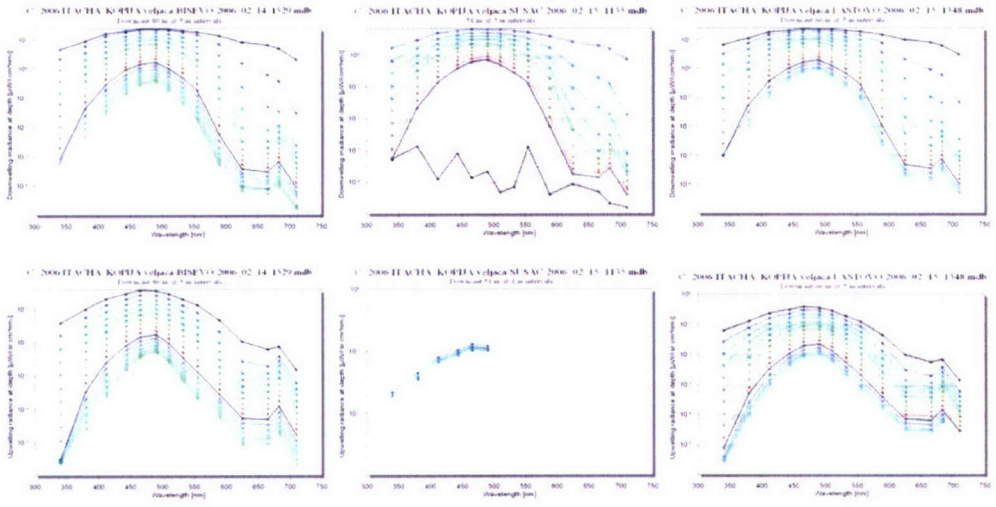

Figure 3.2 Downward irradiance (upper row) and upward radiance (lower row) intensity from the surface to the bottom, measured with a 5 m vertical resolution at stations Bisevo, Susac and Lastovo in February 2006.

Both irradiance and radiance spectra show relative increase of intensity at 683 nm. This wavelength, although highly absorbed by the water itself, is better distinguished with depth. It corresponds to the fluorescence of phytoplankton chlorophyll-like pigments.

In September the irradiance spectra (Figure 3.3, upper row) have very similar properties as in February. Both are characterized by the wavelength of 490 nm with highest intensity at all depths. The shape of the spectral curve is very similar for the three stations.

Upward spectra (Figure 3.3, lower row) are similar but narrower and have two orders of magnitude lower intensities than the irradiances for the same depth. Both spectra

become more narrow with depth, but with a peak at 490 nm. In both spectra the peak at 683 nm is observed, corresponding to chlorophyll fluorescence; this signal becomes better distinguished with increasing depth.

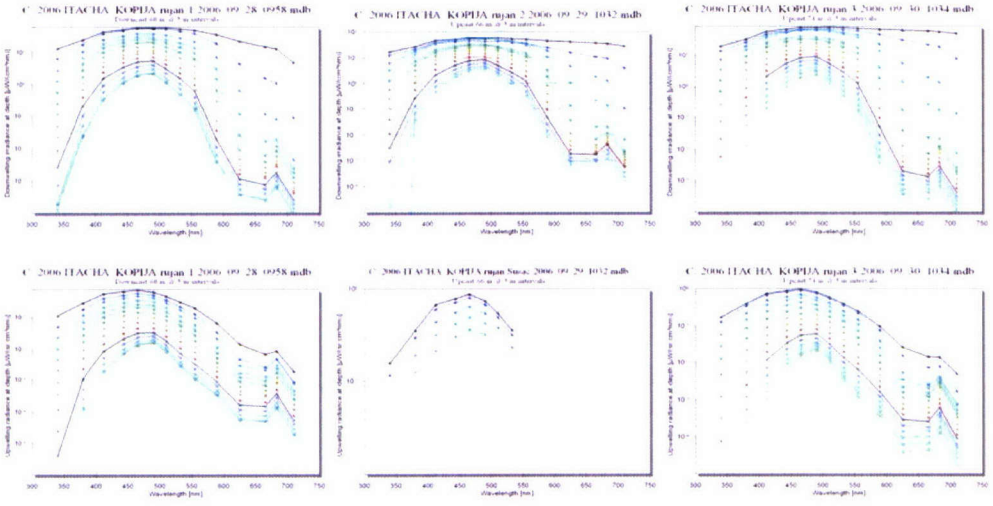

Figure 3.3 Downward irradiance (up) and upward radiance (down) intensity from the surface to the bottom, measured with a 5 m vertical resolution at stations Bisevo, Susac and Lastovo in September 2006.

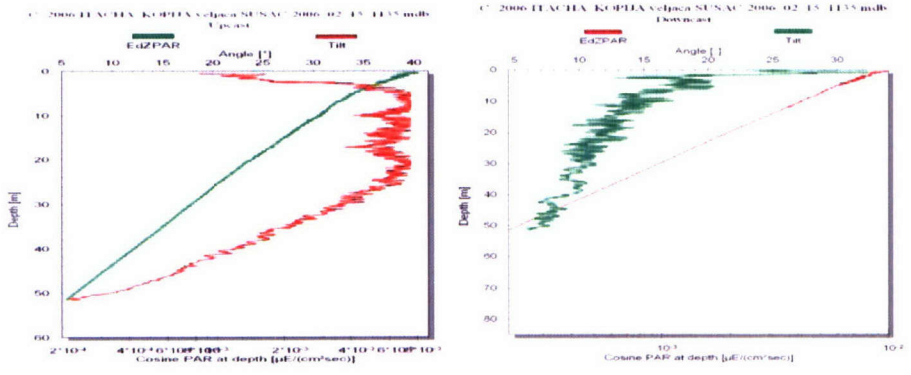

Figure 3.4 PAR attenuation depending on depth and tilt of the instrument.

Both the downcast and the upcast sections of the file have high tilt values for station Susac in February 2006 (Figure 3.4), implying that the data taken at the 5-25 m depths for the upcast and at the first 10 m depths for the downcast should be discarded. Further processing has been done for some parameters, but fluorescence data were missing and chlorophyll could not be obtained.

At station Susac the measurements of radiance of longer wavelengths failed in September 2006 and below 20 m the radiance measurements failed completely. This was probably caused by unfavorable measurement conditions, most probably related to strong currents that caused high tilt of the radiance sensor (Figure 3.5). Due to the shape of irradiance collector the irradiance sensor is much less affected by possible inclination of the instrument with respect to the vertical. However, because of this obstacle, it was not possible to calculate radiance attenuation coefficients, except for some wavelengths and for shallow depths. Also, since fluorescence (as well as radiance at 683 nm) was not measured it was not possible to estimate chlorophyll concentrations.

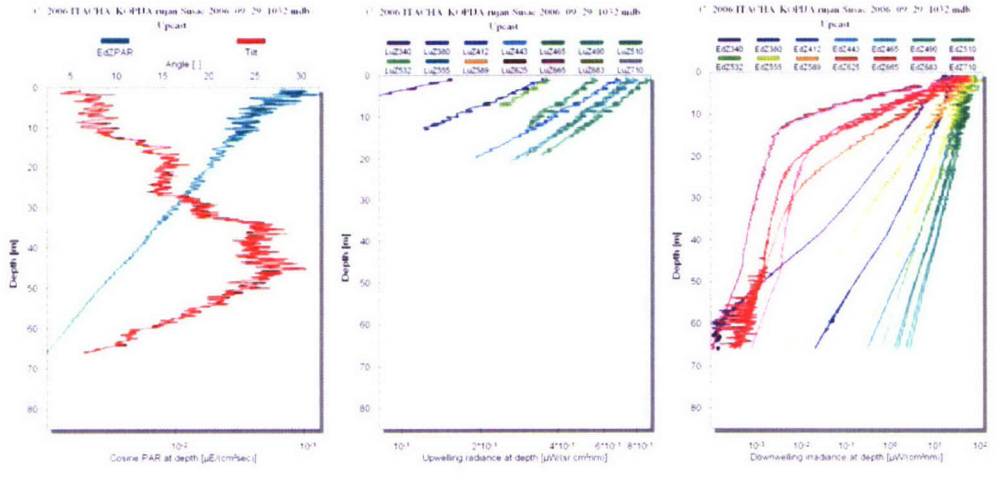

Figure 3.5 PAR attenuation depending on depth and tilt of the instrument (left), radiance distribution depending on depth (middle) and irradiance distribution depending on depth (right).

In Figure 3.6 and Figure 3.7 attenuation coefficients are shown for downward irradiance (left) and upward radiance (right) for February and September. In February the coefficients for downward irradiance attenuation are highest for longer wavelengths and lowest for the most transparent wavelength of 490 nm. At the shortest wavelengths there is a smaller increase of attenuation coefficients relative to the minimum values. The coefficients for radiance attenuation are lower, especially for the longer wavelengths, and in some cases somewhat higher for the shortest wavelengths.

PAR attenuation coefficients (Figure 3.8) for stations in February were more uniformly distributed with depth than in September. Coefficients for PAR attenuation show highest values in the surface layer, where they are higher in September than in February.

From the relative irradiance distribution with depth (Figure 3.9) it is possible to determine the levels of irradiance, like the levels of 10% or 1% of light (euphotic zone depth) relative to the subsurface layer.

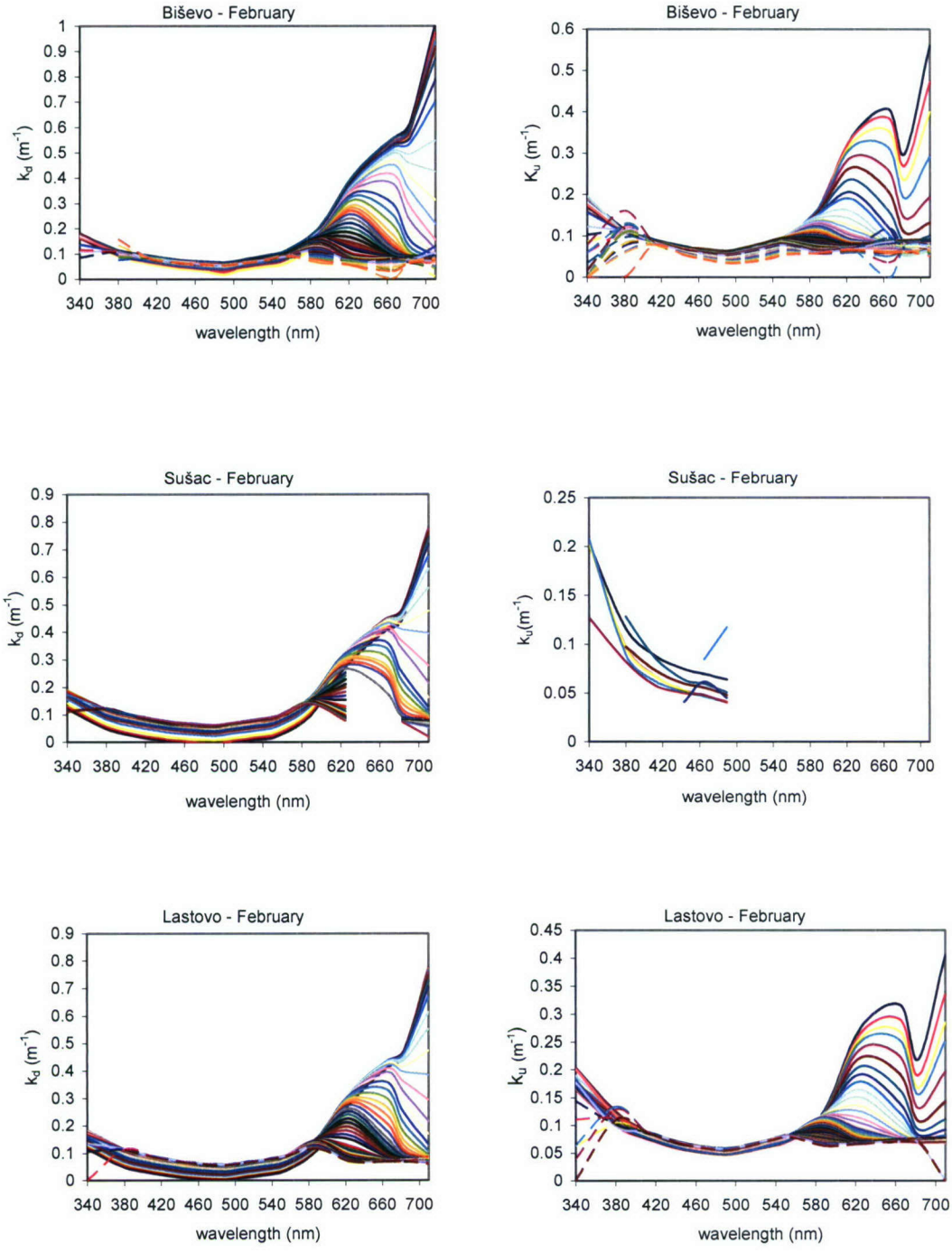

Figure 3.6 Spectral dependence of the attenuation coefficients for downward irradiance (left) and upward radiance (right) for different depths and for stations Bisevo, Susac and Lastovo, in February 2006.

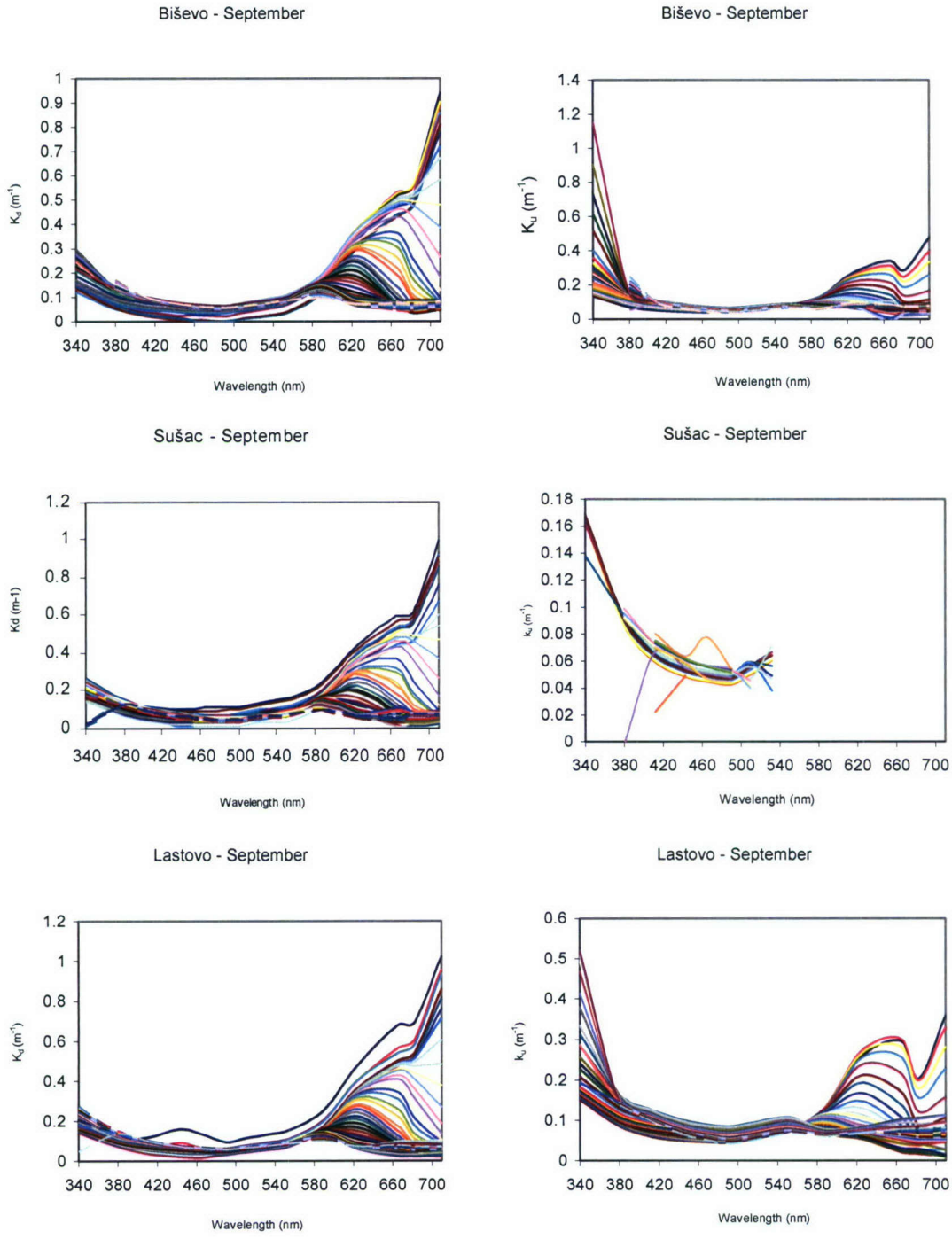

Figure 3.7 Spectral dependence of attenuation coefficients for downward irradiance (left) and upward radiance (right) for different depths and for stations Bisevo, Susac and Lastovo, in September 2006.

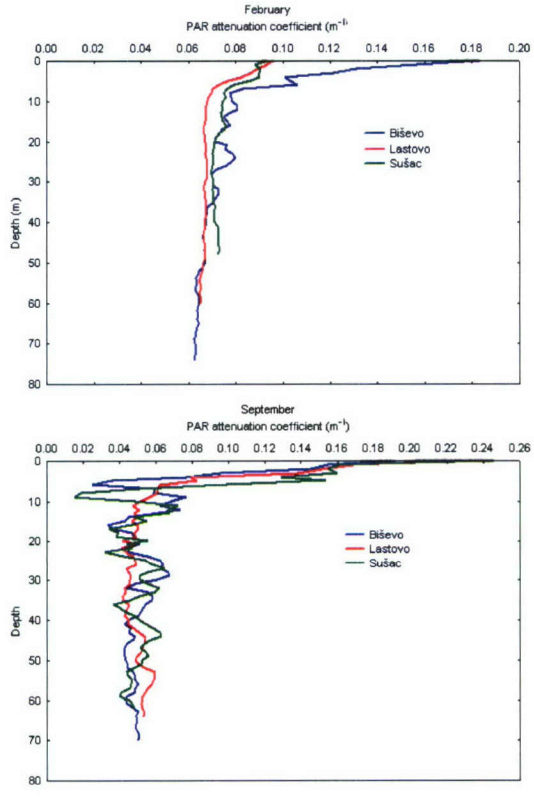

Figure 3.8 Dependence of attenuation coefficients for PAR with depth, for stations Bisevo, Susac and Lastovo, in February (up) and in September 2006 (down).

Chlorophyll concentrations (Figure 3.10) have 1.5-3 times higher values at the surface in February than in September. Estimated values of chlorophyll-like pigments (Biospherical software) are relatively high for the open sea area and, if compared to the estimated values from the WetLabs fluorescent sensor, are almost double. However, the measurements were neither simultaneous in time nor performed at the same position: WetLabs measured off the coast along the transect, while Biospeherical probe measured closer to the coasts of the islands, and the two instruments could sense different conditions in the environment.

Figure 3.11 and Figure 3.12 represent measurements with the SeaBird CTD, additionally supplied with WetLabs instruments for beam attenuation, fluorescence and oxygen measurements. Thermohaline properties from the period of investigation cover two distinct conditions: completely mixed water column in February and highly stratified layers in September (Figure 3.11 and Figure 3.12, down, right). Oxygen distribution (Figure 3.11 and Figure 3.12, down, left) shows differences that correspond

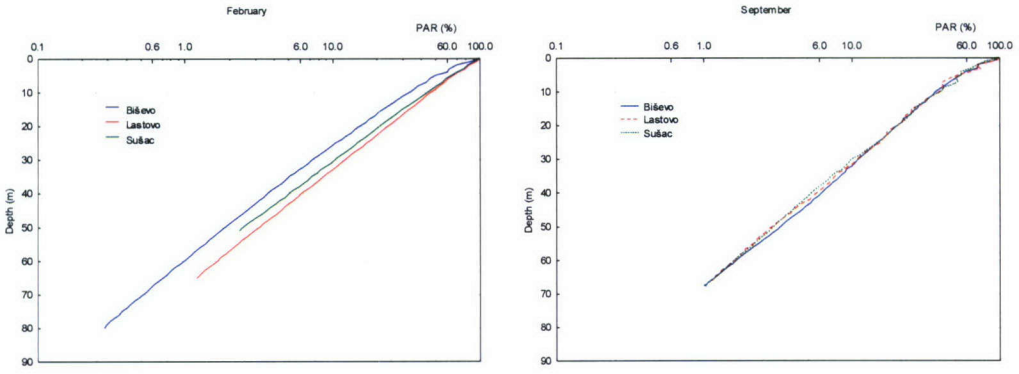

Figure 3.9 Percentage PAR irradiance relative to the subsurface irradiance in February (left) and September 2006 (right) for stations Bisevo, Susac and Lastovo.

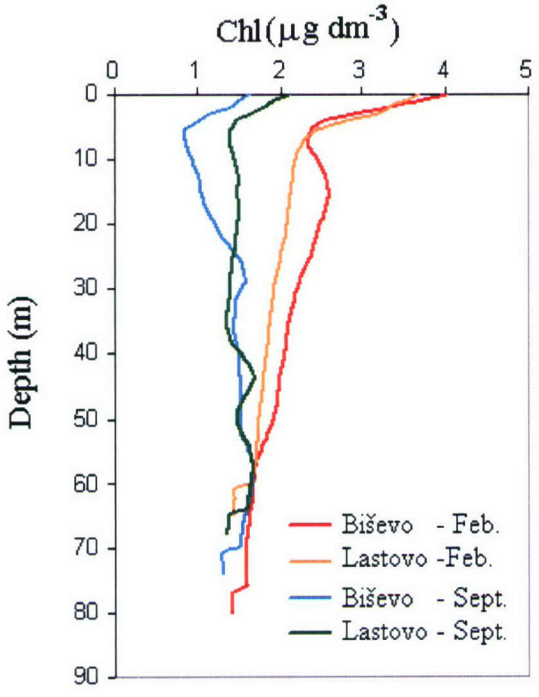

Figure 3.10 Estimated concentration of chlorophyll-like pigments (from WetLabs sensors) in February and September 2006.

to different stratification – vertically mixed conditions in February and horizontally stratified conditions in September. Beam attenuation and chlorophyll also show similar properties in the surface layer, but not so distinguished as oxygen. Beam attenuation coefficients strongly increase towards the bottom going southwards, especially in February, while in September maximum beam attenuation coefficients in the bottom

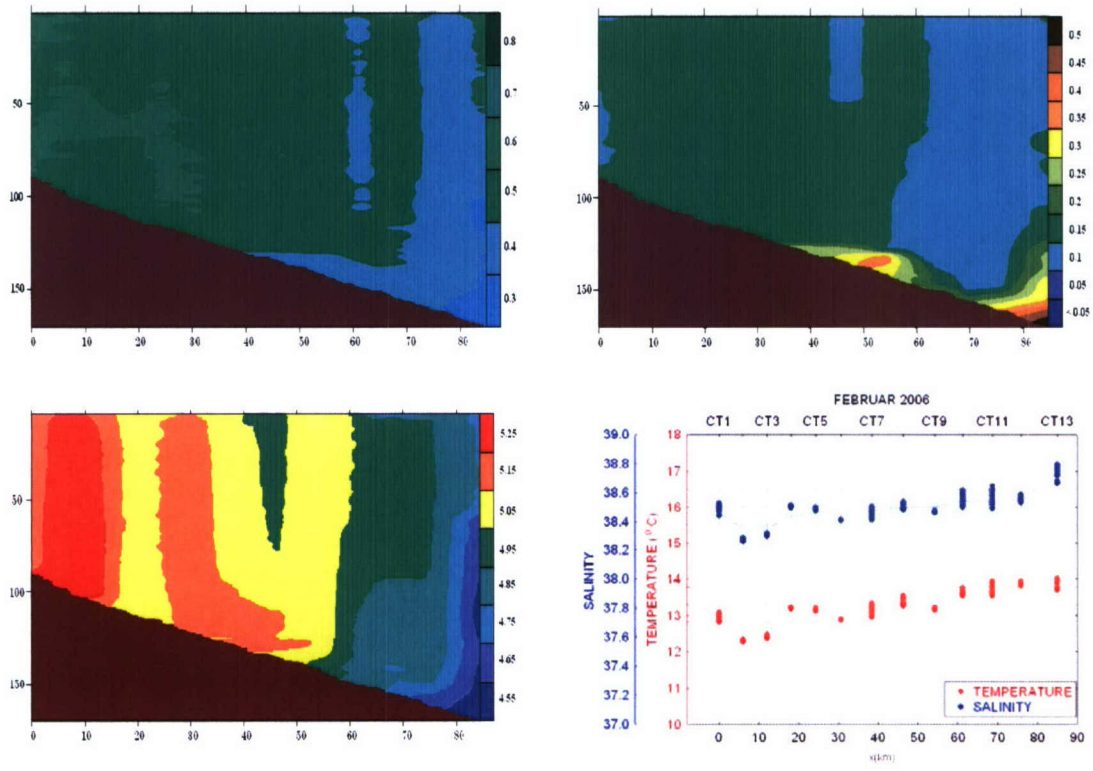

Figure 3.11 Beam attenuation coefficients and fluorescence (up) and oxygen and thermohaline properties (down) at the CTD stations in February 2006.

layer are not found so much southwards but closer to the middle of the transect. Fluorescence was higher at the northern part of the profile in February and in the southern part in September.

The chlorophyll concentrations determined from MODIS (Figure 3.13) show lower values than those determined from the two *in situ* fluorescence measurements for the surface layer during both cruises.

3.4. Concluding remarks

The area of ITHACA measurements is situated in unpolluted areas and optical characteristics of the three stations Bisevo, Susac and Lastovo are in some ways similar. The differences were higher regarding the measurements in different seasons than between the stations in one season, except for the bottom layer. Optical measurements were sensitive to a number of disturbances like waves, currents, cloudiness, and other. Strong currents occurring during the optical measurements at station Susac during both cruises represented significant disturbance for performing radiance (and fluorescence) measurements with PRR800, but not for irradiance measurements. Generally, irradiance and radiance spectra had maximum intensity wavelength at 490 nm and the spectrum

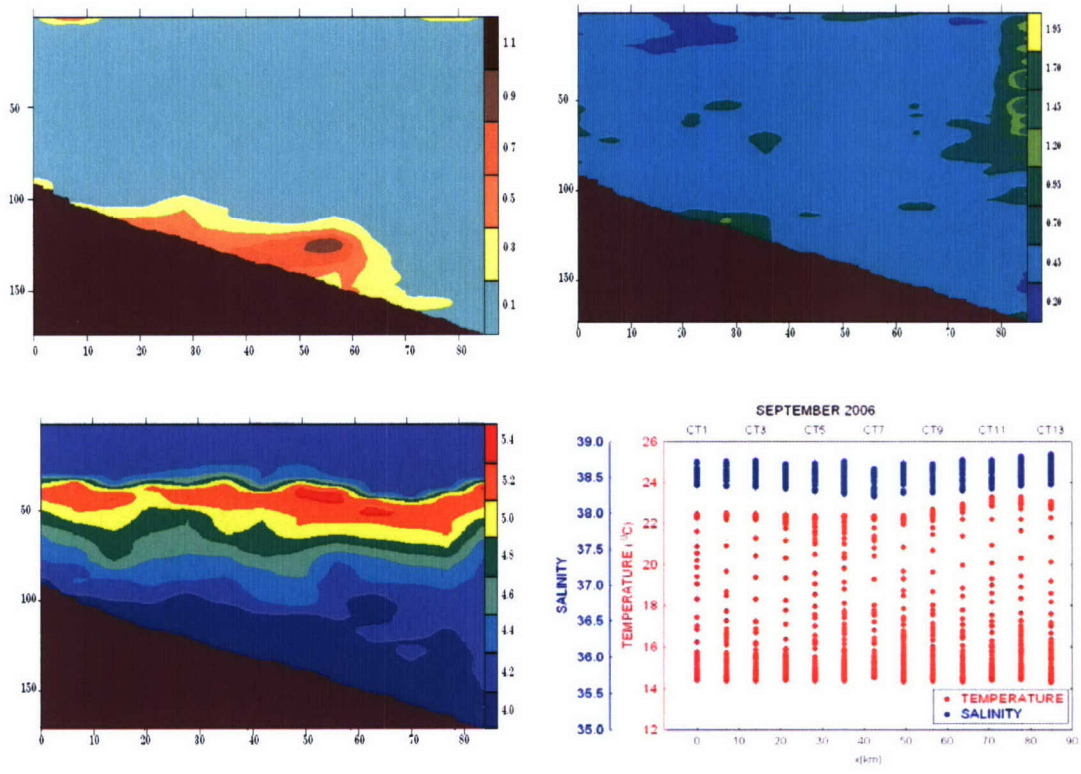

Figure 3.12 Beam attenuation coefficients and fluorescence (up) and oxygen and thermohaline properties (down) at the CTD stations in September 2006.

became narrower with depth. The peak at 683 nm that corresponds to fluorescence was clearly observed, and became more distinguished with depth. Both statements are valid also for the radiance spectrum.

The irradiance attenuation coefficients were higher than the coefficients for radiance attenuation, and with somewhat different spectral distribution. Generally, the attenuation coefficients were higher in February than in September 2006 as were the chlorophyll estimates.

Beam attenuation coefficients, oxygen and fluorescence (from SeaBird) had different distributions in February (mixed) than in September 2006 (stratified), with similarity in vertical distribution for beam attenuation which increased towards the bottom.

In the future, other values could be retrieved from PRR measurements like: the amount of light available for photosynthesis, euphotic zone depth, productivity estimation, optical signature of chlorophyll-like pigments (for comparison of chlorophyll signature from remote sensing) and different optical functions like reflectance or relations between different radiance bands, etc. Also relation between the measured values from the two instruments should be analyzed.

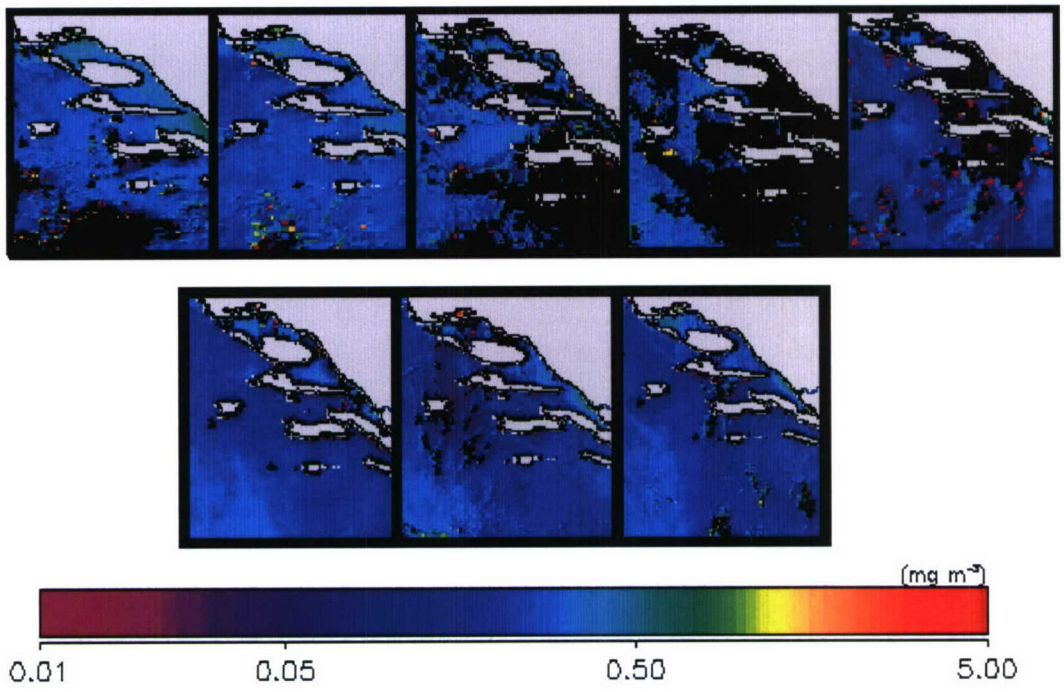

Figure 3.13 Evolution of MODIS pigment concentrations for the period during and prior to February ITHACA cruise (up) (for 11, 12, 13, 14 and 15 February 2006) and for September cruise (down) (for 28, 29 and 30 September 2006) (GOS-ISAC, Rome).

4. CTD measurements and thermohaline properties

The measurements of temperature and salinity took place in the second year of the ITHACA project, between February and September 2006, at the ITHACA section stretching from the island of Vis towards the South Adriatic Pit. The main characteristics of kinematics and dynamics revealed by the preliminary data analysis are presented in this chapter.

4.1. Data acquisition

The measurements of temperature and salinity were performed at 13 CTD stations (Figure 3.1) on the hydrographic section extending from the island of Vis (CT1) towards the Adriatic shelf break (CT13). The measurements of temperature and salinity were carried out during five cruises (Table 4.1), of which the third was accomplished through the DART project. Additionally, dissolved oxygen measurements were performed during ITHACA01, DART, ITHACA03a and ITHACA03b cruises. Temperature and conductivity (salinity) were measured by three probes: SeaBird SBE25 (probe 1), SBE17 (probe 2) and SBE911+ (probe 3), having accuracy of at least 0.002°C in temperature, 0.0003 S/m in conductivity and 0.1% of full-scale range in pressure. The data were preprocessed and averaged along vertical every 1 m. Intercalibration of the first two probes was carried out during the ITHACA cruises. The use of the probes is documented in Table 4.1.

Table 4.1 List of cruises carried out at the ITHACA section.

Cruise	Date	Probe	Stations
ITHACA01	14/15 February 2006	1	CT1 to CT13
ITHACA02	26 June 2006	2	CT1 to CT13
DART	20/21 September 2006	3	CT1 to CT10
ITHACA03a	28 September 2006	1	CT1 to CT13
ITHACA03b	29/30 September 2006	1	CT1 to CT10

4.2. Ambient characteristics

The analyses of spatial and temporal thermohaline properties in the eastern Adriatic shelf break area will be performed by using vertical profiles at the ITHACA section (Figure 4.1 to Figure 4.5).

First and foremost, the influence of the processes at the ocean surface can be noticed during all examined months. Vertical homogeneity was observed in February (Figure 4.1) after heat losses and vertical mixing induced by the wind, which had occurred in the previous months. However, horizontal variability can be detected both in temperature, salinity and dissolved oxygen fields. A band of low temperature and salinity water with higher dissolved oxygen values at CT2 and CT3 is probably a result of the eastern Adriatic rivers, in particular of the Neretva River which strongly affects thermohaline properties in the middle Adriatic channels. An increase in temperature and salinity and decrease in dissolved oxygen can be noticed closer to the shelf break (CT11-CT13), where an inflow of the Levantine Intermediate Water (LIW, Vilibic and Orlic, 2001, 2002), with temperature of about 13.5°C and salinity larger than 38.7, is prevailing.

More complex situation was found in June 2006 (Figure 4.2). Strong heating at the surface resulted in rather warm surface layer (down to 15 m) with high surface temperatures at some spots (up to 26°C). Nevertheless, very low salinity (< 37.5) is preserved at the whole transect at the very surface (down to 5-10 m), with minimum values at CT11 and CT12 (about 37.2). Obvious question arises: Where this water comes from? It may be a filament of the middle Adriatic waters as the circulation differed from the usual pattern at that time. It may be also a result of Albanian rivers (Bojana, Drim) which have a maximum outflow in spring due to snow melting and could be advected along the southeastern shelf and shelf break. Last but not least, it may be influenced by the West Adriatic Current (WAC) which has a maximum at that time due to maximum in the Po River runoff; these waters could be pushed towards the eastern coast over the Palagruza Sill region and could reach outer Croatian islands. An increase in temperature and salinity may be seen in the bottom layer, which could be attributed to enhanced LIW inflow being triggered by the wintertime large scale thermohaline circulation (Orlic et al., 2006).

Similar situation in the bottom layer remained until September (Figure 4.3 to Figure 4.5). The presence of LIW is additionally supported by the low dissolved oxygen values (< 4.5 ml/l, Figure 4.3 and Figure 4.4), denoting an old water mass (LIW is such a mass, traveling a few years before reaching the Adriatic). A deepening of well-developed thermocline/pycnocline may be found already on 20/21 September (20-25 m) with respect to the June cruise, but strong winds (sirocco) which blew between 21 and 28 September pushed it down to 30-45 m in just one week. Surface salinity increased a lot (>38.2) with respect to June 2006, as the freshwater discharge substantially decreased during summertime, resulting in fresher coastal waters being kept close to the shore.

An interesting feature may be found in salinity field in the last two cruises (Figure 4.4 and Figure 4.5). Namely, an area of low salinity (S<38.3) was found on ITHACA03a cruise stretching from CT6 to CT10 stations and encompassing the whole surface layer (down to pycnocline depth of 35 m). The same feature was found also on ITHACA03b cruise, but between CT4 and CT7 stations. Consequently, the along-transect velocity of

that freshened fraction may be estimated at about 14 km/31 h or at about 12.5 cm/s, and its direction is roughly northwestward. Although the closest source of fresh waters to the ITHACA polygon is the middle Adriatic (Neretva and Cetina rivers), and such fractions can be also brought from Albanian rivers via the East Adriatic Current (EAC), it seems that this eddy- or filament-like feature is advected from the WAC which brings the Po River waters along the Italian coastline down to the Otranto Strait. Figure 4.6 shows two snapshots of the Adriatic chlorophyll_a surface fields (28 and 30 September), on which the cross-basin transport of freshened Po River waters may be seen (high chlorophyll concentration) directed along the Palagruza Sill towards the ITHACA polygon. Although the concentration rapidly decreased due to mixing of these waters with the EAC, a small fraction entered ITHACA polygon between Susac and Lastovo islands, and it was shifted towards the island of Vis. In fact, the whole filament of the WAC waters propagated towards the northwest, presumably being a result of strong sirocco forcing which prevailed in preceding days and thus pushed the surface waters northwestward throughout the Palagruza Sill area.

Finally, T-S diagram of all ITHACA cruises (Figure 4.7) puts temperature and salinity measurements in the context of average ambient characteristics. In particular, deep water masses can be detected near the bottom, especially during the February 2006 cruise. Three of four major water masses can be found there: LIW, Middle Adriatic Deep Water – MadW, and South Adriatic Deep Water – SadW (North Adriatic Dense Water – NAdW – is usually flowing along the western shelf and filling the north Adriatic and Jabuka Pit; see Vilibic et al., 2004). Apart from deep water masses, vertical homogeneity in salinity can be found in the upper layer for all cruises except for June 2006. As already mentioned, rather low salinity appeared at the section, without a clue which may be used for the detection of water source. However, other collected data (ADCP, thermistor chain) may enable an explanation to be arrived at; intercomparison of various data sets is planned for the third project year.

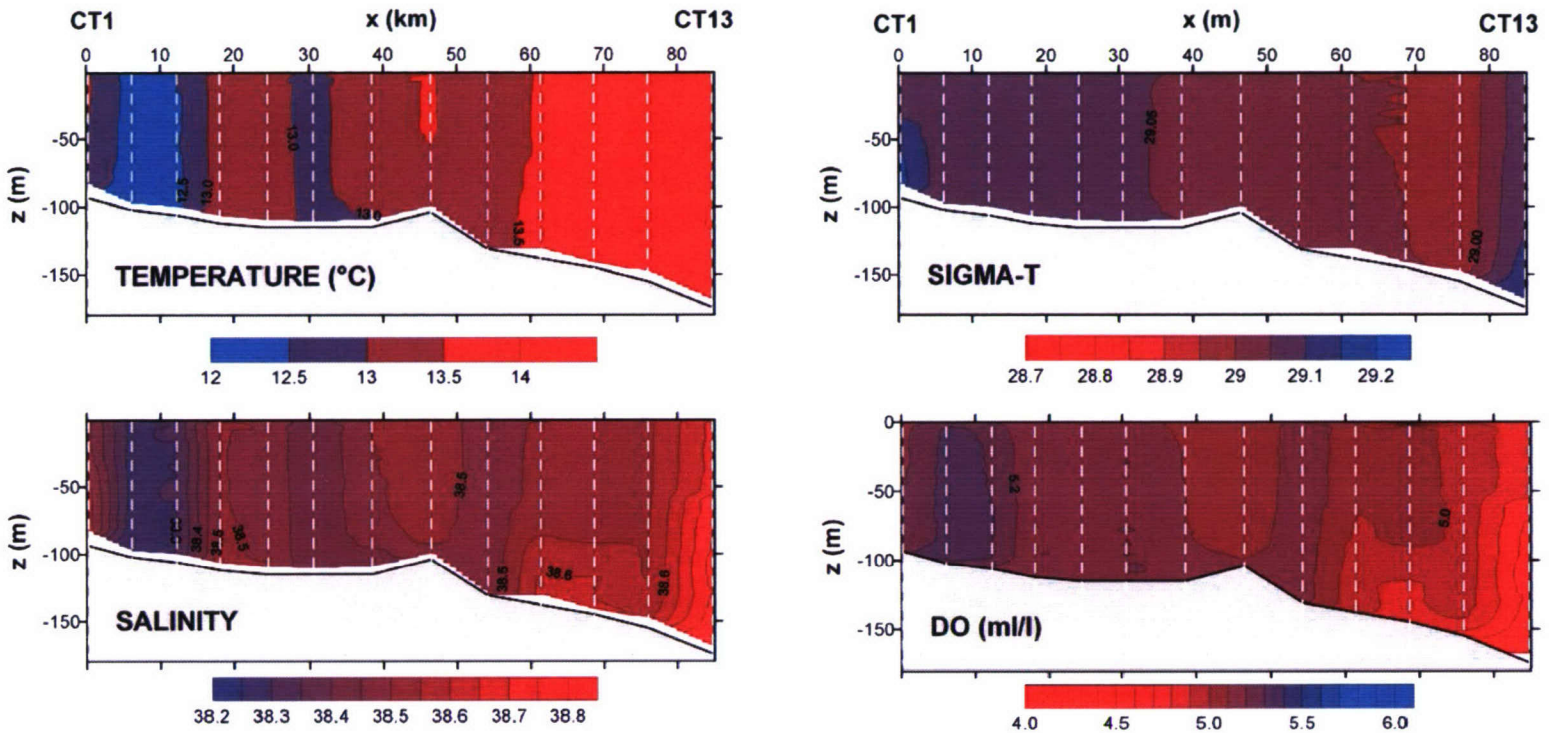

Figure 4.1 Vertical profiles of temperature, salinity, sigma-t and dissolved oxygen measured on 14/15 February 2006.

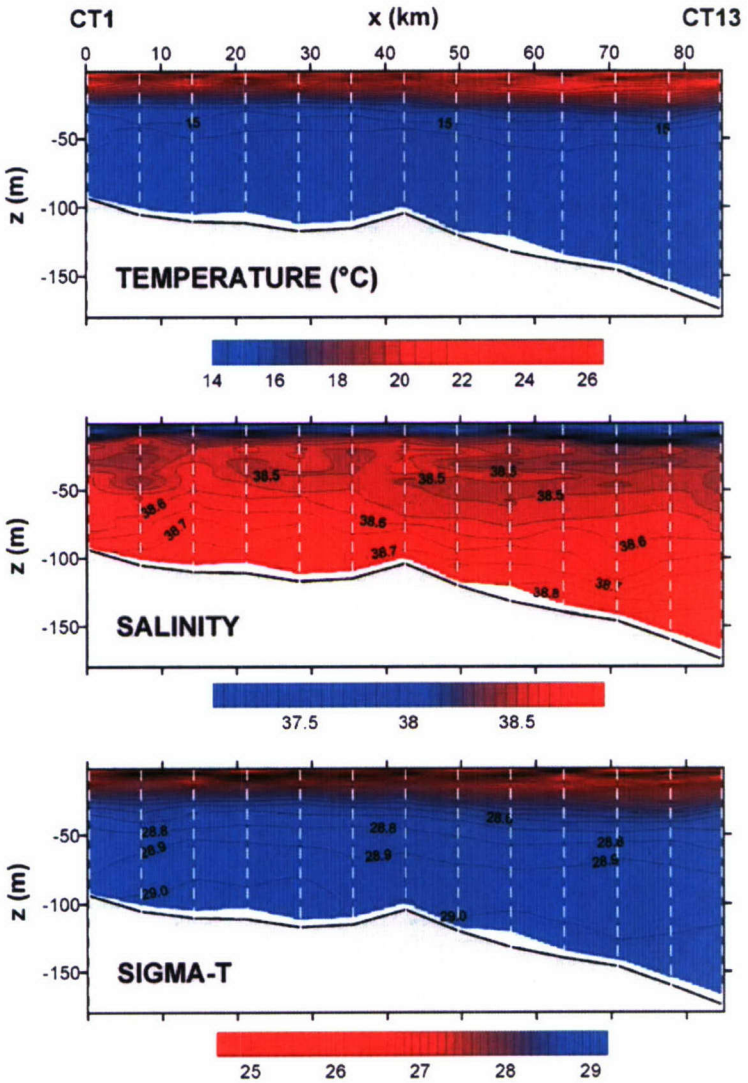

Figure 4.2 Vertical profiles of temperature, salinity and sigma-t measured on 26 June 2006.

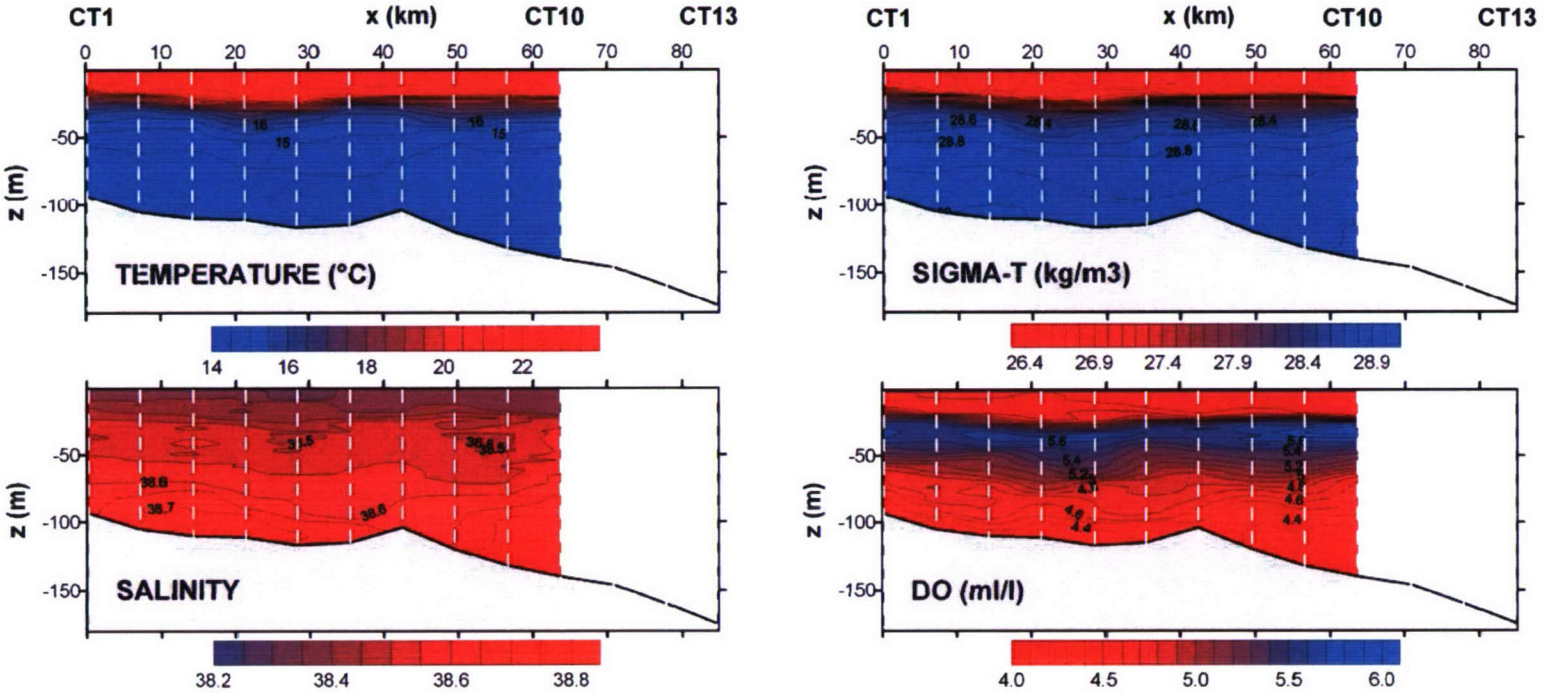

Figure 4.3 Vertical profiles of temperature, salinity, sigma-t and dissolved oxygen measured on 20/21 September 2006.

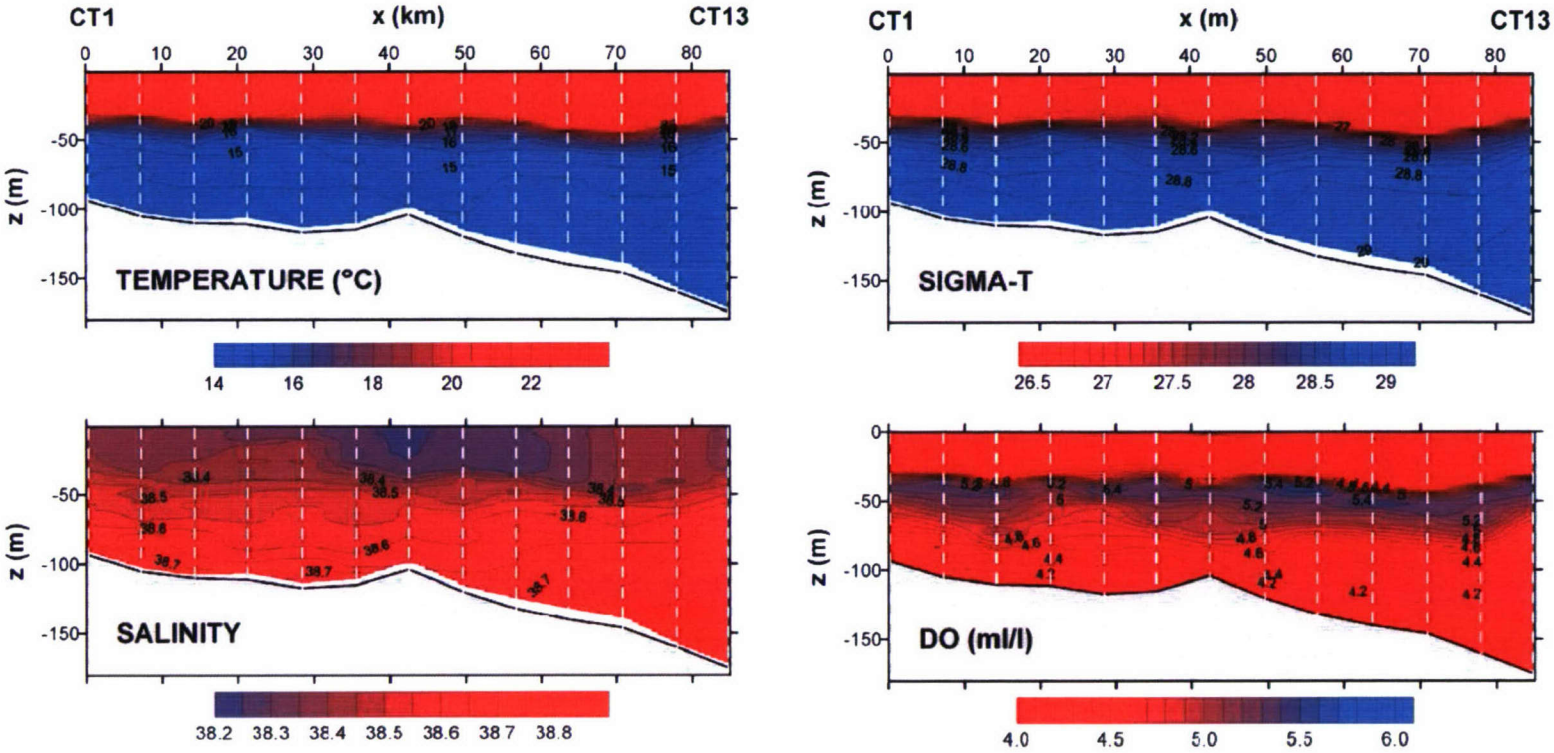

Figure 4.4 Vertical profiles of temperature, salinity, sigma-t and dissolved oxygen measured on 28 September 2006.

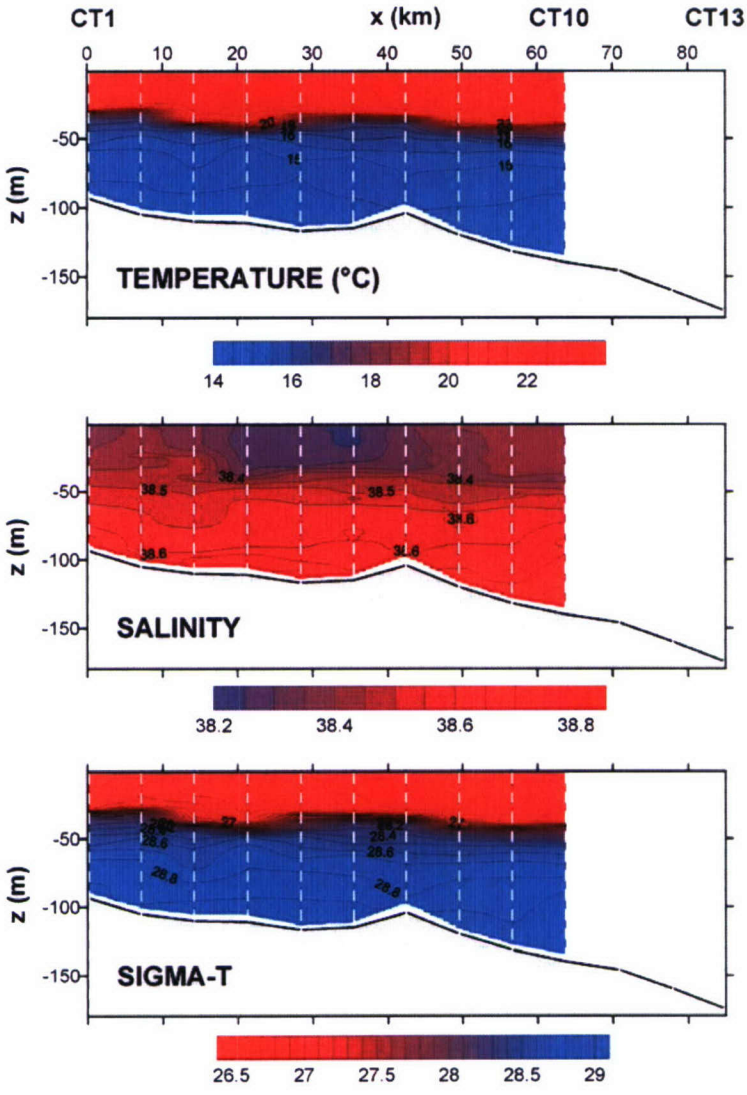

Figure 4.5 Vertical profiles of temperature, salinity and sigma-t measured on 29/30 September 2006.

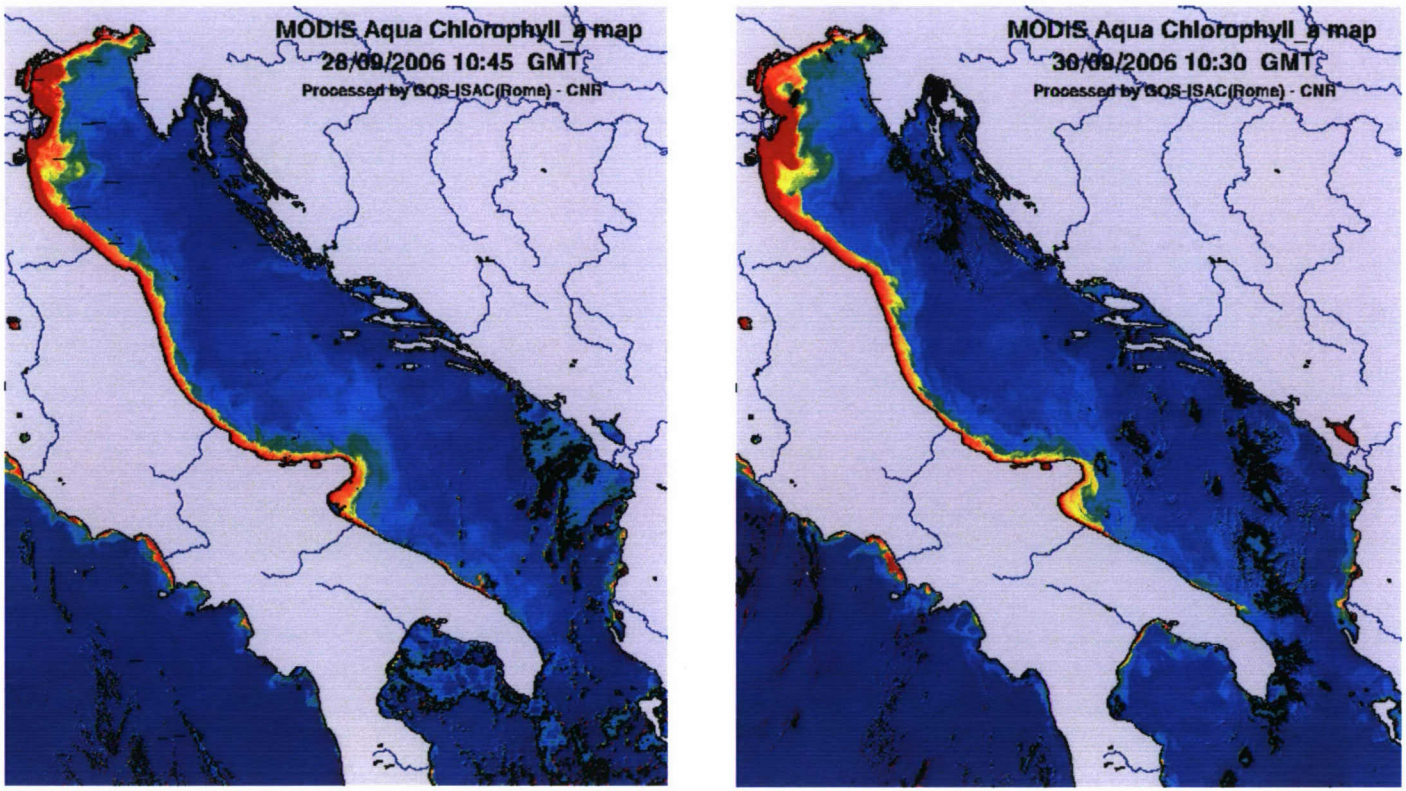

Figure 4.6 MODIS chlorophyll_a satellite images of the Adriatic Sea on 28 and 30 September 2006 (courtesy of GOS-ISAC, Rome).

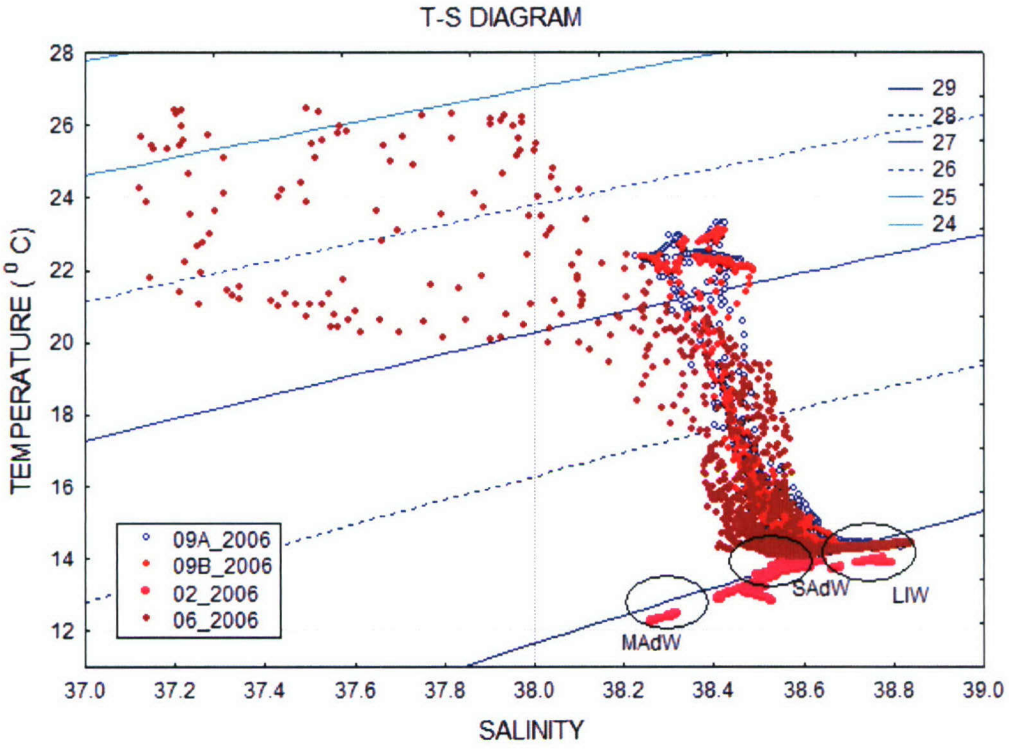

Figure 4.7 T-S diagram obtained for all ITHACA CTD cruises. Characteristic values for the deep Adriatic water masses (MAdW, SAdW, LIW) are shown too (taken from Vilibic and Orlic, 2001).

4.3. Internal waves

A preliminary analysis of baroclinic oscillations and internal waves, in particular of internal tides, will be attempted through CTD transects (Figure 4.8 to Figure 4.11) zoomed in the first 60 m. In addition, a simple two-layer modeling approach will be applied in order to quantify some processes, which presumably occur in the area. The latter will be based on the zero-level approximation, which includes (i) shallow-water equations (e.g. Cushman-Roisin, 1994) with two homogeneous layers, (ii) flat constant-depth bottom, and (iii) internal waves being progressive and having constant velocity. The velocity of linear internal waves V_{it} in the two-layer homogeneous fluid equals:

$$V_{it} = \sqrt{GH}\ ,\ G = g\varepsilon\frac{h}{H+h},\quad \varepsilon = 1-\frac{\rho_h}{\rho_H},$$

where ρ_h and ρ_H are mean densities of the surface and bottom layers having the respective thicknesses h and H, while g is the acceleration due to gravity (9.81 m/s^2).

Table 4.2 gives the wavelengths estimated by assuming that the oscillations are diurnal internal tides (period of 24 h) as suspected from the literature (Mihanovic, 2005; Mihanovic et al., 2006). Average depth is set to 120 m, while the depths h and H are roughly estimated from the CTD sections, associating the pycnocline depth with the largest vertical density gradients. The same estimate is done by examination of wave-like structures, which may be observed in the sections (Table 4.3). The sampling of the progressive waves was undertaken in time, so the Galileo's coordinate transformations should be included in the estimates. This is done again by assuming that internal oscillations are in fact diurnal internal waves.

One may see that fairly good matching between theoretical and empirical internal wave parameters is reached during neap tides. However, a large difference (more than double) appears during spring tides, leading to the conclusion that these waves are not internal diurnal tides, but possibly semidiurnal tides or a different baroclinic process that is more pronounced at the time. In fact, a coupling of different internal tides may occur, but it is not possible to precisely extract the tides from CTD sections only. In addition to both diurnal and semidiurnal internal tides, the observed wave-like structures in CTD data may be consequence of internal Adriatic seiche (21.2 h, Vilibic, 2006) generated at the shelf break, as barotropic currents were observed and modeled to be quite strong in the area (Leder and Orlic, 2004). Also, inertial oscillation (period of 17.6 h) may be visible in the hydrographic sections. Consequently, true classification of these internal waves should result from a simultaneous analysis of CTD, thermistor and ADCP data, which is planned for the last year of ITHACA project.

Table 4.2 Theoretical wavelength ($\lambda_{it,t}$) and velocity ($V_{it,t}$) of internal waves, computed via the two-layer model and assuming that they are diurnal internal tides (period of 24 h). The depths h and H and densities ρ_h and ρ_H are estimated from CTD sections.

Cruise	h	H	ρ_h	ρ_H	$V_{it,t}$	$\lambda_{it,t}$
26 Jun 2006	8	112	25.2	28.8	0.51 m/s	43.7 km
20/21 Sep 2006	24	96	26.6	28.8	0.63 m/s	54.8 km
28 Sep 2006	38	82	26.7	28.8	0.72 m/s	62.3 km
29/30 Sep 2006	38	82	26.7	28.8	0.72 m/s	62.3 km

Table 4.3 Empirical wavelength ($\lambda_{it,e}$) and velocity ($V_{it,e}$) of internal waves, computed from CTD sections assuming that they are influenced by diurnal internal tides (period of 24 h). λ_{CTD} is the non-transformed wavelength estimated from the transects, Δt is the time needed for the sampling of one internal wave, while A is the tentatively estimated wave amplitude.

Cruise	λ_{CTD}	Δt	A (tent.)	Tides	$V_{it,e}$	$\lambda_{it,e}$
26 Jun 2006	35 km	5 h	2-4 m	neap	0.50 m/s	42.3 km
20/21 Sep 2006	50 km	6 h	7-8 m	neap	0.72 m/s	62.5 km
28 Sep 2006	28 km	-4 h	4/12 m	spring	0.27 m/s	23.3 km
29/30 Sep 2006	37 km	-5 h	8-10 m	spring	0.34 m/s	29.3 km

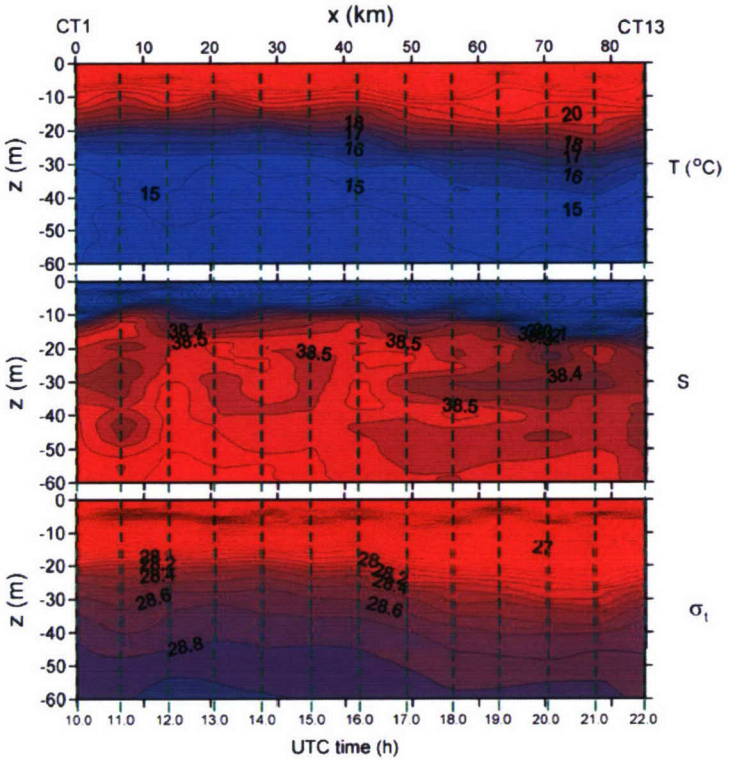

Figure 4.8 Vertical profiles of temperature, salinity and sigma-t measured on 26 June 2006 in the first 60 m. CTD sampling times are indicated too.

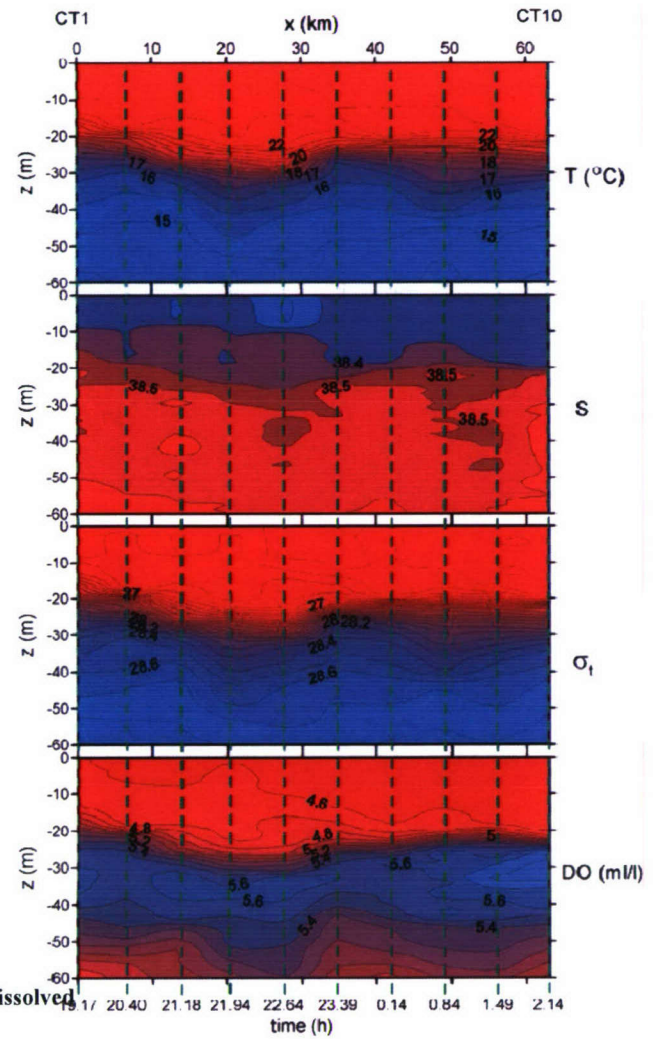

Figure 4.9 The same as Figure 4.8, but with dissolved oxygen and on 20/21 September 2006.

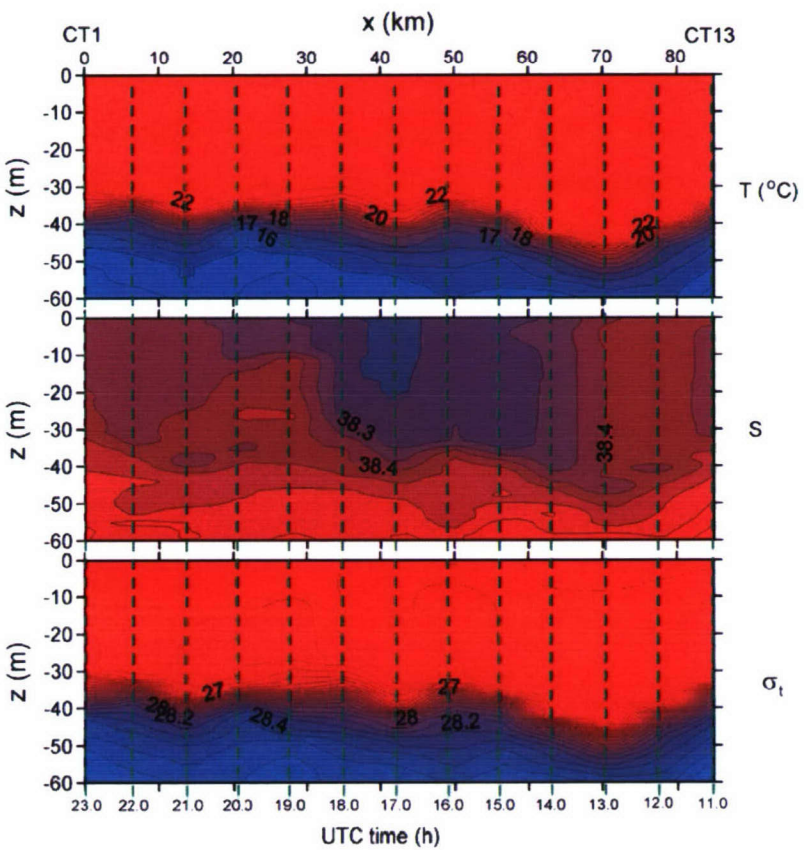

Figure 4.10 Vertical profiles of temperature, salinity and sigma-t measured on 28 September 2006 in the first 60 m. CTD sampling times are indicated too.

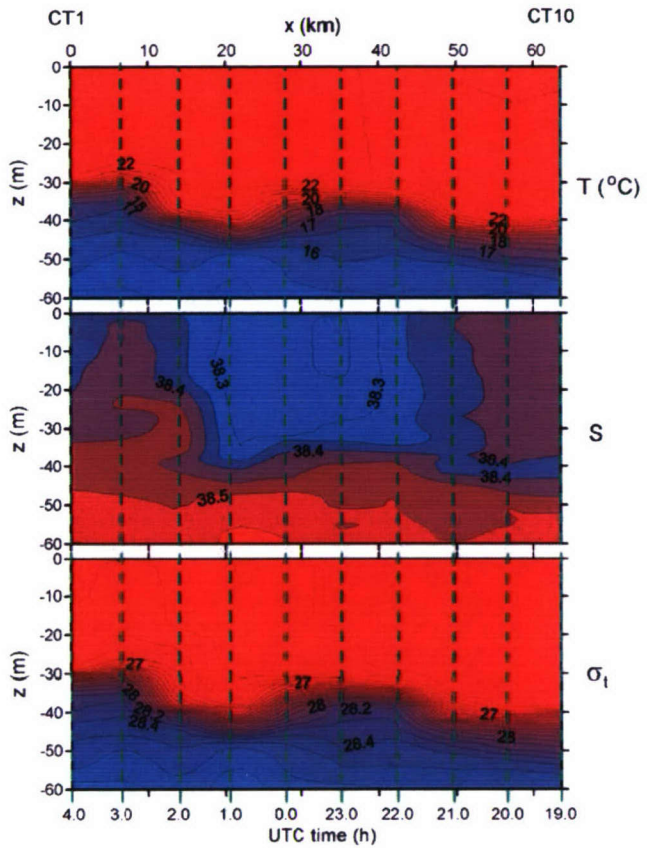

Figure 4.11 Vertical profiles of temperature, salinity and sigma-t measured on 29/30 September 2006 in the first 60 m. CTD sampling times are indicated too

5. Thermistor time series

One of the objectives of ITHACA project was to investigate diurnal internal tides, their generation at the Adriatic shelf break, propagation across the Palagruza Sill and dependence on stratification and currents in the area (Orlic et al., 2005). Besides optical, CTD and ADCP measurements, the work comprised thermistor measurements in the Adriatic shelf break area.

5.1. Data acquisition

Temperature measurements were carried out between 7 March and 30 September 2006 at the islands of Bisevo, Susac and Lastovo using thermistors (Figure 5.1) deployed on steep underwater cliffs opened to the southeast (Figure 5.2 – underwater profiles of cliffs at Bisevo, Susac and Lastovo). The positions of these cliffs are indicated in Figure 3.1, and the exact coordinates are given in Table 5.1. Previous long-term temperature measurements from Lastovo (Cape Struga) showed that strong diurnal and inertial oscillations develop during stratified season (Mihanovic, 2005; Mihanovic et al., 2006). Intense diurnal temperature oscillations that lasted for several days were observed at 22 m depth in June 2001 and 15 m depth during July-August 2001. Detailed analysis showed that during July-August 2001 oscillations were correlated with diurnal sea-level changes and diurnal wind variations. However, pronounced diurnal temperature oscillations may also occur at a time of rather insignificant wind forcing, as documented by data collected in June 2001, when diurnal sea level changes achieved annual maxima. The most significant diurnal thermocline oscillations also occurred in June 2001. They were in phase with sea level variations and the range of diurnal sea level oscillations was close to 19 cm, whereas the range of resulting thermocline variability was about 5.4 m.

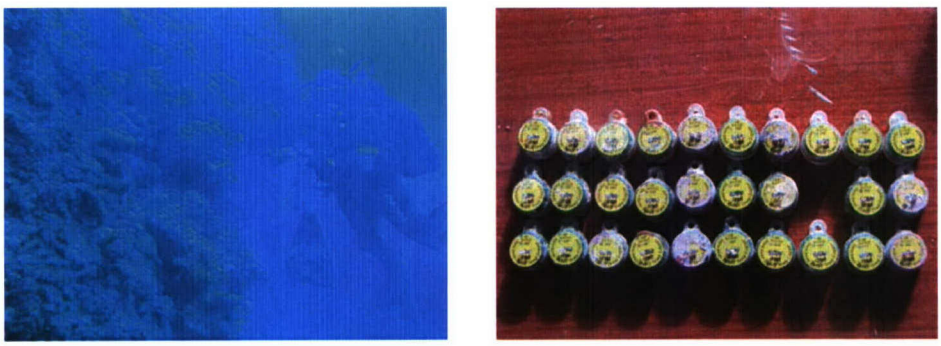

Figure 5.1 TidbiT thermistors while being deployed (left) and after recovery (right).

Table 5.1 Coordinates of the locations at which thermistor sensors were attached to the submarine cliffs opened to the southeast (WGS 84).

Station	φ	λ
Bisevo	42° 57.312' N	16° 00.261' E
Susac	42° 44.925' N	16° 29.545' E
Lastovo	42° 43.432' N	16° 53.040' E

In the present study TidbiT type thermistors were used, with 3 x 10 equidistant sensors distributed between the depths of 4 and 40 m (4 m vertical resolution). The instruments recorded the sea temperature with 10 min resolution and an accuracy of ±0.2°C at 21°C. The experiment was very successful, with 29 sensors being recovered, and only one lost at the depth of 32 m at Susac island. After the instruments were recovered, the divers performing the task informed us that some of the sensors at Bisevo island were found at different depths than originally positioned. A simple verification was performed, in order to check the new depths and time coordinate corresponding to the depth change. Figure 5.3 shows ten-day running average of sea temperature data measured at Bisevo, advancing in time with one-day step. There were two suspicious sensors, 16 m sensor which was found at 23 m and 28 m sensor recovered at 29 m. It was almost impossible to determine the exact time of vertical shift of 28 m sensor, while the 16 m sensor fell off the original position in the middle of April 2006, when the sea was almost homogeneous. The same procedure showed that the sensors recovered at Susac and Lastovo were positioned at designed depths throughout the period of measurement.

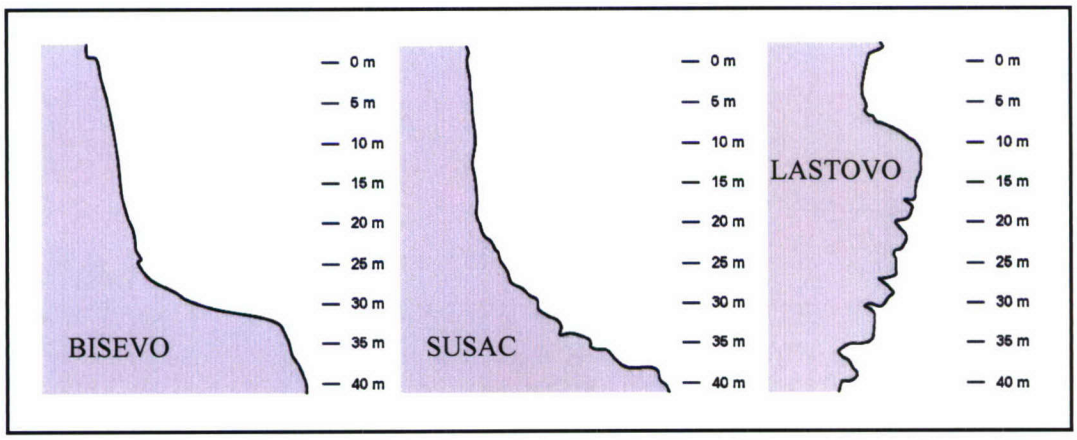

Figure 5.2 Underwater profiles of cliffs located at Bisevo, Susac and Lastovo islands. The profiles at Bisevo and Susac were drawn by Andjelko Novosel and adapted for this report. The profile at Lastovo (Cape Struga) is based on Figure 2 from Novosel et al. (2004).

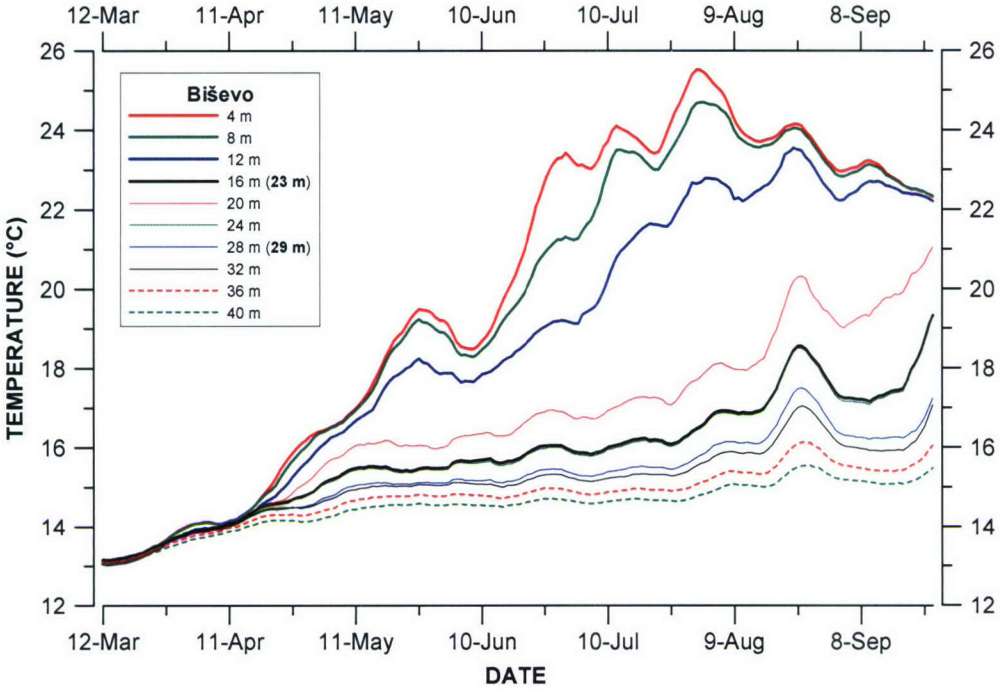

Figure 5.3 Ten-day running average of sea temperature data measured at Bisevo, advancing in time with one-day step; it was used to verify the change of depths of sensors located at 16 and 28 m.

5.2. Comparison between TidbiT measurements at Cape Struga and Aanderaa thermistor string measurements off Cape Struga

During DART06b cruise (*R/V Alliance*) in August 2006 four thermistor strings were deployed in the region, one of them about 0.75 km to the SE of Lastovo (Cape Struga). Thermistor string TCH2 had the following coordinates: φ = 42° 43.101' N; λ = 16° 53.373' E. An Aanderaa thermistor string was used, with 11 equidistant sensors between the depths of 23 and 73 m (5 m vertical resolution). Temperature was recorded every 5 min with an accuracy of ±0.1°C. The comparison between 28 m sensors from Lastovo (Cape Struga) and TCH2 is shown in Figure 5.4, for the period extending from 17 August to 11 September 2006. The linear fit coefficient of determination (r-squared) between these two time series was equal to 0.867. The correspondence is best evident when temperature profiles between 23 and 40 m (overlapping depths) are investigated (Figure 5.5). Intense temperature changes recorded at the end of August 2006 and during last two days of overlying time series are very similar on both locations, confirming that cliff measurements are representative for the region close to the islands.

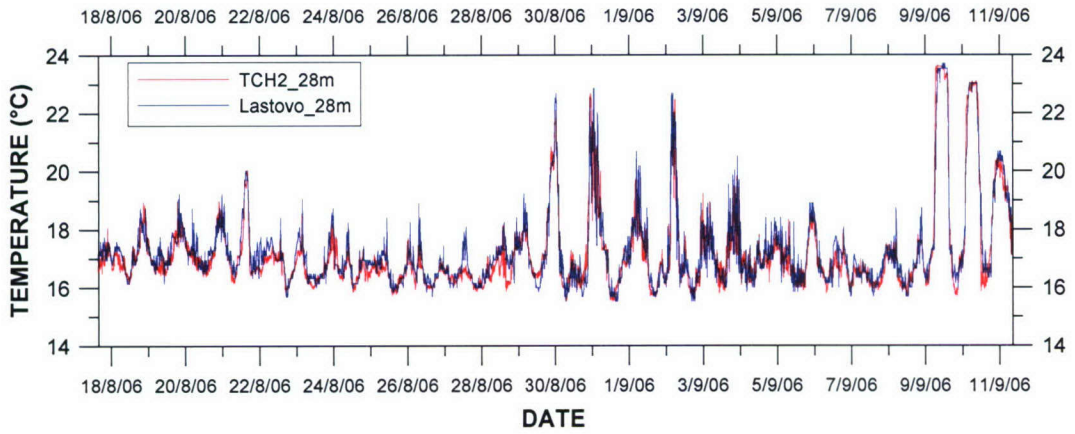

Figure 5.4 Sea temperature at the depth of 28 m as measured by TidbiT thermistor sensor (Lastovo) and Aanderaa thermistor string (station TCH2) for the interval between 17 August and 11 September 2006.

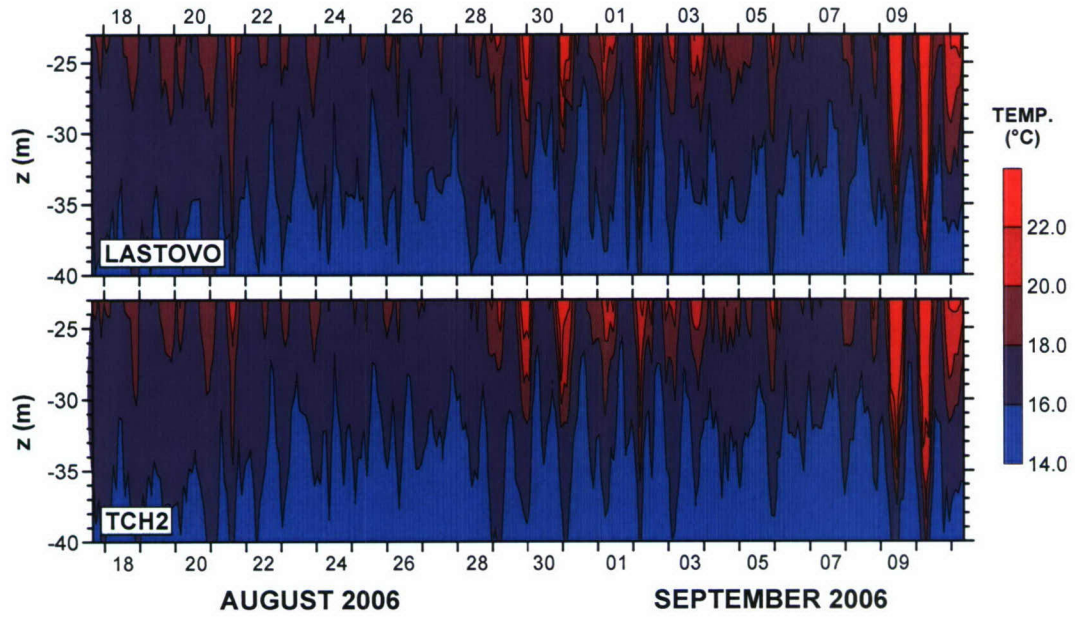

Figure 5.5 Vertical profiles of sea temperature between 23 and 40 m (overlapping depths) at Lastovo (Cape Struga) and station TCH2 for the interval between 17 August and 11 September 2006.

5.3. Stationary spectral analysis of thermistor data collected at Bisevo, Susac and Lastovo

The first step in the analysis of temperature data was a stationary spectral analysis performed by using Welch's method (Welch, 1967) at three island locations. It enabled determination of the most energetic temperature oscillations during the period of research. The results are presented as contours in Figure 5.6 and separately in Figure 5.7 to Figure 5.9. Vertical profiles of power spectral density show that diurnal temperature variations were particularly strong at Lastovo, whilst inertial oscillations were significant at all three locations. Strong diurnal temperature oscillations at Lastovo were discussed in previous study of long-term temperature measurements at Cape Struga (Mihanovic et al., 2006). Inertial oscillations are also a well-known feature of the Adriatic under stratified conditions (e.g., Orlic, 1987). Diurnal variations were noted at all depths at Lastovo, and down to 12 m at Bisevo and Susac. Inertial oscillations at Bisevo and Lastovo were significant between 8 and 40 m, and from 12 to 40 m at Susac. Moreover, semidiurnal oscillations seemed to exist at Bisevo between 32 and 40 m, close to the surface at Susac (down to 12 m) and between 8 and 20 m at Lastovo. There is also a noteworthy 10.2 h oscillation at Susac (36 and 40 m) and an 8 h oscillation between 8 and 20 m at Lastovo.

More detailed investigation of energy distribution during the stratified season will be carried out in the next section of this chapter, by using wavelet analysis. It will point out exact intervals in which significant diurnal and inertial oscillations were present, thus enabling more exhaustive analysis of these occurrences.

5.4. Wavelet analysis of thermistor data collected at Bisevo, Susac and Lastovo

Stationary spectral analysis enables a good distinction of energy maxima. However, having time series almost seven months long, it is necessary to apply spectral method that facilitates the study of temporal changes in energy distribution. Therefore, the wavelet spectral analysis was performed, being especially efficient in time-frequency localization of significant oscillations. The choice of non-dimensional frequency equaling 6 results in good time-frequency localization and convenient approximate equality between wavelet scale and respective Fourier frequency (Torrence and Compo, 1998).

Stratified season started in the middle of April 2006, and the data analyzed in this section cover the interval between 16 April and 26 September 2006 (corresponding to the start of the stratification and the end of measurements at Lastovo). It is important to note that the corrected depths at Bisevo also match with this period. Special emphasis was placed on diurnal and inertial oscillations (period around 17.6 h). By extracting wavelet spectra at diurnal and inertial periods at all depths and by normalizing them by the respective variance and significance level so that the confidence level at 95% equals 1, vertical profiles of wavelet spectrum could be presented (Figure 5.10 for diurnal

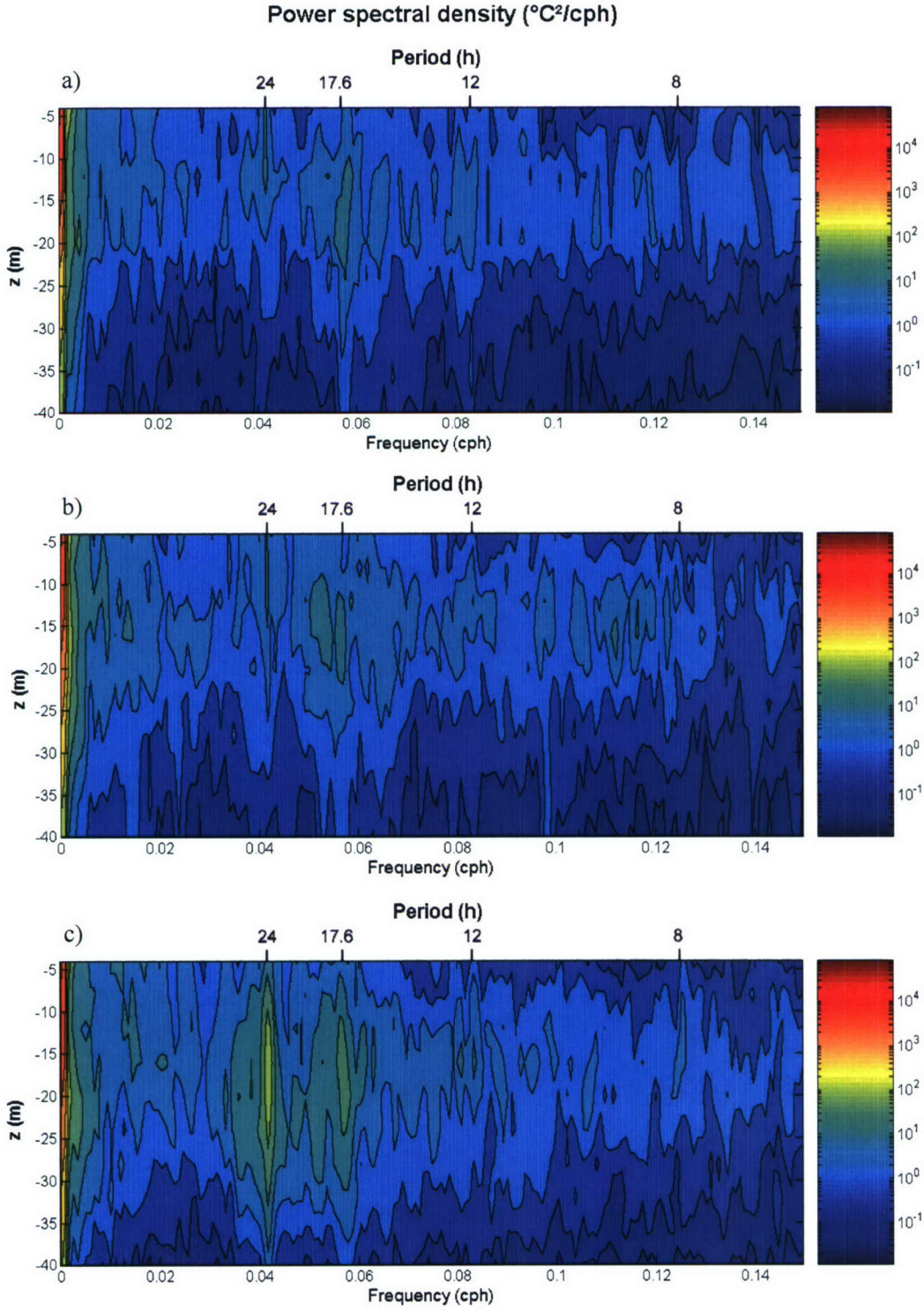

Figure 5.6 Vertical profiles of power spectral density of sea temperature measured at Bisevo, Susac and Lastovo over the period extending from 7 March to 27 September 2006.

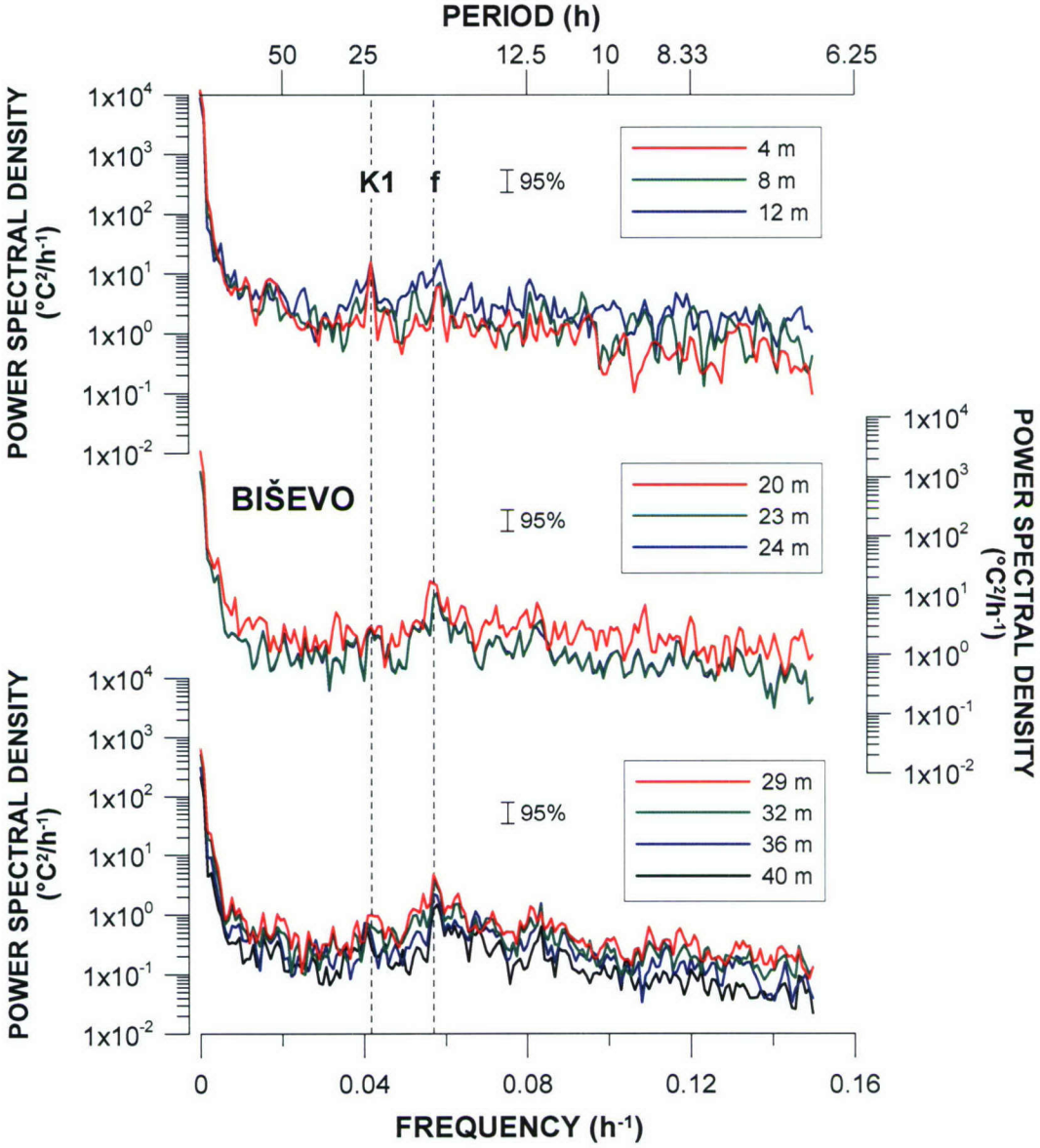

Figure 5.7 Power spectral density of sea temperature measured at Bisevo, for the interval extending from 7 March to 27 September 2006. The corresponding 95% confidence interval is also shown. Dashed lines indicate the K1 tidal period and the local inertial period.

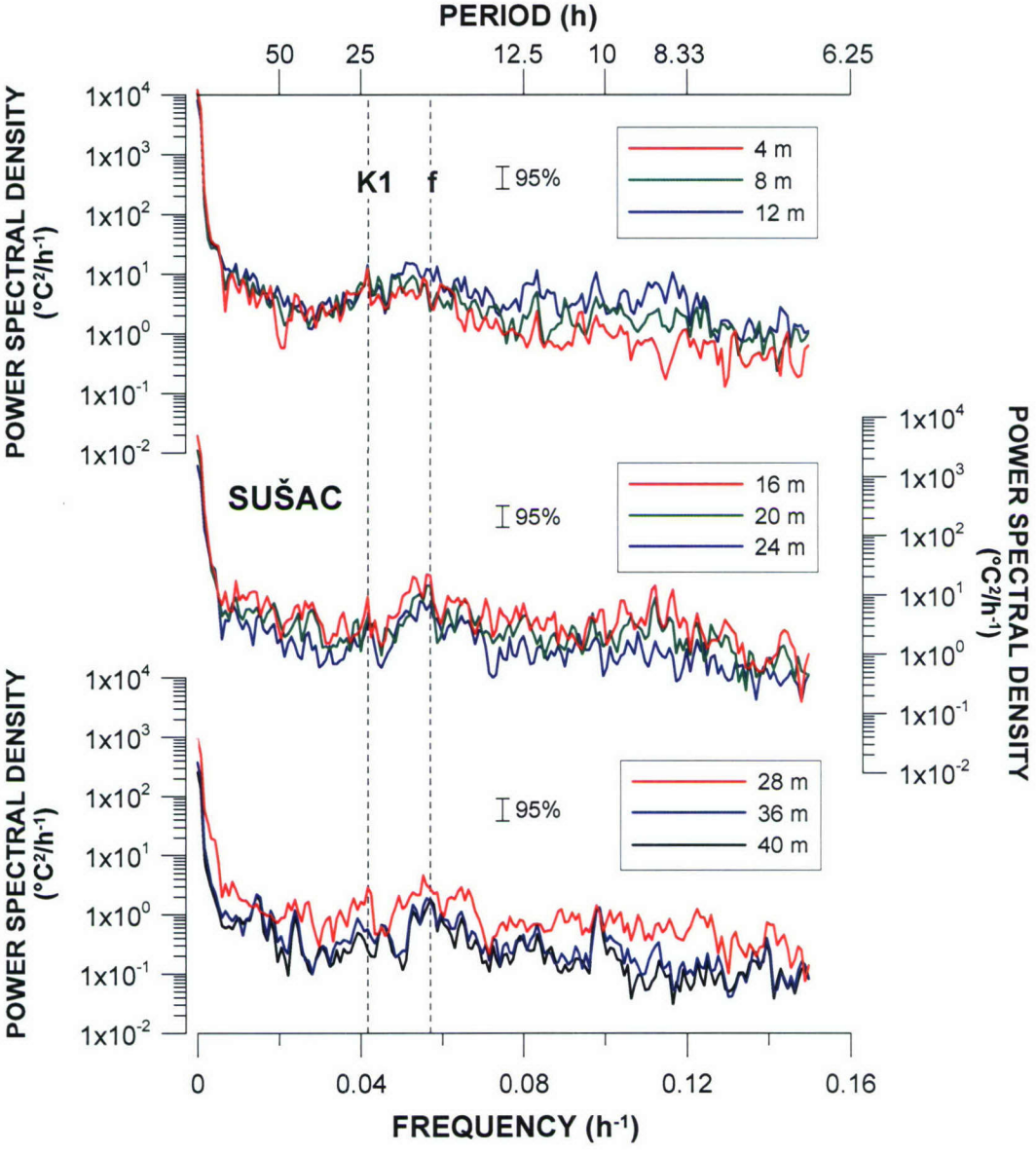

Figure 5.8 Power spectral density of sea temperature measured at Susac, for the interval extending from 7 March to 27 September 2006. The corresponding 95% confidence interval is also shown. Dashed lines indicate the K1 tidal period and the local inertial period.

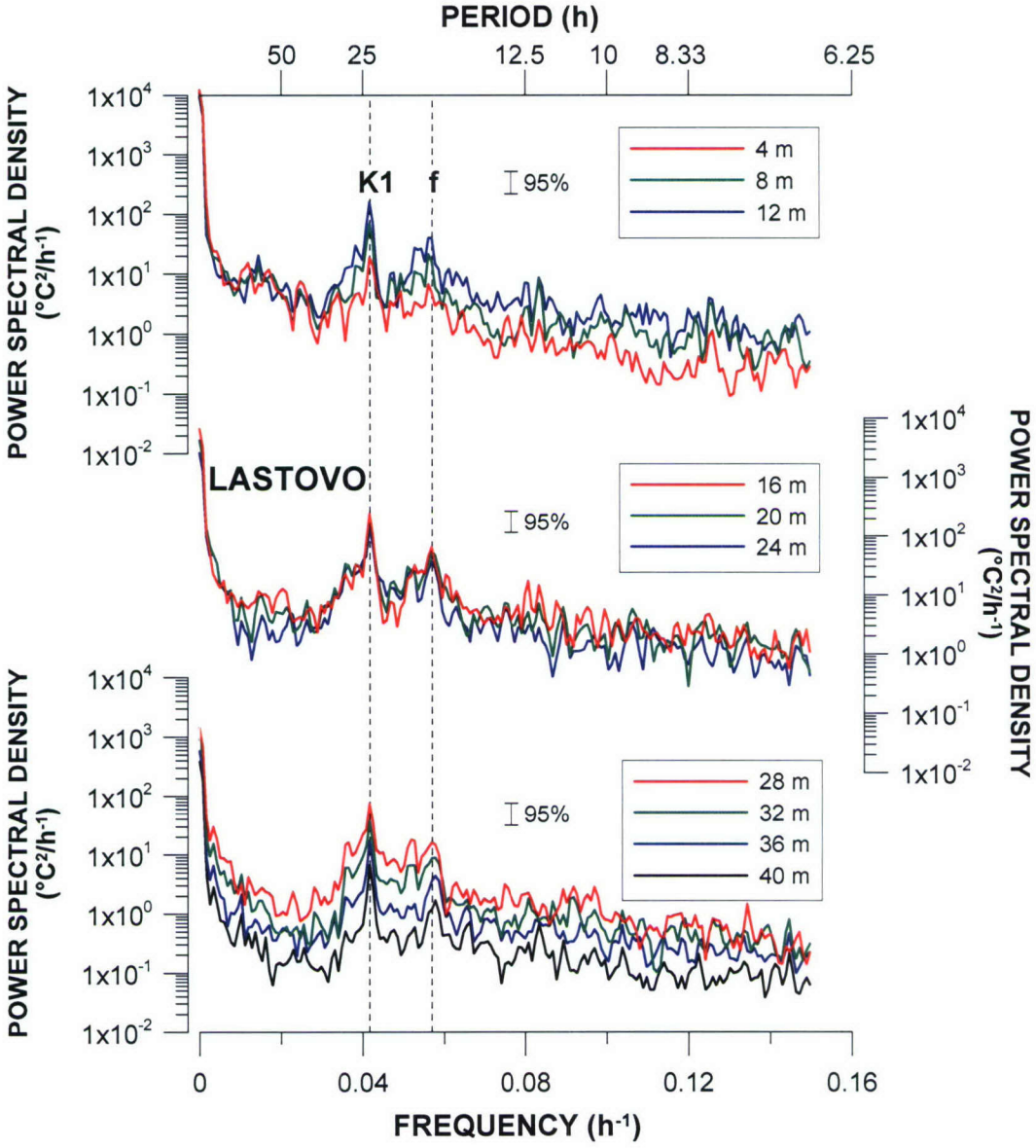

Figure 5.9 Power spectral density of sea temperature measured at Lastovo, for the interval extending from 7 March to 27 September 2006. The corresponding 95% confidence interval is also shown. Dashed lines indicate the K1 tidal period and the local inertial period.

period and Figure 5.11 for inertial period). Red contour encloses regions of greater than 95% confidence (Torrence and Compo, 1998).

Diurnal oscillations were more significant at Lastovo than at the other two locations (Figure 5.10). Important diurnal temperature variations at Bisevo were recorded in the second part of June 2006 and at the beginning of July 2006 in the subsurface layer. In the middle of July 2006 there was a short period of significant diurnal oscillations at the depth of 12 m. The results are somehow similar for Susac, with important diurnal oscillations in the subsurface layer (4 and 8 m depth) in the middle of July 2006. On the other hand, Lastovo had several periods with intense diurnal oscillations between June and September 2006, lasting for several days. To be more precise, these intervals are as follows: the end of June; the beginning, the middle and the end of July; the end of August/the beginning of September; and the middle of September 2006. They correspond to the deepening of the thermocline during summer, so that in June most significant oscillations took place close to the surface (down to 20 m), as also in July when they occurred down to 20 m depth at the beginning and the end of the month. However, the most important period with diurnal oscillations happened in the middle of July 2006 (several diurnal oscillations between 16 and 28 m had a diurnal variation of about 8°C). They were significant throughout the water column between 4 and 40 m. In August 2006 diurnal variations slightly decreased and regained strength at the end of August and during September 2006, at depths larger than 16 m.

Inertial temperature variations had even more intervals with significant energy at all three locations (Figure 5.11). Generally, they were important between June and September 2006. They occurred closer to the surface in June and the first half of July 2006, in the mid-layer at the end of July and in August, and in deeper layers during September 2006 (between 16 and 40 m). However, oscillations recorded at Lastovo were more important with respect to those at Bisevo and Susac. The period with the strongest oscillations was recorded at the end of July and the beginning of August 2006, when the range of inertial oscillations was almost 9°C at Lastovo (at the depth of 16 m). They were also important at Bisevo between 4 and 12 m at the beginning of August (up to 6°C), but not at Susac at the same time, where the largest range was recorded in September 2006 (more than 5°C at 24 m depth).

It has to be emphasized that during episodes of exceptionally strong oscillations, significant energy at an investigated period could mean that the maximum of oscillations was not exactly at that period. That is why significant diurnal oscillations at Bisevo and Susac need to be analyzed more thoroughly to see if they are an artifact of the method or the real result. To provide a more precise insight into time-frequency distribution of normalized energy at chosen depths several examples are going to be given for Bisevo, Susac and Lastovo. For each location two depths were chosen and presented in this report as normalized wavelet energy contours for the periods between 4 and 60 h and the time interval extending from 16 April to 26 September 2006 (Figure 5.12a to Figure 5.14a).

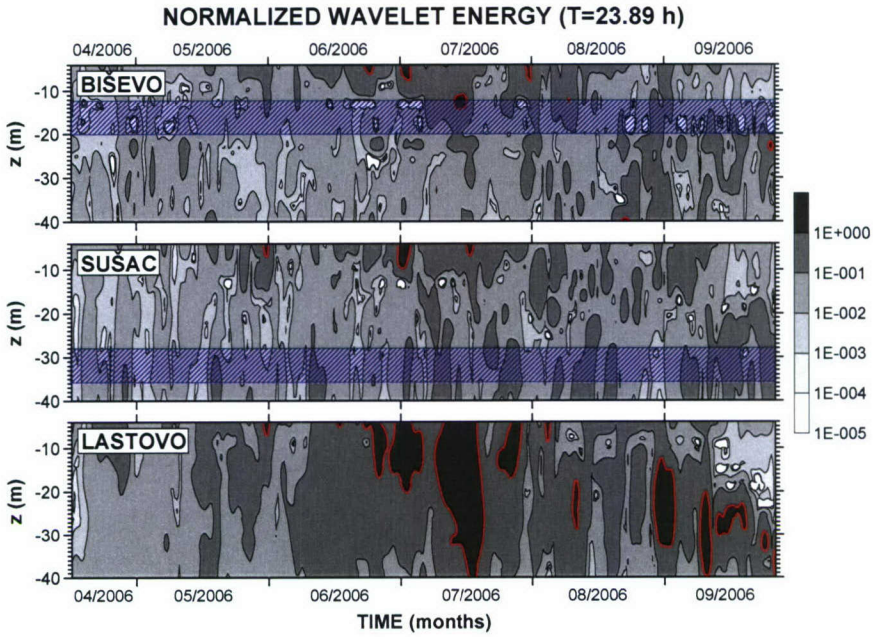

Figure 5.10 Vertical profile of wavelet spectra at Bisevo, Susac and Lastovo, at diurnal period, normalized by the respective variance and significance level so that the confidence level at 95% equals 1. Red contour encloses regions of greater than 95% confidence. Blue areas denote depth intervals that are missing in the 4 m vertical resolution setting (missing depth ± 4 m).

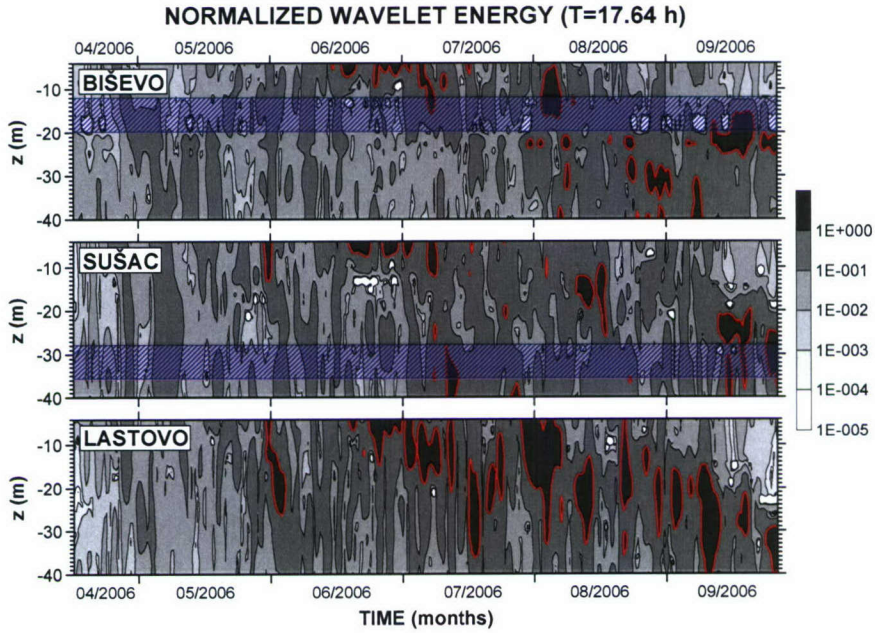

Figure 5.11 Vertical profile of wavelet spectra at Bisevo, Susac and Lastovo, at inertial period, normalized by the respective variance and significance level so that the confidence level at 95% equals 1. Red contour encloses regions of greater than 95% confidence. Blue areas denote depth intervals that are missing in the 4 m vertical resolution setting (missing depth ± 4 m).

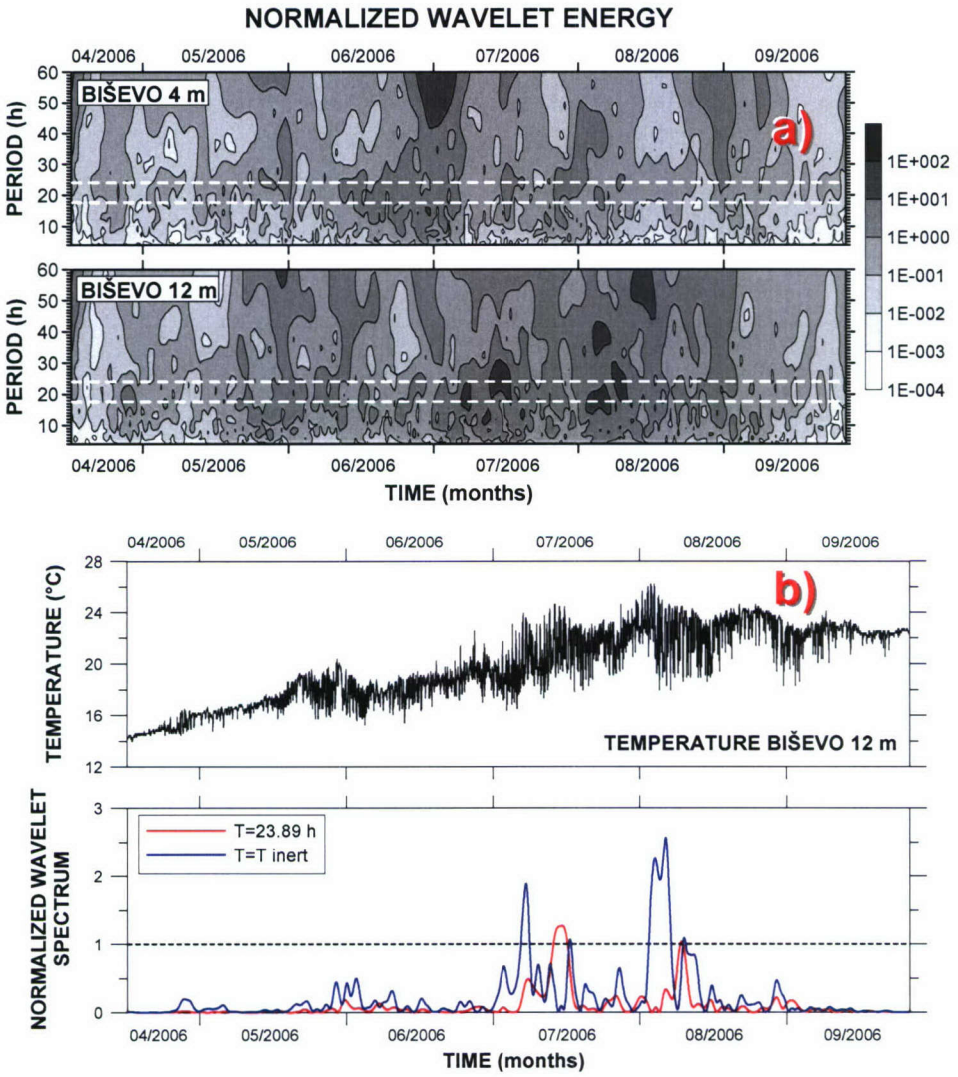

Figure 5.12 a) Wavelet spectrum of sea temperature measured at 4 and 12 m at Bisevo, for the interval extending from 16 April to 26 September 2006. The spectrum is normalized by the respective variance. Dashed lines denote the K1 and inertial periods. b) Sea temperature measured at 12 m depth at Bisevo and respective wavelet spectra at the K1 tidal period and inertial period for the interval extending from 16 April to 26 September 2006. The spectra are normalized by the respective variances and significance levels, so that the confidence levels at 95% equal 1.

In addition, time series of temperature data and their corresponding normalized wavelet spectra at diurnal and inertial period are also presented for a selected depth (Figure 5.12b to Figure 5.14b). Significance levels depend on the length of time series and their variance. As a result, when shorter intervals are analyzed, oscillations that seem to be insignificant for overall series can turn out to be significant for that specific period.

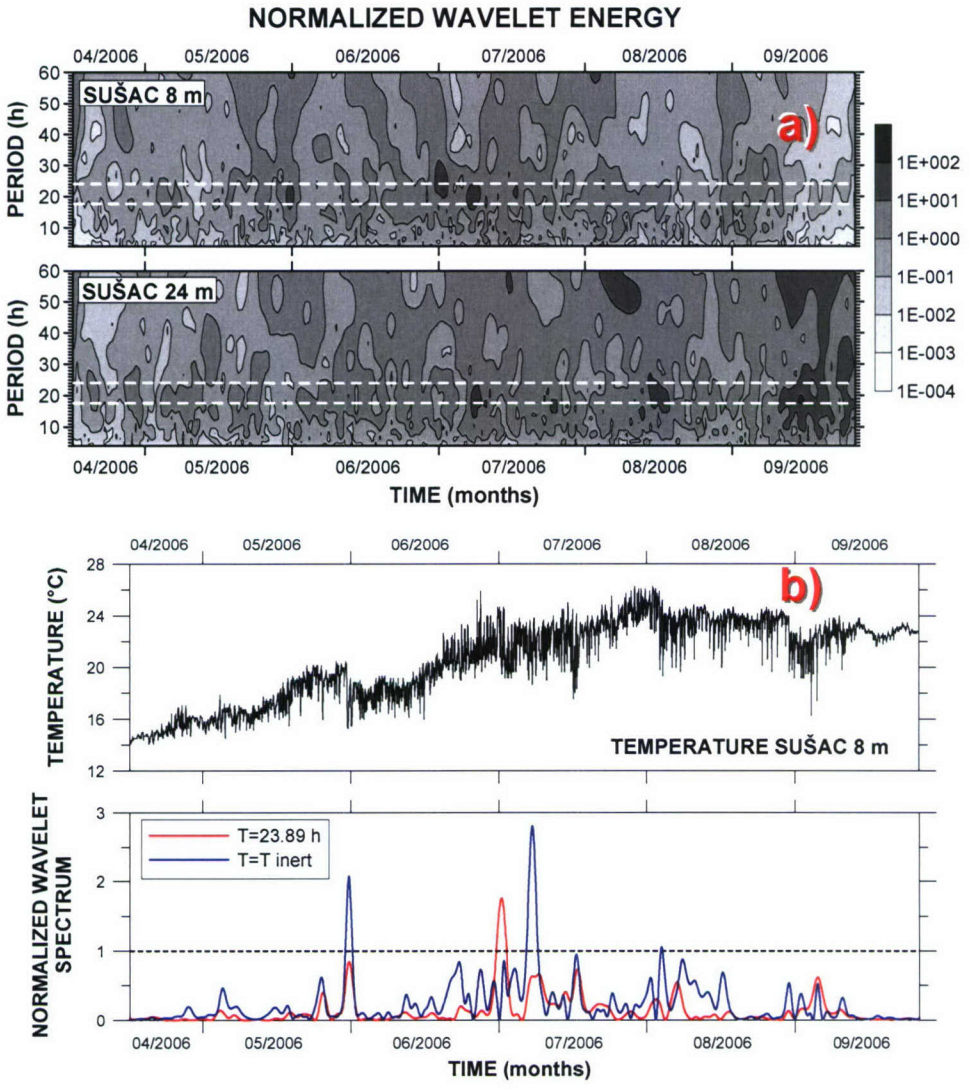

Figure 5.13 a) Wavelet spectrum of sea temperature measured at 8 and 24 m at Susac, for the interval extending from 16 April to 26 September 2006. The spectrum is normalized by the respective variance. Dashed lines denote the K1 and inertial periods. b) Sea temperature measured at 8 m depth at Susac and respective wavelet spectra at the K1 tidal period and inertial period for the interval extending from 16 April to 26 September 2006. The spectra are normalized by the respective variances and significance levels, so that the confidence levels at 95% equal 1.

Time series of wavelet spectra enable precise determination of intervals with significant temperature oscillations at a chosen period. For instance, the 12 m depth wavelet spectrum at Bisevo shows that in the middle of July 2006 diurnal oscillations were significant, whereas inertial oscillations had their maxima at the beginning of July and the beginning of August 2006 (Figure 5.12b).

On the other hand, wavelet spectra at the depth of 8 m at Susac reveal significant diurnal variations at the beginning of July 2006 and important inertial oscillations

evidenced at the beginning of June and in the first half of July 2006 (Figure 5.13b). Still, inertial oscillations were strongest in the middle of September at 24 m depth (Figure 5.13a).

Diurnal and inertial temperature oscillations were strongest at Lastovo. As examples, wavelet spectra at 16 and 24 m together with time series and related wavelet spectra at diurnal and inertial period at 24 m depth are given in Figure 5.14. Two intervals with significant diurnal oscillations can be observed, one in the middle of July 2006, and the other at the end of August/the beginning of September 2006, more pronounced at 24 m depth. Yet wavelet analysis shows that this second maximum was positioned around 27 h. Even stationary spectral analysis of sea temperature at the depth of 28 m at two nearby locations (Cape Struga and TCH2 station) for overlapping period between 17 August and 11 September 2006 confirms this result, with wide energy maximum having peaks at 24 and 28 h (Figure 5.15). That is why the correlation between sea temperature data and sea-level changes and wind variations is to be especially important, in order to distinguish between intervals dominated by internal tidal oscillations and periods with strong diurnal wind-related variability.

Diurnal temperature variations in the middle of July at 24 m at Lastovo were so important that they "eclipsed" other significant intervals with important but less vigorous 24 h oscillations. That is why some other periods (e.g. June 2006) will have to be analyzed separately in further analysis, in order to correlate them with two maxima of diurnal sea-level oscillations that occur in June. Inertial oscillations at 24 m were important around 10 August 2006, in addition to the beginning and the middle of September 2006 (the most energetic interval). When diurnal and inertial oscillations were particularly energetic, energy maxima were recorded at a wider period range, so that in the middle of July 2006 inertial oscillations seemed to be important as a result of broader energy maximum around diurnal period (Figure 5.14b).

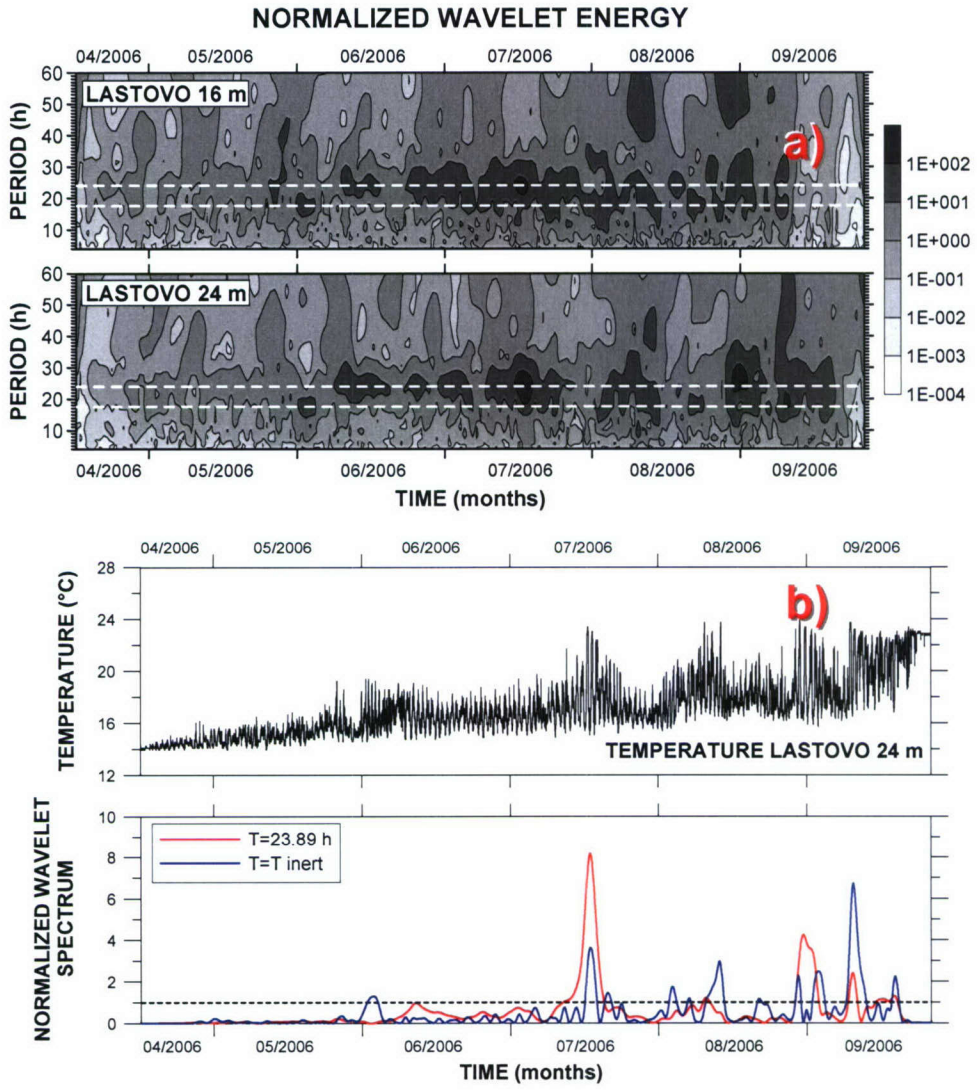

Figure 5.14 a) Wavelet spectrum of sea temperature measured at 16 and 24 m at Lastovo, for the interval extending from 16 April to 26 September 2006. The spectrum is normalized by the respective variance. Dashed lines denote the K1 and inertial periods. b) Sea temperature measured at 24 m depth at Lastovo and respective wavelet spectra at the K1 tidal period and inertial period for the interval extending from 16 April to 26 September 2006. The spectra are normalized by the respective variances and significance levels, so that the confidence levels at 95% equal 1.

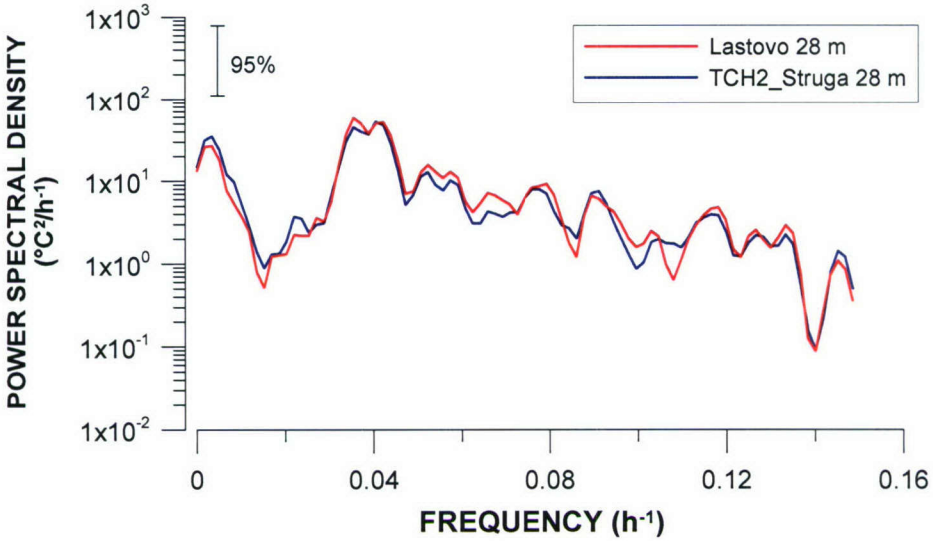

Figure 5.15 Power spectral density of sea temperature measured at 28 m at Lastovo (red) and TCH2 station (blue) for the interval extending from 17 August to 11 September 2006. The corresponding 95% confidence interval is also shown.

6. Results of ADCP measurements

The ITHACA field work comprised ADCP measurements at three stations. These resulted in the first long time series of currents recorded in the area.

6.1. Data acquisition

Sea currents were measured at two stations, ITHACA 1 (IT1) and ITHACA 2 (IT2) (Figure 3.1), between 8 March and 1 September 2006. The measurements were made by 300 kHz Workhorse Sentinel ADCPs, produced by RDI, USA. The ADCPs were placed on the sea bottom within barny frames (Proteco, Italy). The barnys were also equipped with CART releases (Edgatech, USA) to retrieve the equipment at the end of the observation period. The Edgatech command unit model 9300 was used to activate the releases. The deployment of the equipment was made by NATO *R/V Alliance* and the recovery by *R/V Bios* (Figure 6.1). In addition to the measurements made at IT1 and IT2 that were set up especially for the ITHACA experiment, we had at our disposal current measurements at nearby station HR1 (Figure 3.1) of the Institute of Oceanography and Fisheries (IOF), Split. It was equipped with the same type of ADCP as IT1 and IT2, but here it was mounted on a stainless steel frame placed inside a spherical buoy that was developed at IOF (Figure 6.2). The buoy was made of synthetic foam, with two parallel IXEA Sea Shallow Water Acoustic Releases AR701 AE fixed to it. The buoy was anchored by a 150 kg concrete block. In such setting the ADCP was positioned 1.8 m above the sea floor. Station HR1 was deployed on 23 April 2006 and released on 1 September 2006 by *R/V Bios*. During release the sea surface was rough (sea state 3) and, upon sending codes to IXEA releasers, neither the ADCP nor the buoy were found. Fortunately, the ADCP, the buoy and the two releasers, both released, were found by a fisherman on 10 September 2006 about 18 nm to the NW of HR1.

At all the three stations measurements were made with a 15 min sampling interval, in burst mode (60 pings sent continuously during the first minute and stand by mode for the rest of the interval), at a vertical resolution of 3 m. The bottom depth at IT1, IT2 and HR1 was 114, 95 and 105 m, and with approximately upper 6% of water column being contaminated, this yielded 33, 28 and 30 layers, respectively (Table 6.1).

Table 6.1 Location, bottom depth, number of uncontaminated layers and depth of the (center of) the top and bottom layer, at each station.

	Latitude (deg)	*Longitude (deg)*	*Bottom depth (m)*	*No. of layers*	*Top layer (m)*	*Bottom layer (m)*
IT1	49.6615 N	17.1381 E	114	33	12.4	108.4
IT2	42.7508 N	16.6817 E	95	28	8.4	89.4
HR1	43.0000 N	16.3205 E	105	30	11.0	98.0

Figure 6.1 ADCP and pop-up float (left) and barny (right) after recovery.

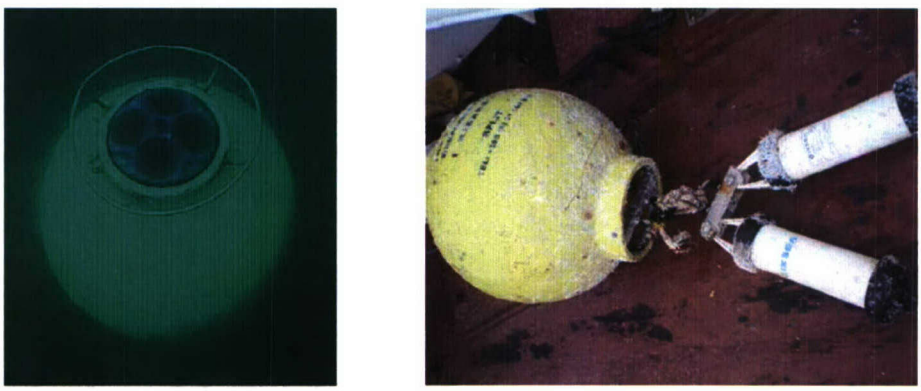

Figure 6.2 Foam buoy with ADCP sentinel in the sea (left) and with releasers on the board of *R/V Bios* (right).

6.2. Main statistical features

Standard deviation ellipses along vertical at each station (Figure 6.3) give an insight into the main features of flow, with blue arrows showing strength and direction of the main current and ellipses giving distribution of standard deviation, with the major axis pointing in the direction of maximum variance.

The mean current is weak (2-3 cm/s) at IT1 and generally westward, veering southwestward with depth. It is strongest at IT2 (5-8 cm/s), northwestward, in the deeper layers turning westward. The mean flow at HR2 is similar (4-8 cm/s) to that at IT2, but for the direction which is northwestward throughout the water column. The current variability is largest at IT2. At all three sites surface currents are very weakly polarized, but become more polarized in the deeper layers, again turning left at IT1 and IT2; at IT2 the flow in lower layers is cross-shore, but at HR1 it maintains alongshore direction.

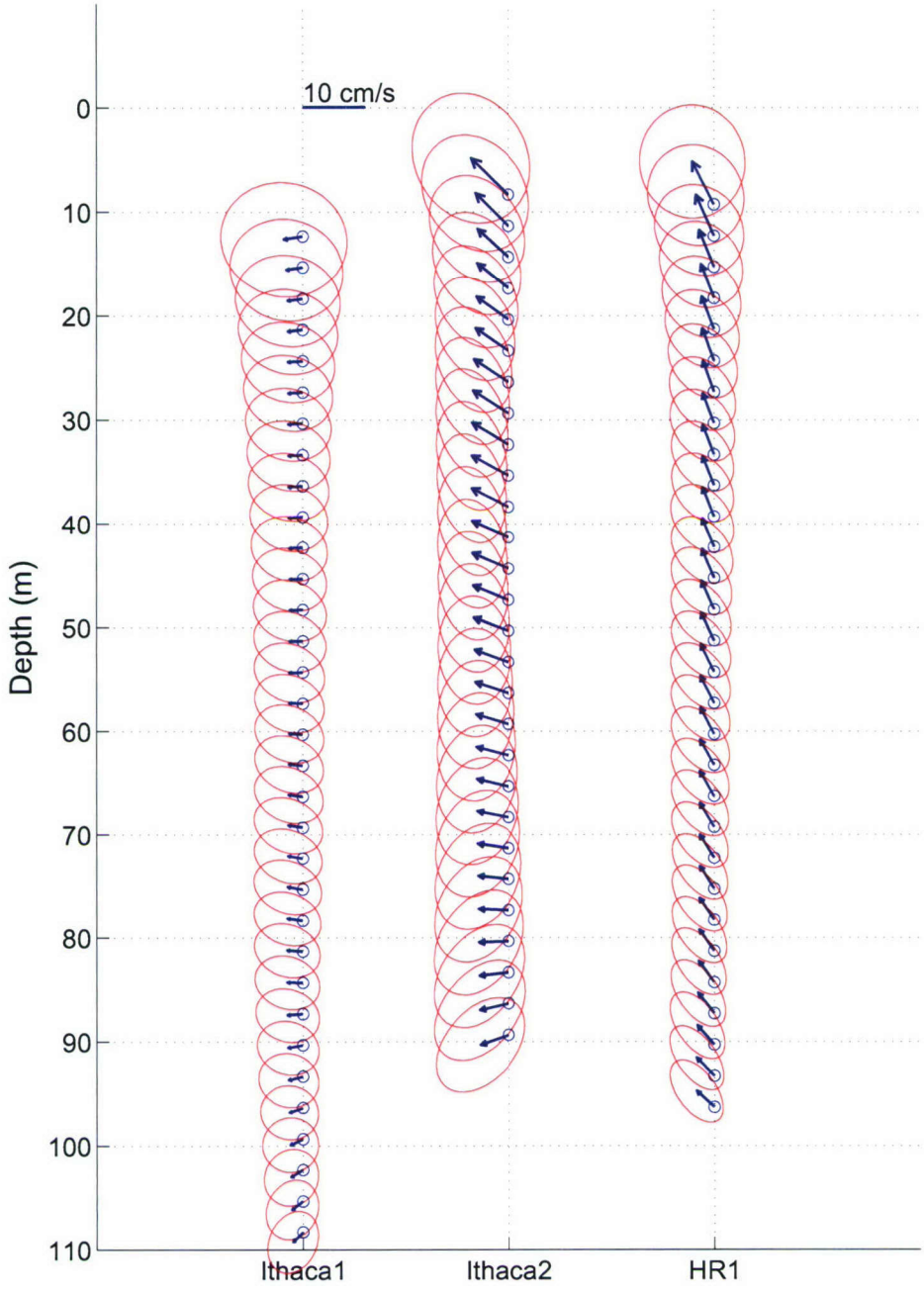

Figure 6.3 Current standard deviation ellipses along the water column at the three ADCP sites.

6.3. Time series analysis

In the following an overview of the main current features is given, going from seasonal to smaller time scales.

6.3.1. Monthly mean currents

Seasonal variability of the current flow is documented by monthly mean currents (Figure 6.4). At IT1 the currents are generally much weaker than at the other two stations, the flow following bottom topography. In June at IT1 a reversal in the surface layer is observed, with generally western surface currents now flowing eastward, but already in July a southwestern flow is established. Currents at IT2 and HR1 do not show large seasonal variability until July, when a pronounced baroclinic structure is evident, especially at IT2. There, the flow in the surface layer is perpendicular to the permanent southwestern current of the bottom layer. In August again an almost barotropic flow is reestablished, the flow becoming stronger especially at IT1.

6.3.2. Daily currents

In order to examine daily-to-weekly variability, the original currents were subjected to a low-pass digital filter (half-power point at 48 h, half-filter length equal to 7 days) and subsampled once a day. As an example Figure 6.5 shows daily currents in June 2006. The daily time series show the already observed pattern – currents at HR1 and IT2 have common features, while at IT1 the flow is quite different. At HR1 and IT2 several episodes of strong flow may be noticed, likely related to wind, since at these time scales the flow, at least in the upper part of water column, is mostly driven by wind. At HR1 the flow is more uniform along the vertical, while at IT2 there is a clearly visible upper layer with prevailing northwesterly flow and a bottom layer with southwesterly currents. At the same time currents at IT1 are very weak. However one interesting episode may be noticed in mid-June. On 11 June and several preceding days strong northwesterly flow was evident at HR1 and IT2 while at IT1 the flow was very weak. During the following days currents at HR1 and IT2 persisted with changing amplitude, while at IT1 an anticyclonically rotating flow started to develop, reaching maximum on 18 June, the entire episode lasting for some ten days. A similar episode was also noticed in mid-July. These events are likely related to the divergence/curl in the wind field.

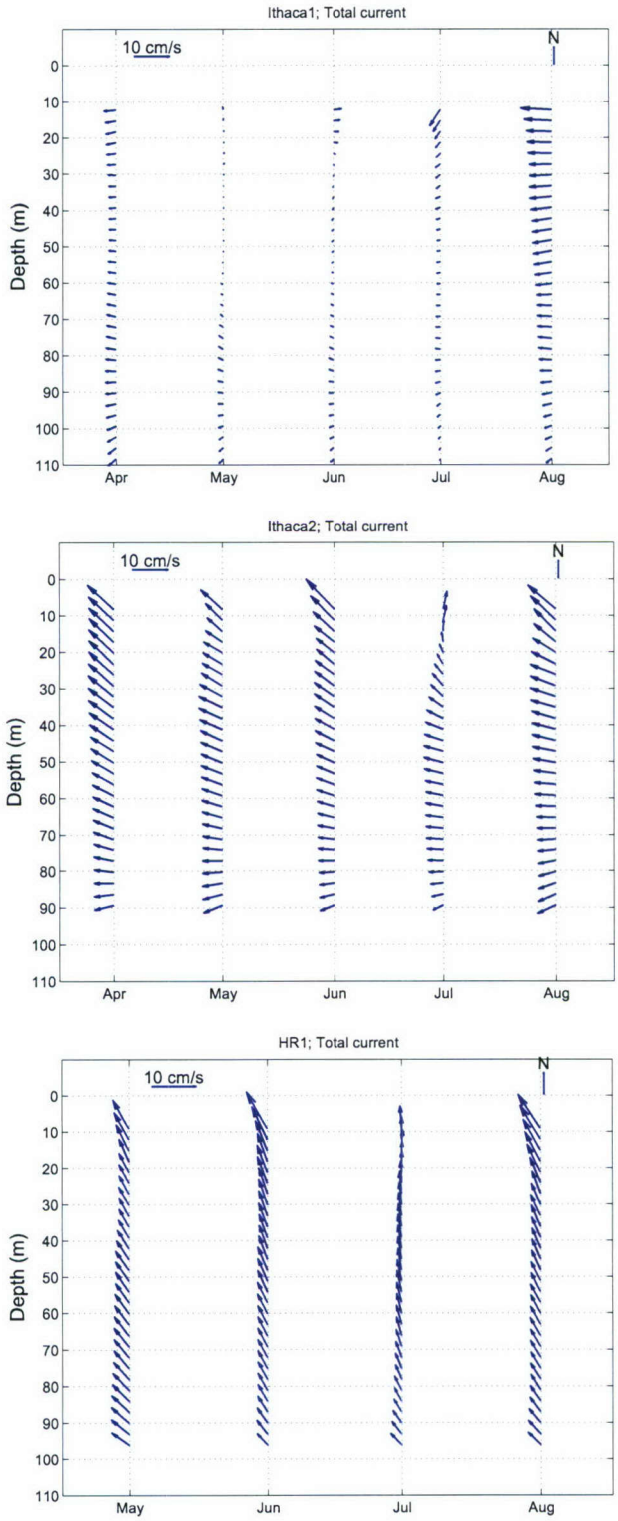

Figure 6.4 Monthly mean currents at IT1 (top), IT2 (middle) and HR1 (bottom), calculated for complete months of data only.

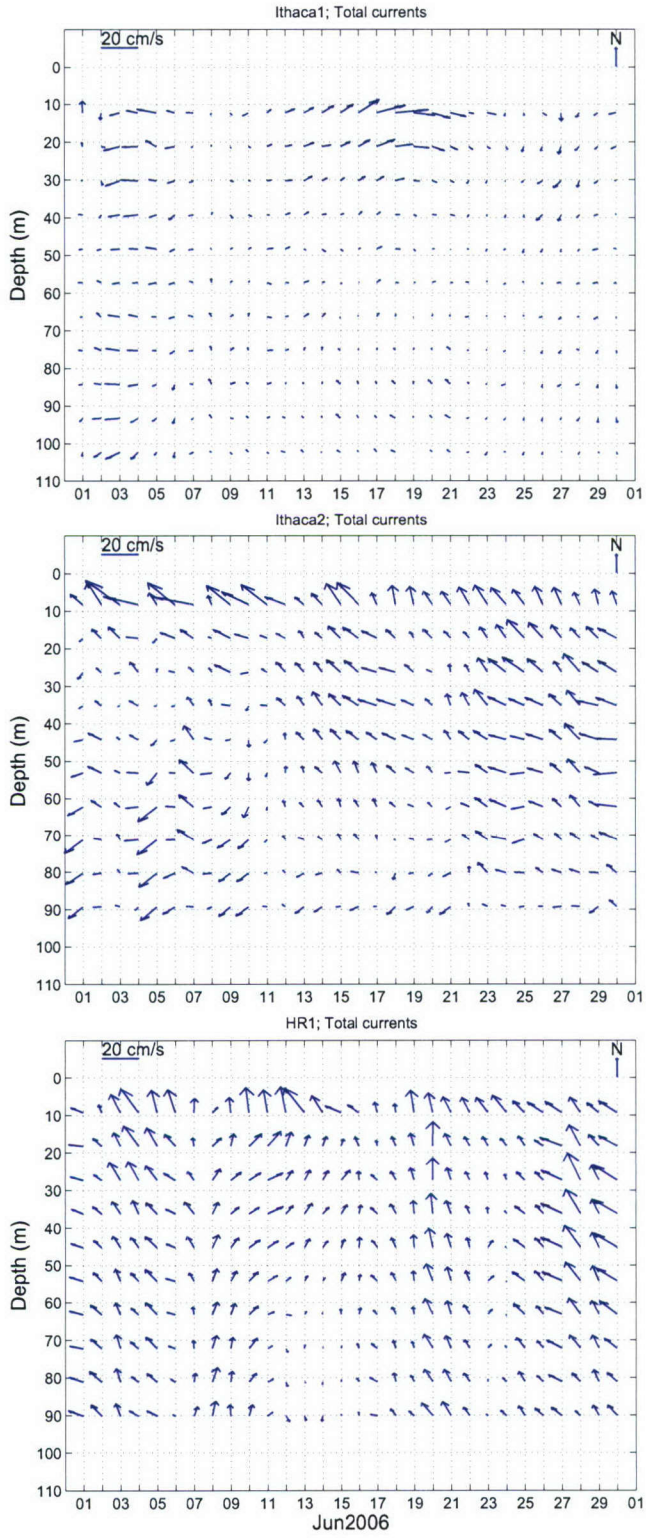

Figure 6.5 Daily currents at IT1 (top), IT2 (middle) and HR1 (bottom) in June 2006, shown at every third layer starting from surface.

6.3.3. Variability at diurnal and shorter time scales

Power density spectra of current speed were calculated from the original 15 min data in order to identify major processes that govern current variability at shorter time scales. The spectra were determined by Welch method, using 30 day long, half-overlapping Hamming windows.

Figure 6.6 shows spectra at different depths, plotted as contours of power density. On the upper horizontal axes some characteristic periods are marked – the local inertial period (17.6 h), the period of the principal Adriatic mode (21.2 h), along with the 24, 12 and 8 h periods.

A strong diurnal oscillation, accompanied by semidiurnal and 8 h signal, is evident at IT2 and HR1; at HR1 the currents are largely barotropic, while at IT2 a pronounced baroclinic structure emerges, with maximum current speed at 30-40 m depth and in the bottom layer. At IT1 the tidal signal is very weak; here a signature of the Adriatic seiche is seen in the upper layers.

Harmonic analysis

Tidal currents have been determined using T-TIDE package provided by Pawlowicz et al. (2002), which follows the Foreman method (1978). Axes of tidal ellipses for seven major tidal constituents in the Adriatic (O1, P1, K1, N2, M2, S2 and K2) are shown in Figure 6.7. The tidal currents at HR1 and IT1 are barotropic to a high degree. The diurnal K1 component is dominant, with elongated, alongshore oriented tidal ellipses. The observed tidal ellipses agree well with modeled barotropic K1 tide (Cushman-Roisin and Naimie, 2002), with respect to direction as well as magnitude. At IT1 the flow in the lower layers is notably affected by bottom friction, resulting in veering of currents and reduction of speed. On the other hand, at IT2 all tidal constituents show a pronounced baroclinic profile. The surface currents are strongly polarized in the alongshore direction but with depth tidal ellipses become more circular, with anticyclonically rotating current vectors. In the bottom layer cross-shore orientation prevails at diurnal frequencies.

In order to eliminate the barotropic tide from time series, harmonic analysis was performed on vertically averaged currents, where the two deepest layers were left out from the averaging, and the synthesized barotropic tidal current was subtracted from the data measured at each level. All of subsequent analyses were done using the residual (i.e. detided) currents obtained that way. Following the general Adriatic orientation, the current vectors were decomposed into a longitudinal (L, northwestward) and transverse (T, northeastward) component.

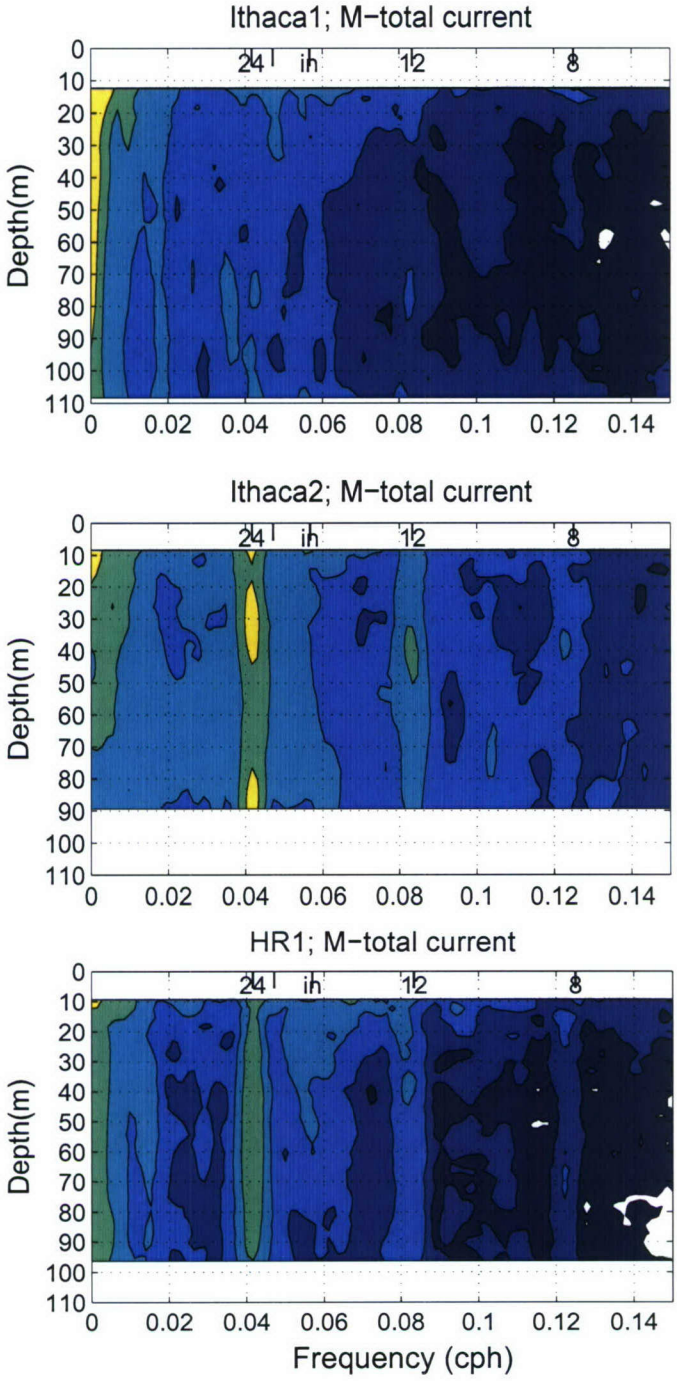

Figure 6.6 Power density spectra of current speed at IT1 (top), IT2 (middle) and HR1 (bottom).

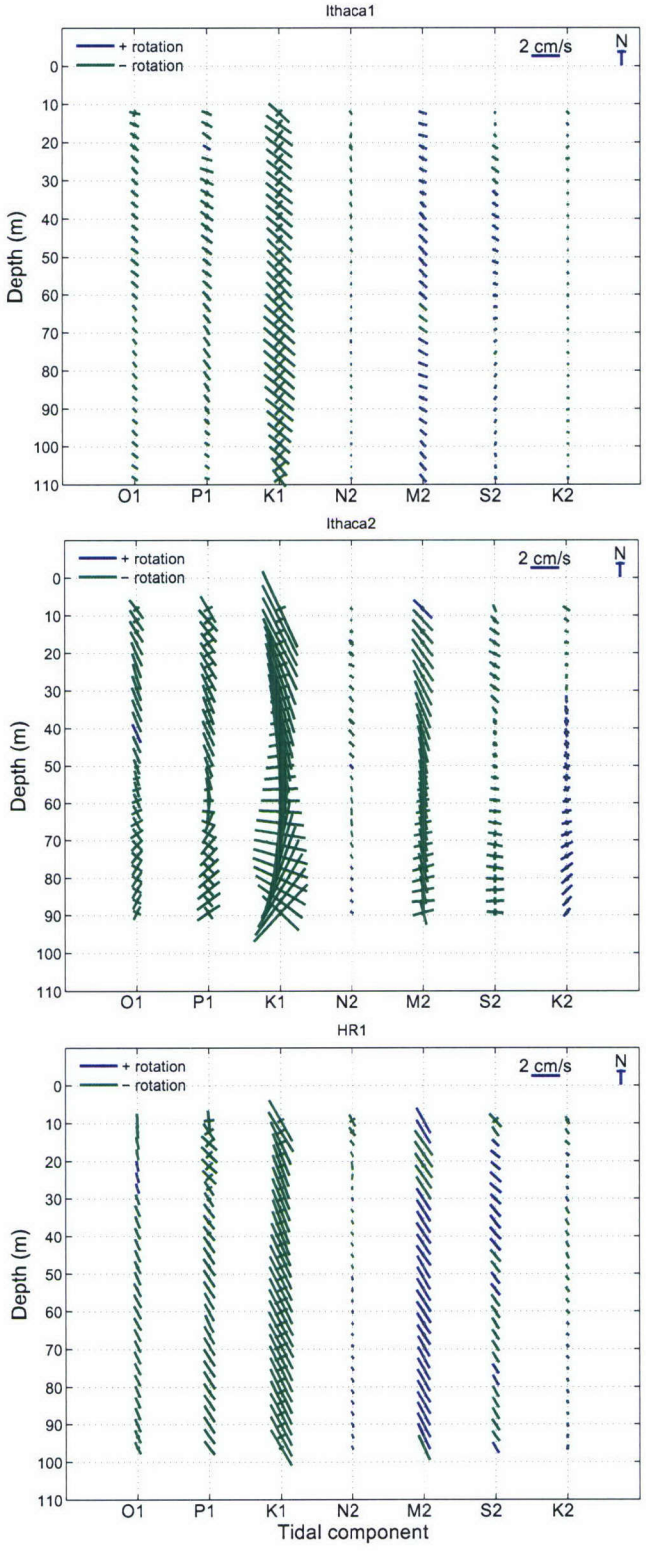

Figure 6.7 Tidal ellipses for seven major tidal constituents.

Spectral analysis

Power density spectra of residual currents are shown in Figure 6.8. Oscillations at the inertial period are observed at all the three sites, especially pronounced at the most remotely positioned station IT1. The signal is strongest in the surface layer, diminishes with depth but is present down to ca. 50 m depth. At the two stations closer to the coast, especially at HR1, signal at the inertial frequency is concealed by a broad energy maximum that spans from about 21 to 14 h periods. The most appealing feature is a strong oscillation observed at IT2 at diurnal frequency. Oscillations of less intensity are seen at semidiurnal as well as at 8 h periods. It is interesting to note that the 24 and 8 h signals are significantly stronger in the bottom layers and in the cross-shore (T) component. The diurnal signal evident in bottom layers at IT1 might be an artifact of an overestimated barotropic tide being subtracted from the measured data.

Additional information on current variability may be obtained through cross-spectra computed between surface currents and those at different depths. Coherence squared amplitude and phase spectra at stations IT1, IT2 and HR1 are shown in Figures 6.9a to 6.9c, respectively. At IT1, the inertial oscillation is the most prominent feature (Figure 6.8). Surface inertial currents show maximum coherence with those at about 50 m depth, the two having opposite direction, as is expected (Figure 6.9a). In addition, in the upper 50 m of the L-component, a coherent signal related to a 10 day variability can be noticed. Finally, seasonal circulation at IT1 is characterized by a coherent flow that stretches much deeper (to about 50 m) than at the other two stations. At IT2 (Figure 6.9b) strong currents at diurnal and 8 h period occupy the bottom 20 meters. Phase spectra show that the bottom currents are in the opposite direction to the surface currents. Increased coherence between surface and deeper layers and phase difference close to π is found in the broad band between 12 and 20 h. Finally, a ten-day variability is also manifested at IT2, with minimum intensity in the middle part of water column. The most striking feature at HR1 (Figure 6.9c) is the large coherent region related to the already mentioned broad energy maximum at periods 14-21 h. Equal intensity and similar pattern in both current components and phase shift close to π between surface and deeper (below ca. 30 m) layers suggest that it may be related to the inertial oscillations.

As many of the observed baroclinic phenomena are related to the changing stratification, time evolution of energy at different time scales was examined. Power density spectra were computed over 30 day long sliding intervals, advancing at 5 day time steps. Within each interval, power spectrum was determined over three half-overlapping windows. Sliding spectra thus obtained from detided currents at the surface, around 30 m depth and at the bottom, are shown in Figures 6.10a – 6.10c. Episodes of intense inertial oscillations have been recorded at the end of May and in the first part of June, at IT1 (Figure 6.10a). Episodes of strong diurnal variability at IT2 can be observed in the second part of April and the beginning of June and the strongest one took place in mid-June (Figure 6.10b). Finally, variability at periods between 14 and 21 h at HR1 was more intense in the first and the last part of the experiment, having a break during July (Figure 6.10c).

Diurnal variability

Finally, let us examine time series that are related to the strong baroclinic signal observed at diurnal frequency at IT2. To that end a narrow band-pass digital filter (of half-length equal to 14 days) was designed to pass unaffected all signals between 23 and 26 h, and to completely remove periods shorter than 22.4 h which is the highest reported period of the principal Adriatic mode. The filtered time series of currents at IT2 are shown in Figure 6.11. The time series show, as we have already inferred from the spectral analysis, that largest oscillations at the diurnal frequency take place in the bottom layer, and are more pronounced in the cross-shore direction. During episodes of strong activity diurnal currents in the bottom layer can reach 8.5 cm/s. When looking at the modulation curves one may notice that (*i*) maxima in the cross-shore component occur at the time of minima in the alongshore component and vice versa and (*ii*) the maxima seem to propagate from the bottom towards the upper layers.

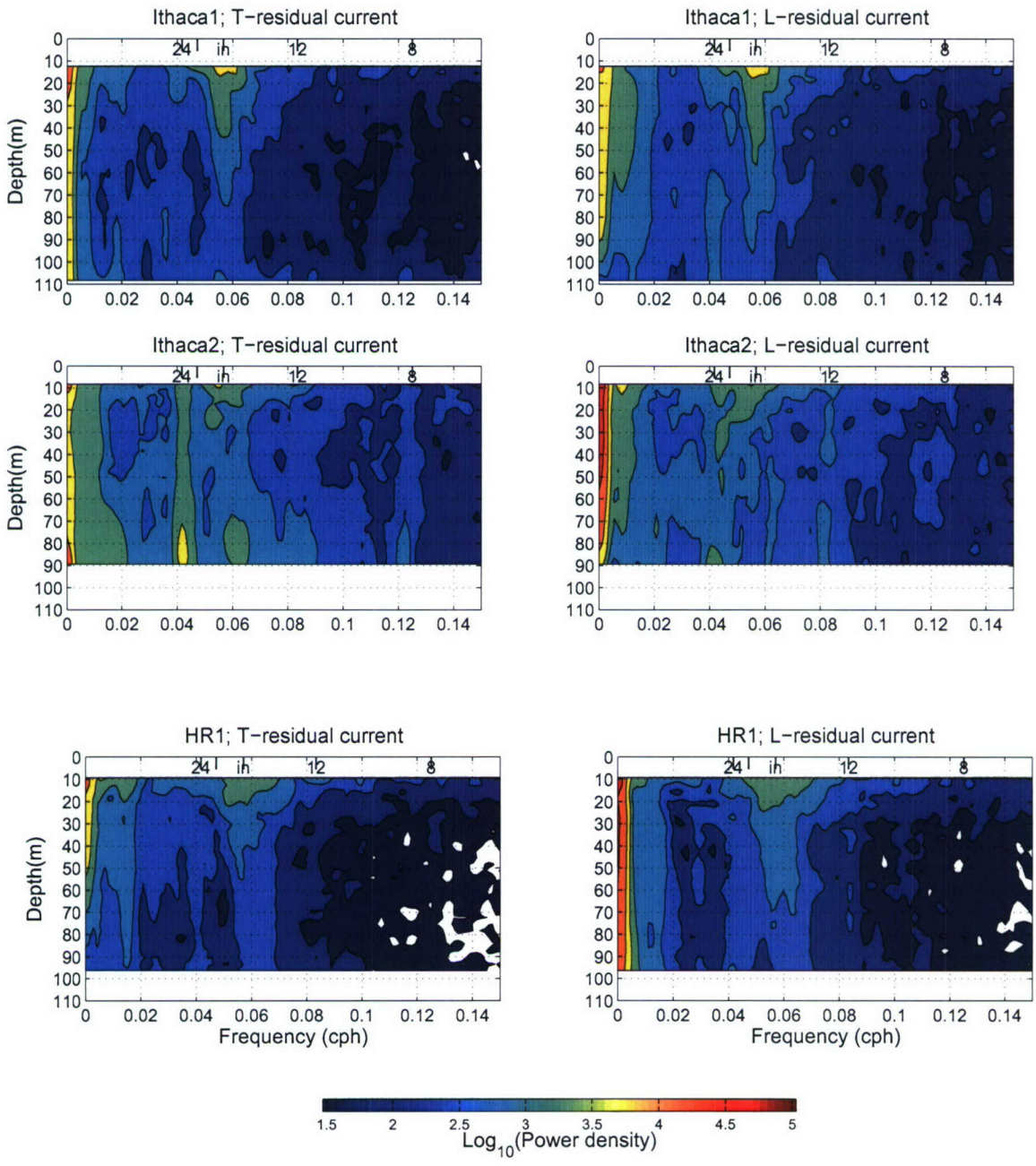

Figure 6.8 Power density spectra of cross-shore (T, left)) and alongshore (L, right) component of detided currents.

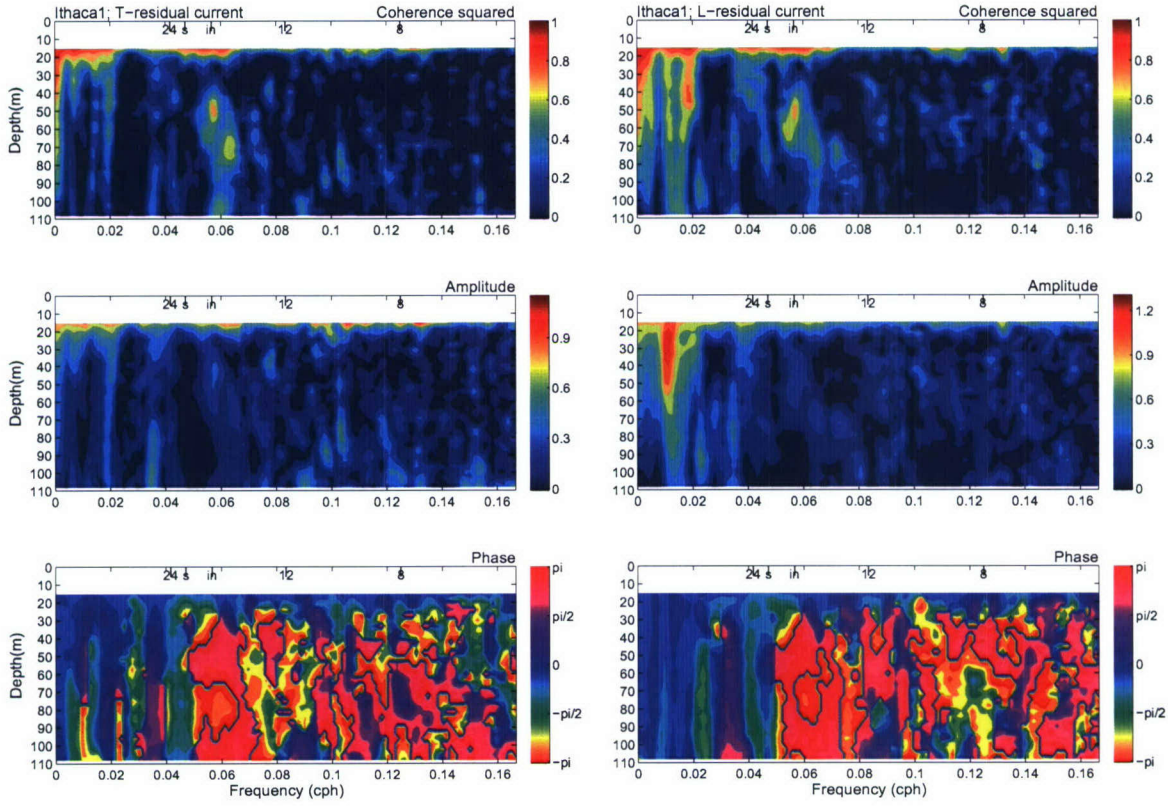

Figure 6.9a Coherence squared (top), amplitude (middle) and phase (bottom) computed between surface currents and currents at each depth, at station IT1, for the cross-shore (left) and alongshore (right) component.

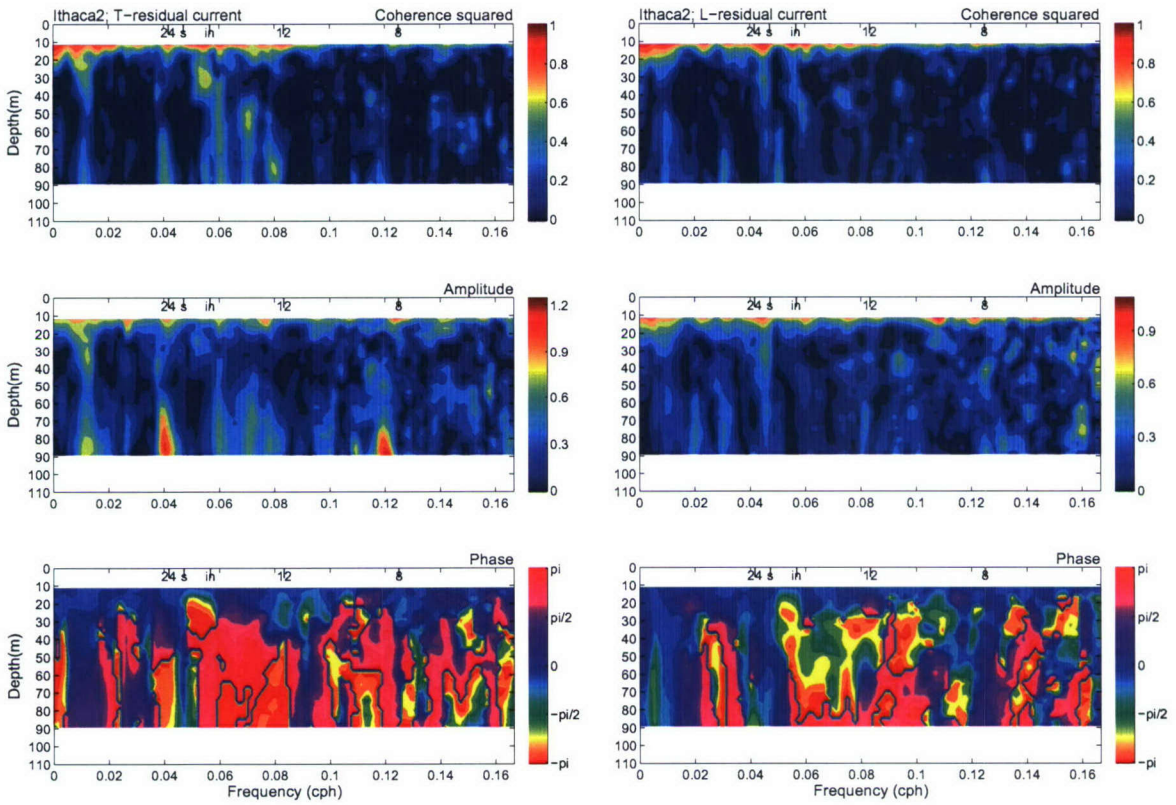

Figure 6.9b The same as in Figure 6.9a, but for station IT2.

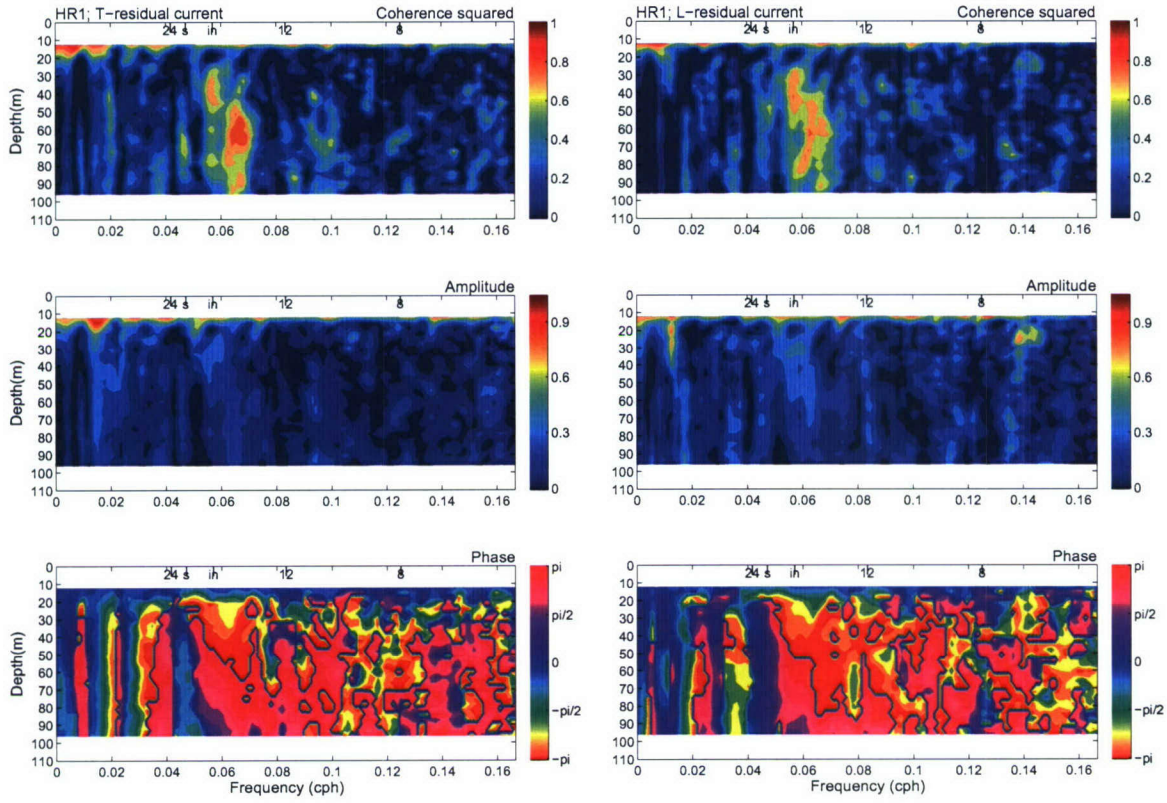

Figure 6.9c The same as in Figure 6.9a, but for station HR1.

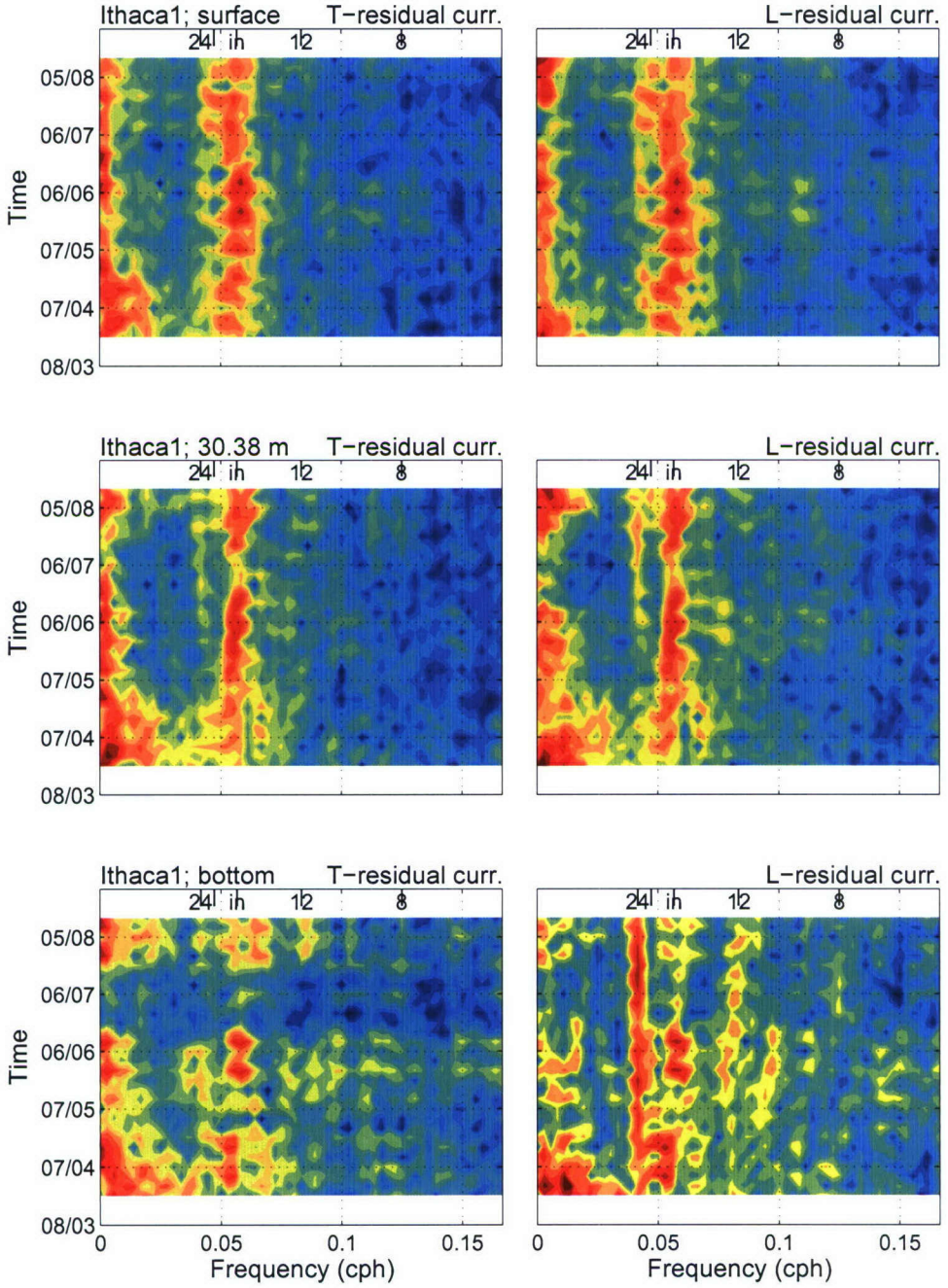

Figure 6.10a Sliding power density spectra of cross-shore (left) and alongshore (right) component of residual current, at the uppermost (top), 30 m (middle) and bottom (bottom) layer at IT1. The spectra were computed over 30 day sliding intervals, advancing at 5 day steps.

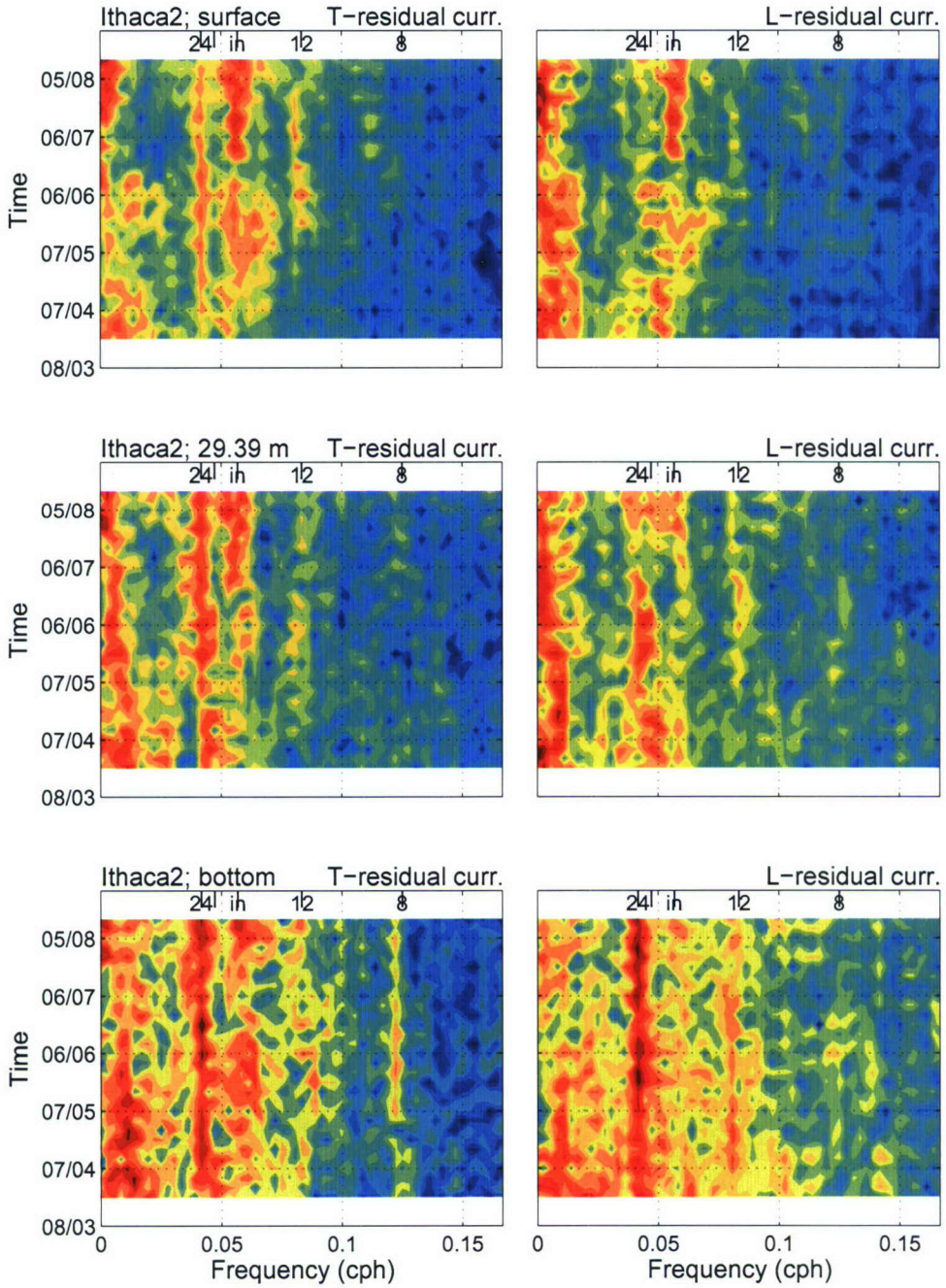

Figure 6.10b The same as in Figure 6.10a, but for IT2.

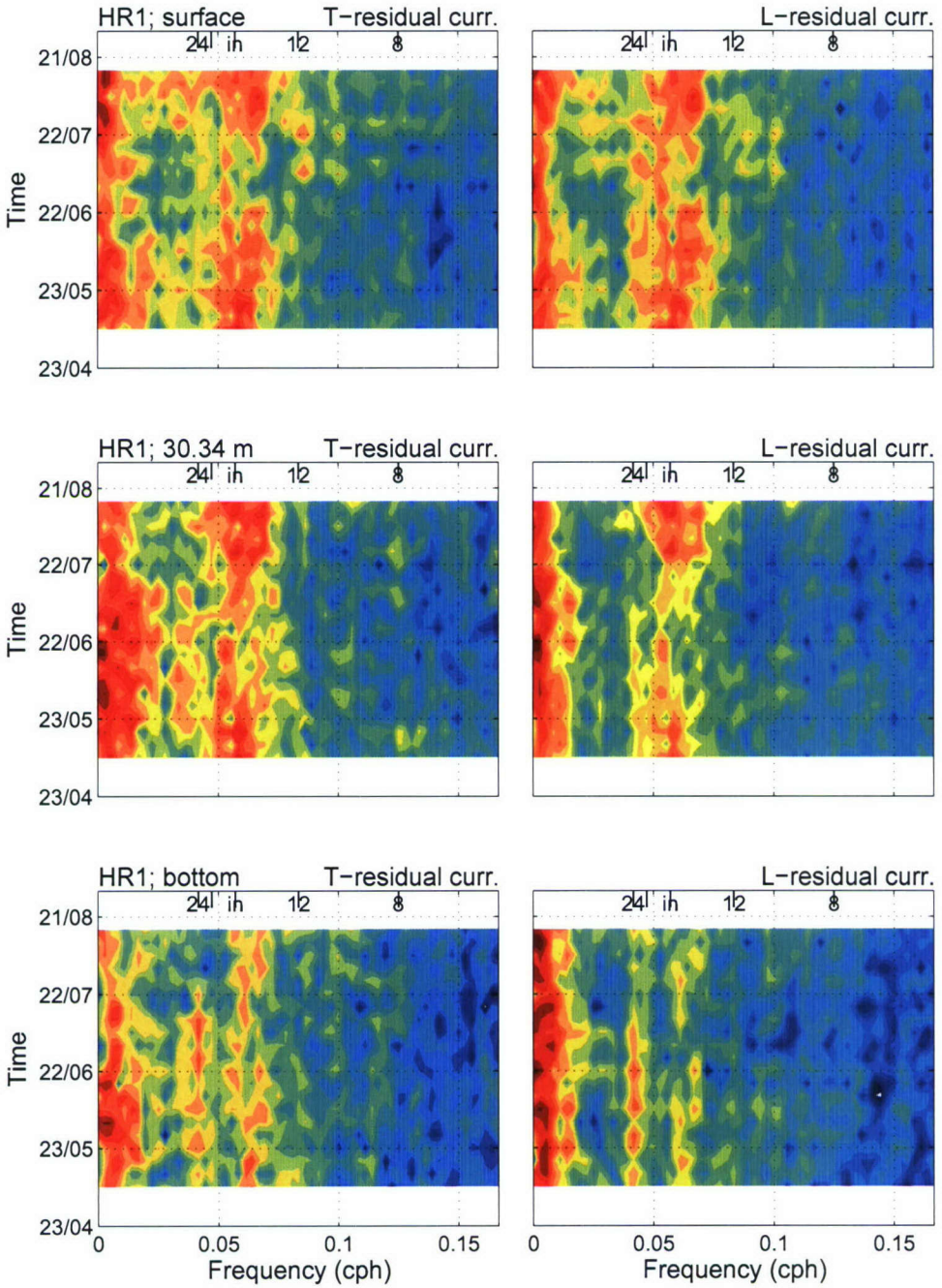

Figure 6.10c The same as in Figure 6.10a, but for HR1.

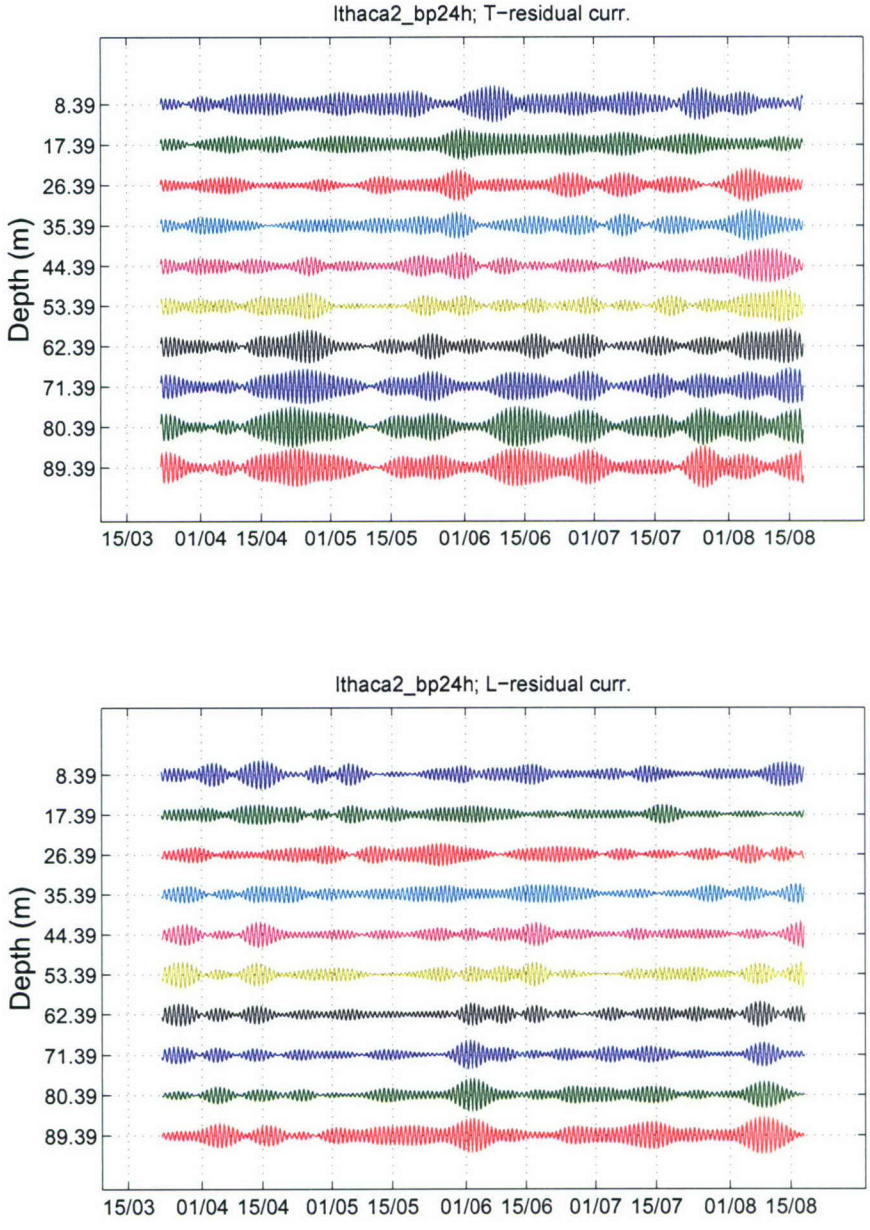

Figure 6.11 Cross-shore (top) and alongshore (bottom) current, band-pass filtered at 24 h, at station IT2. Time series at every third level are drawn with 15 cm/s offset.

7. Sea-level and bottom-pressure time series

ITHACA project plan included as one of its topics sea-level measurements at Dubrovnik and Split tide gauge stations between 1 February and 30 September 2006. It was hypothesized that these measurements will document tidal characteristics in the area between islands of Vis and Lastovo, where other parameters were intensively measured.

7.1. Adriatic sea-level oscillations – short overview

Sea-level variations of the Adriatic Sea are basically generated by tidal and atmospheric influences, primarily by the air pressure and wind. Orlic (2001) analyzed sea level measurements at Bakar since 1930, and concluded on components of the recorded signal: tides, storm surges and seiches, variability driven by planetary atmospheric waves, seasonal cycle, interannual variability and long-term trend.

Studies concerned with sea-level measurements in the Adriatic Sea have revealed that tides are of mixed type. One of the striking properties of the Adriatic tides is a well developed amphidromy with semi-diurnal tides having opposite phases in the western and the eastern part of the middle Adriatic (Polli, 1960). Mean tidal ranges are small, rising from the south to the north: Dubrovnik (23 cm), Split (24 cm), Bakar (30 cm) and Trieste (68 cm) (e.g. Leder, 2004).

It has been generally concluded by calculating the percentage of total sum of squares (*tss*), where *tss* is a measure of each constituent's contribution to the total observed tide (e.g. Emery and Thomson, 1997), that Adriatic tides can be adequately described by using seven constituents, four semi-diurnal and three diurnal tides (Cushman-Roisin et al., 2001). Principal semi-diurnal constituents are M2, S2, K2 and N2, while principal diurnal constituents are K1, O1and P1. Tides in the Adriatic are usually described by the largest M2 and K1 constituents (Polli, 1960), while the other semidiurnal and diurnal constituents behave similarly. Harmonic constants have been published by governmental authorities in Italy, Slovenia and Croatia. In Croatia, Hydrographic Institute published harmonic constants in 1973 (Hydrographic Institute, 1973).

Forced oscillations of the sea level – storm surges – are aperiodic and mainly caused by long-lasting and strong winds (synoptic scale atmospheric disturbances) as well as by pronounced air pressure changes. The lower the air pressure the higher the sea level and vice versa. The acting of wind on the sea surface is complex, depending on the topography of the basin and on the wind speed, direction and duration. In the Adriatic Sea the southeast winds (sirocco) raise the sea level, especially in the north Adriatic, where a long-lasting sirocco and low air pressure can raise the water level by up to 1 m (e.g. Orlic, 2001). Storm surges are relatively well examined in the Adriatic Sea (e.g. Leder, 1988; Orlic, 2001).

Free oscillations – seiches – occur as the sea response to sudden changes of the meteorological parameters over the basin, especially the wind and air pressure. Seiche periods are determined by the dimensions and the topography of the basin, whereas the

amplitudes depend on the changes of the wind speed and direction. The most pronounced seiche in the Adriatic Sea is uninodal seiche having a period of 21-22 h, but the second mode with a period of 10-11 h is significant as well (e.g. Vilibic et al., 1998; Raicich et al., 1999; Leder and Orlic, 2004).

The other processes contributing to the Adriatic sea-level variability are less important for the present study.

7.2. Data acquisition and processing

The Split tide gauge station is located in front of the Harbour Master's Office (φ = 43° 30' N, λ = 16° 26' E) in the harbor of Split (Figure 3.1). In Dubrovnik, the tide gauge station is situated on the northern side of Sumartin Bay, on the Lapad Peninsula (φ = 42° 40' N, λ = 18° 04' E, Figure 3.1).

Continuous time series of measurements commenced in 1956 at both tide gauge stations, by using float-type (in stilling well) analog recording gauge A. Ott–Kempten, with registration ratio 1:5. Precision of tide gauge measurements is ± 1 cm. Tide gauges were upgraded in 2003 with OTT Thalimedes A/D converter (Vilibic et al., 2005). Thalimedes is set up to record the data every minute.

Time series, collected with the 1 min sampling interval at Split and Dubrovnik tide gauges between 1 February and 30 September 2006, were digitized and stored in the data logger unit. Sea-level variations were recorded on analog paper charts as well.

The sea-level data measured at Split tide gauge are graphically displayed on the dynamic web pages of the Hydrographic Institute of the Republic of Croatia (*http://www.mijeneonline.hhi.hr/split_mj_n_e.asp*).

One-minute time series of sea level in Split and Dubrovnik were subjected to a low-pass filter (e.g. Emery and Thomson, 1997) with a cut-off period of 20 min in order to extract the sea-level heights with a resolution of 10 min (the same resolution as provided for temperature data by thermistors).

ITHACA 1 SBE pressure gauge station was located southward of Glavat island (φ = 42° 40' N, λ = 17° 08' E, Figure 3.1). Station was active from 8 March to 1 September 2006, with sampling interval of 15 min.

Harmonic analysis of tide gauge and pressure gauge measurements was performed using TASK software (Bell et al., 2000) and T-TIDE software (Pawlowicz et al., 2002). It must be pointed out that T-TIDE software enables calculation of amplitude and phase errors too.

Spectral analysis calculations were carried out via Fast Fourier Transform method (Welch, 1967), while wavelet spectra were calculated according to Torrence and Compo (1998).

7.3. Results

7.3.1. Harmonic analysis

The results of harmonic analysis for Split and Dubrovnik tide gauges and ITHACA 1 SBE pressure gauge are presented in Tables 7.1a to 7.1c. For comparison, the amplitudes and phases of tidal constituents calculated by Hydrographic Institute (1973) for Split and Dubrovnik tide gauge stations are given in Tables 7.1a and 7.1b. It can be seen that all values of amplitudes and phases are in ranges of amplitude and phase errors, except that Hydrographic Institute's phases are slightly higher for K1, M2 and S2 constituents in Split and Dubrovnik and for K2 constituent in Dubrovnik.

Table 7.1.a Harmonic constants for Split tide gauge calculated using TASK and T-TIDE software packages. Values presented in brackets are amplitudes and phases calculated by Hydrographic Institute (1973).

SPLIT TIDE GAUGE						
Tidal constituent	TASK (PSMSL)		T-TIDE (with SNR=10)			
	Amplitude (cm)	Phase (°)	Amplitude (cm)	Amplitude error (cm)	Phase (°)	Phase error (°)
O1	2.89 (2.69)	43.88 (47.5)	2.93	0.43	43.45	7.59
P1	3.23 (2.90)	51.23 (51.8)	3.20	0.46	51.78	8.60
K1	8.96 (8.82)	52.46 (55.9)	8.99	0.45	52.38	2.63
N2	1.23 (1.38)	124.39 (125.6)	1.18	0.17	124.11	8.12
M2	8.04 (7.95)	124.54 (129.0)	8.05	0.16	124.32	1.18
S2	5.46 (5.58)	126.19 (130.8)	5.45	0.16	126.31	1.77
K2	1.51 (1.64)	121.82 (124.1)	1.51	0.11	122.23	4.39
M3			0.30	0.08	11.02	16.59

Table 7.1.b Harmonic constants for Dubrovnik tide gauge calculated by using TASK and T-TIDE software packages. Values presented in brackets are amplitudes and phases calculated by Hydrographic Institute (1973).

DUBROVNIK TIDE GAUGE						
Tidal constituent	TASK (PSMSL)		T-TIDE (with SNR=10)			
	Amplitude (cm)	Phase (°)	Amplitude (cm)	Amplitude error (cm)	Phase (°)	Phase error (°)
O1	1.93 (1.90)	47.64 (47.3)	1.95	0.22	46.80	6.05
P1	1.83 (1.69)	56.45 (60.2)	1.82	0.23	56.95	7.30
K1	5.19 (5.19)	57.92 (62.4)	5.20	0.21	57.86	2.13
N2	1.51 (1.68)	106.04 (110.6)	1.47	0.13	105.16	4.82
M2	9.47 (9.28)	108.25 (115.1)	9.48	0.12	108.11	0.70
S2	5.76 (5.76)	114.23 (120.4)	5.76	0.12	114.37	1.32
K2	1.65 (1.65)	106.42 (115.7)	1.64	0.10	106.76	2.94

7.3.2. Spectral and wavelet analysis

The power spectra of sea-level data at Split and Dubrovnik and pressure gauge data at ITHACA 1 station are shown in Figure 7.1, while the power spectra of the corresponding residual values are shown Figure 7.2. In Figure 7.1 one can observe sharp peaks at periods of the main Adriatic tides. The first and the second mode Adriatic seiches are distinguished from tides by relatively wide peaks (periods of 21-22 h and 10-11 h). It is interesting to notice slightly higher energy for semidiurnal than for diurnal tides in Dubrovnik. At Split station significant peaks also appear at periods of about 4 and 2 h. These oscillations were interpreted by Vilibic et al. (1998) as seiches in the region inside the middle Adriatic island area. Similar power spectrum as shown in Figure 7.1 for Split tide gauge station was presented by Vilibic et al. (1998).

Power spectra of residual values (Figure 7.2) contain expected seiche peaks and relatively high energy at tidal periods. However, the tides were already removed from the series and so this energy is probably a result of nonlinear effects (Cerovecki et al., 1997; Pasaric and Orlic, 2001).

Table 7.1.c Harmonic constants for ITHACA 1 SBE pressure gauge calculated by using TASK and T-TIDE software packages.

ITHACA 1 SBE PRESSURE GAUGE						
Tidal constituent	TASK (PSMSL)		T-TIDE (with SNR=10)			
	Amplitude (mbar)	Phase (°)	Amplitude (mbar)	Amplitude error (mbar)	Phase (°)	Phase error (°)
O1	2.13	42.71	2.14	0.27	42.75	7.48
P1	1.96	49.45	1.91	0.37	58.58	10.03
K1	5.73	51.36	5.78	0.31	51.51	3.24
N2	1.42	99.91	1.47	0.24	99.89	8.48
M2	9.71	103.16	9.72	0.23	103.06	1.29
S2	5.50	108.11	5.45	0.20	108.50	2.16
K2	1.64	103.49	1.48	0.16	130.90	5.91

Sea level measured at Split and Dubrovnik tide gauges together with respective wavelet spectra at the K1 tidal frequency are shown in Figure 7.4 and Figure 7.6 while corresponding normalized wavelet energies, presented as period-time diagrams, are given in Figure 7.3 and Figure 7.5. Wavelet spectra confirm spectral maxima revealed by stationary spectral analysis. Wavelet spectra at the K1 frequency for Split and Dubrovnik are very similar, indicating that CTD cruises carried out on the ITHACA polygon on 14/15 February, 26 June and 28-30 September 2006 (Table 4.1) were very well picked for research of internal tidal waves. Similar pattern can be observed for pressure gauge data measured at ITHACA 1 station (Figure 7.7 and Figure 7.8). It must be pointed out that sometimes the wavelet spectral analysis performed for certain fixed period can not distinguish between two nearby periods. This happens, for example, in cases when the first mode Adriatic seiche coincides with strong K1 tide. Thus, the maxima of normalized wavelet energy on 30 May 2006 (Figure 7.4, Figure 7.6 and Figure 7.8) can be related to seiche signal shown in Figure 7.15.

Wavelet spectra of residual sea level at Split and Dubrovnik (Figure 7.9 and Figure 7.11) and residual pressure gauge data (Figure 7.13) show the same spectral maxima as obtained by stationary spectral analysis (Figure 7.2), but additionally indicate the dates of corresponding maxima.

Time series of residual values and respective normalized wavelet spectra at the period of the first (fundamental) Adriatic mode (Figure 7.10, Figure 7.12 and Figure 7.14) reveal the dates of the individual seiche episodes. The most intensive seiche episode occurred on 30 May 2006; this episode is presented in Figure 7.15 as time series of

residuals. It is interesting to note an occurrence of the sea-level rise and pressure decrease (28 May 2006) in the period before the seiche were triggered. This situation is typical for the seiche generation in the Adriatic (e.g. Leder and Orlic, 2004). Furthermore, seven oscillations of the seiche period are observed confirming longevity of the Adriatic seiches (e.g. Raicich et al., 1999).

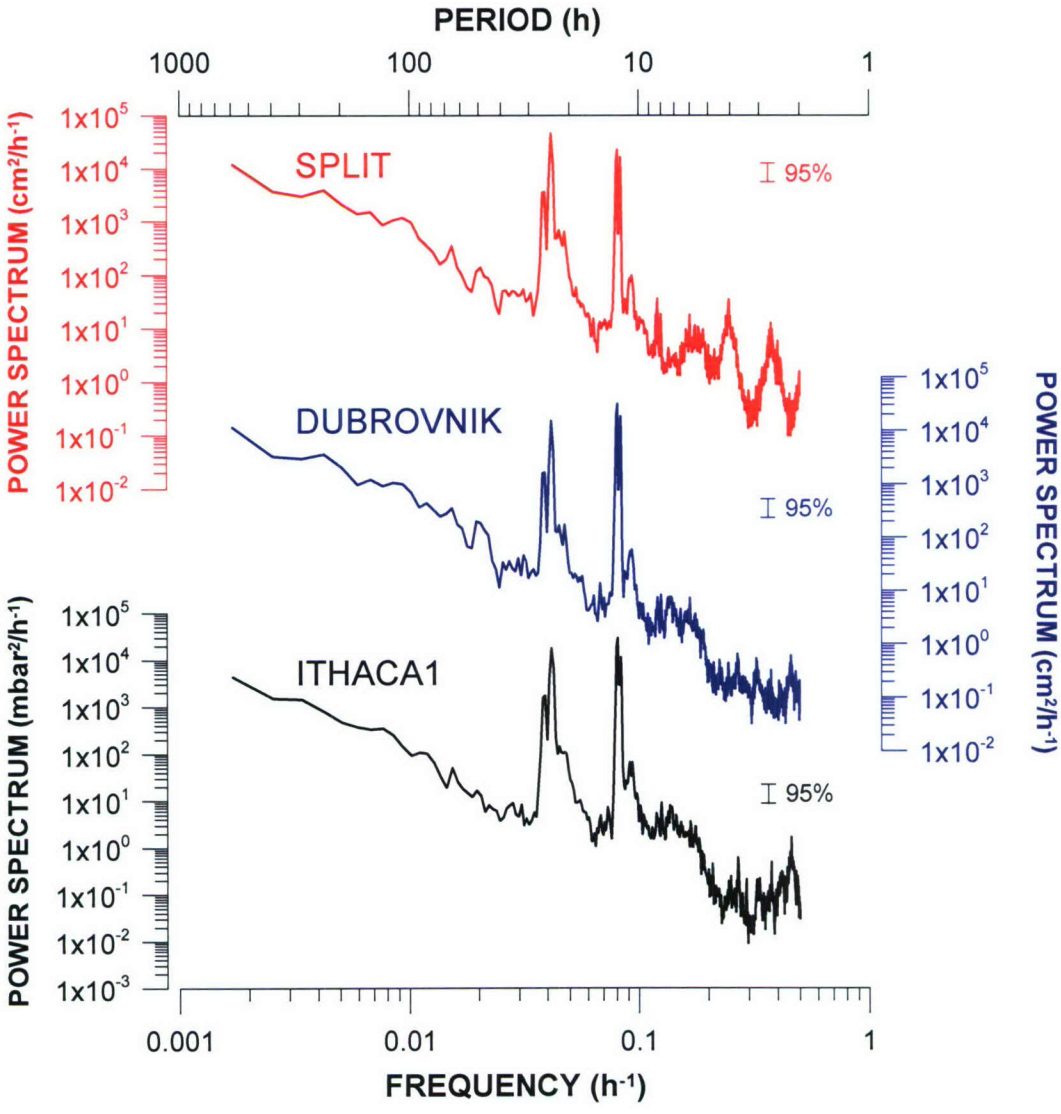

Figure 7.1 Power spectrum of sea level data at Split and Dubrovnik and pressure gauge data at ITHACA 1 station for the interval extending from 1 February to 30 September 2006 (Split and Dubrovnik) and from 8 March to 1 September 2006 (ITHACA 1).

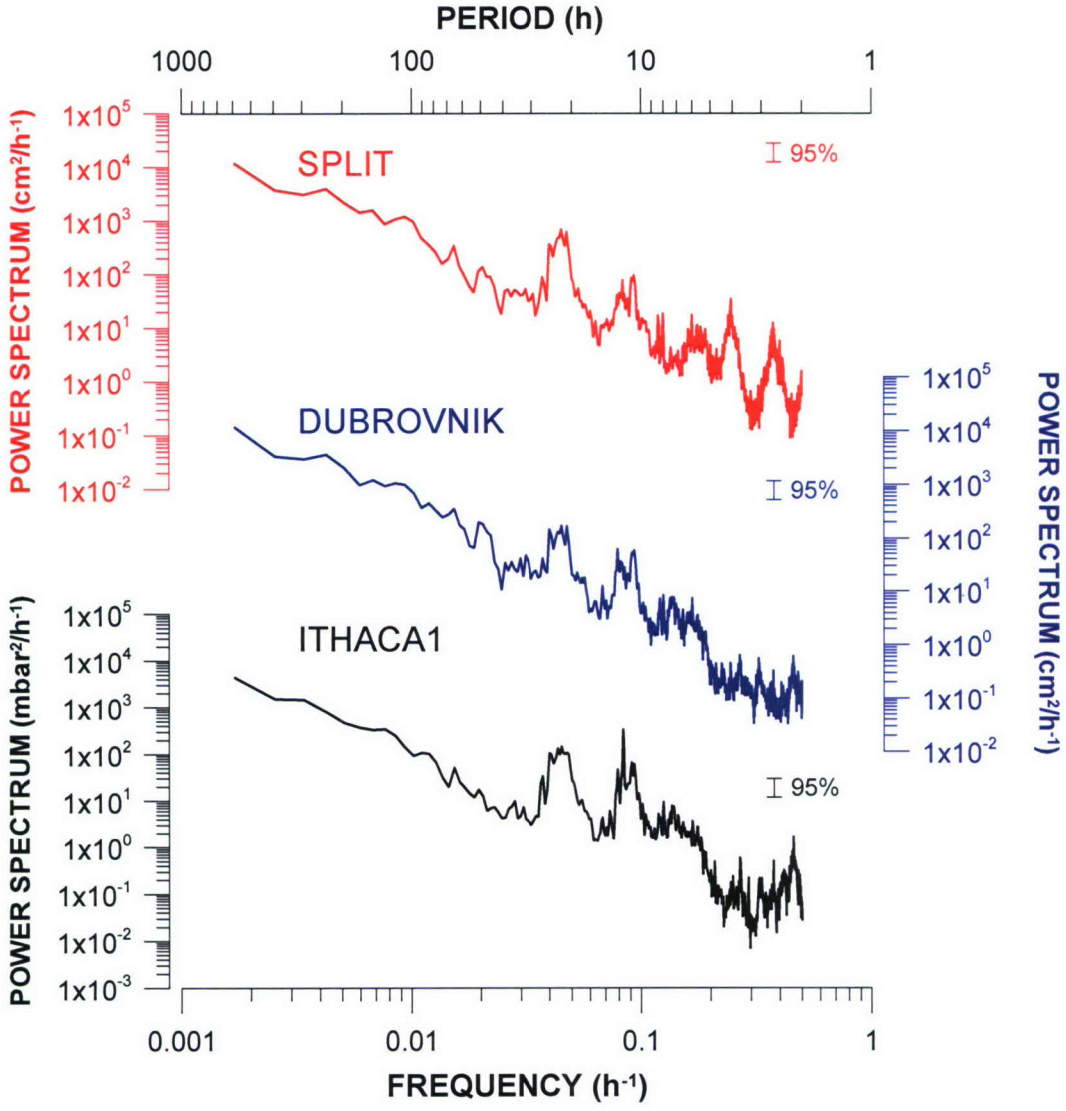

Figure 7.2 Power spectrum of residual sea level at Split and Dubrovnik and residual pressure at ITHACA 1 station for the interval extending from 1 February to 30 September 2006 (Split and Dubrovnik) and from 8 March to 1 September 2006 (ITHACA 1).

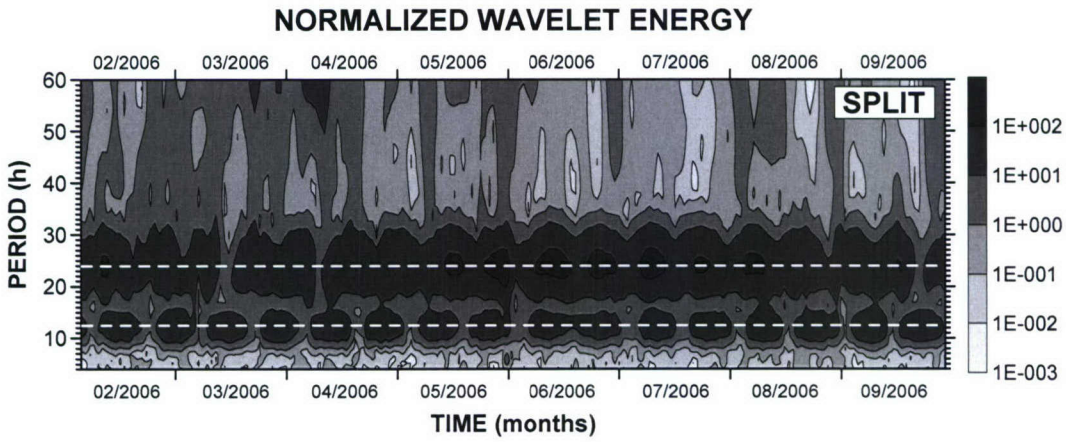

Figure 7.3 Wavelet spectrum of sea level measured at Split tide gauge, for the interval extending from 1 February to 30 September 2006. The spectrum is normalized by the respective variance. Dashed lines denote the K1 and M2 tidal periods.

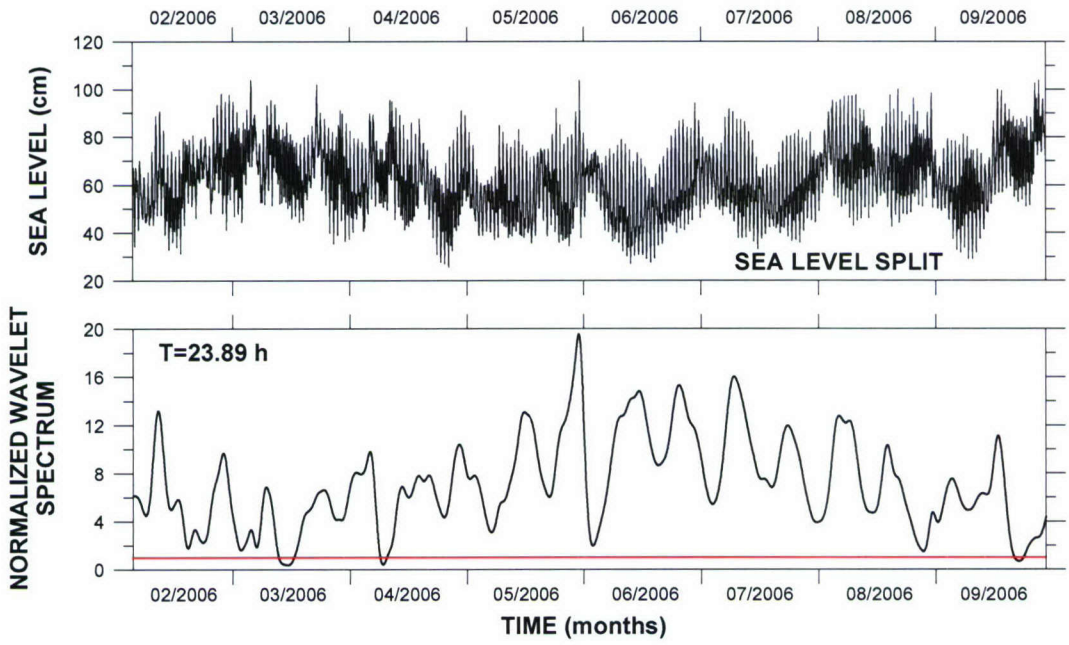

Figure 7.4 Sea level measured at Split tide gauge and respective wavelet spectrum at the K1 tidal frequency for the interval extending from 1 February to 30 September 2006. The spectrum is normalized by the respective variance and significance level, so that the confidence level at 95% equals 1.

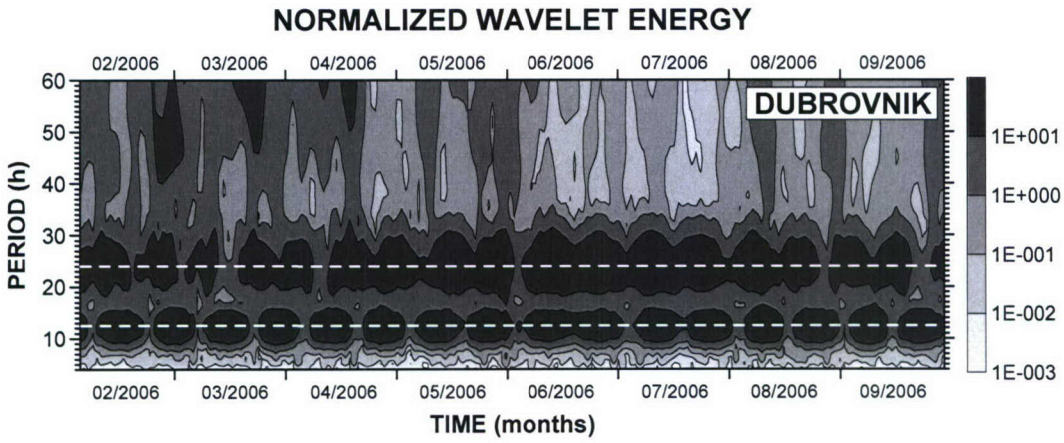

Figure 7.5 Wavelet spectrum of sea level measured at Dubrovnik tide gauge, for the interval extending from 1 February to 30 September 2006. The spectrum is normalized by the respective variance. Dashed lines denote the K1 and M2 tidal periods.

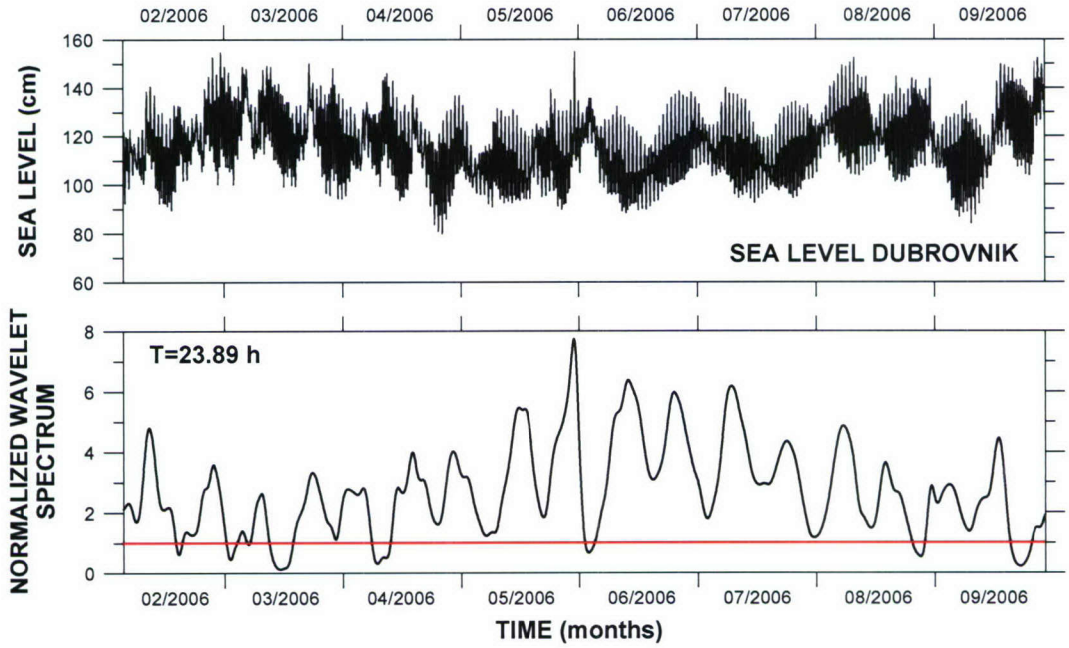

Figure 7.6 Sea level measured at Dubrovnik tide gauge and respective wavelet spectrum at the K1 tidal frequency for the interval extending from 1 February to 30 September 2006. The spectrum is normalized by the respective variance and significance level, so that the confidence level at 95% equals 1.

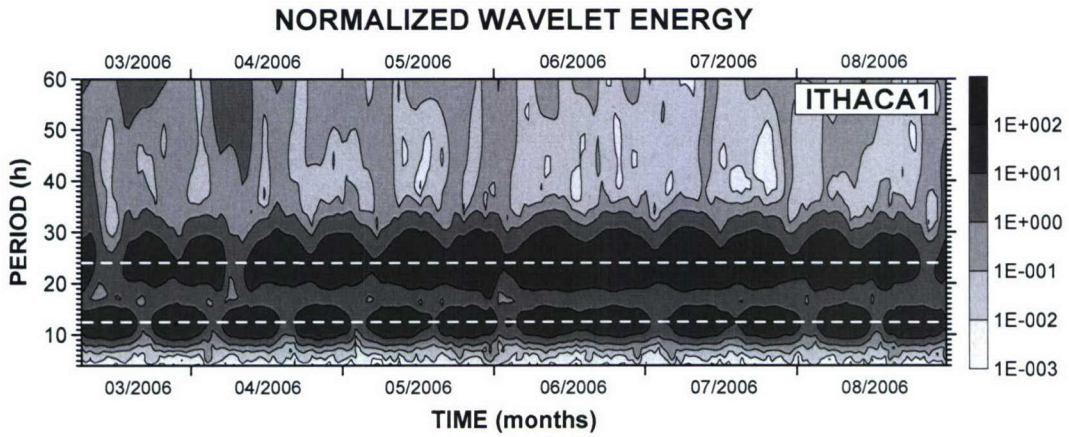

Figure 7.7 Wavelet spectrum of pressure gauge data measured at ITHACA 1 station, for the interval extending from 8 March to 1 September 2006. The spectrum is normalized by the respective variance. Dashed lines denote the K1 and M2 tidal periods.

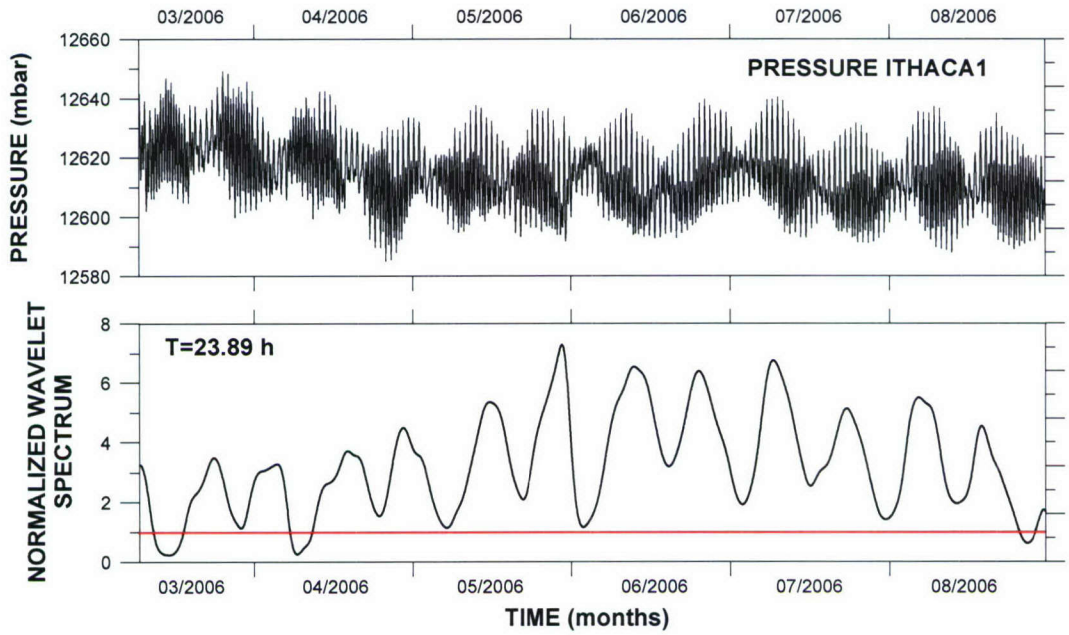

Figure 7.8 Bottom pressure measured at ITHACA 1 station and respective wavelet spectrum at the K1 tidal frequency for the interval extending from 8 March to 1 September 2006. The spectrum is normalized by the respective variance and significance level, so that the confidence level at 95% equals 1.

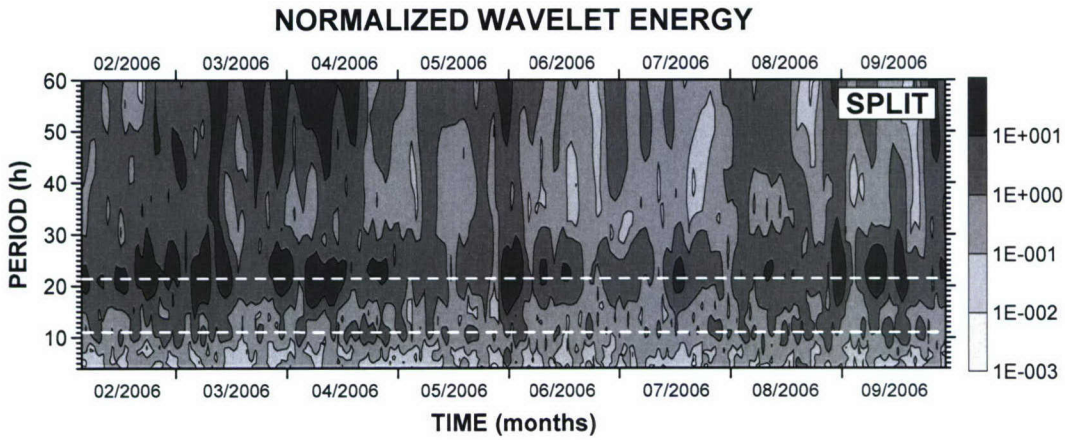

Figure 7.9 Wavelet spectrum of residual sea level at Split tide gauge, for the interval extending from 1 February to 30 September 2006. The spectrum is normalized by the respective variance. Dashed lines denote periods of the fundamental and second Adriatic mode.

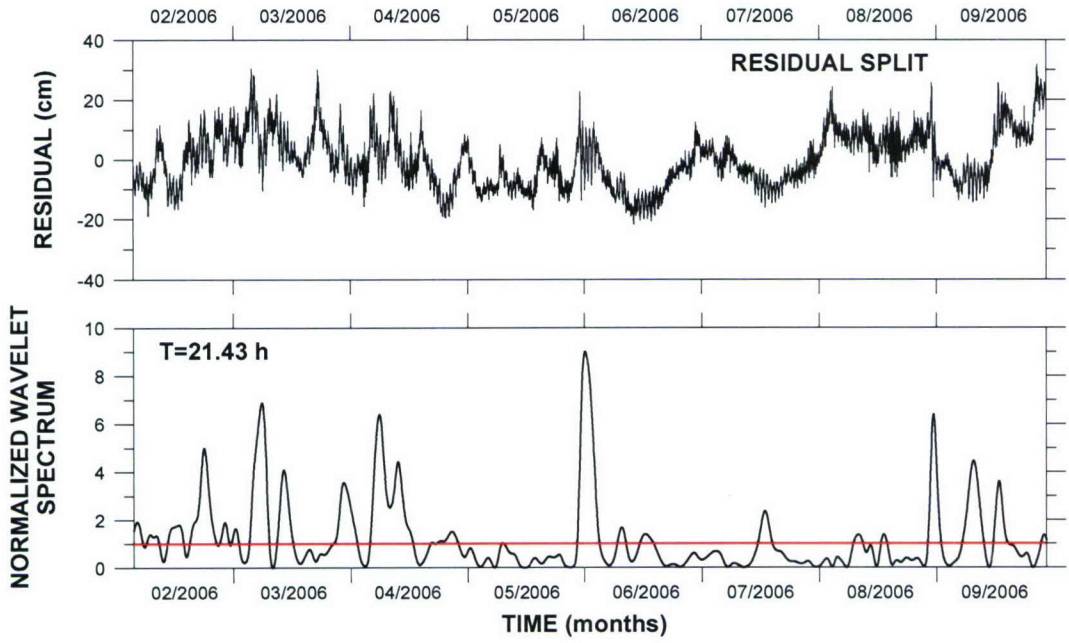

Figure 7.10 Residual sea level at Split tide gauge and respective wavelet spectrum at the period of fundamental Adriatic seiche for the interval extending from 1 February to 30 September 2006. The spectrum is normalized by the respective variance and significance level, so that the confidence level at 95% equals 1.

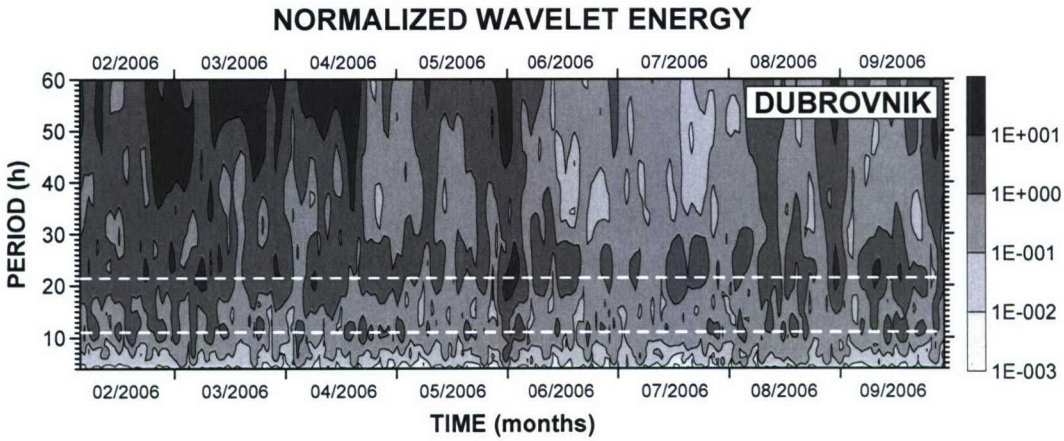

Figure 7.11 Wavelet spectrum of residual sea level at Dubrovnik tide gauge, for the interval extending from 1 February to 30 September 2006. The spectrum is normalized by the respective variance. Dashed lines denote periods of the fundamental and second Adriatic mode.

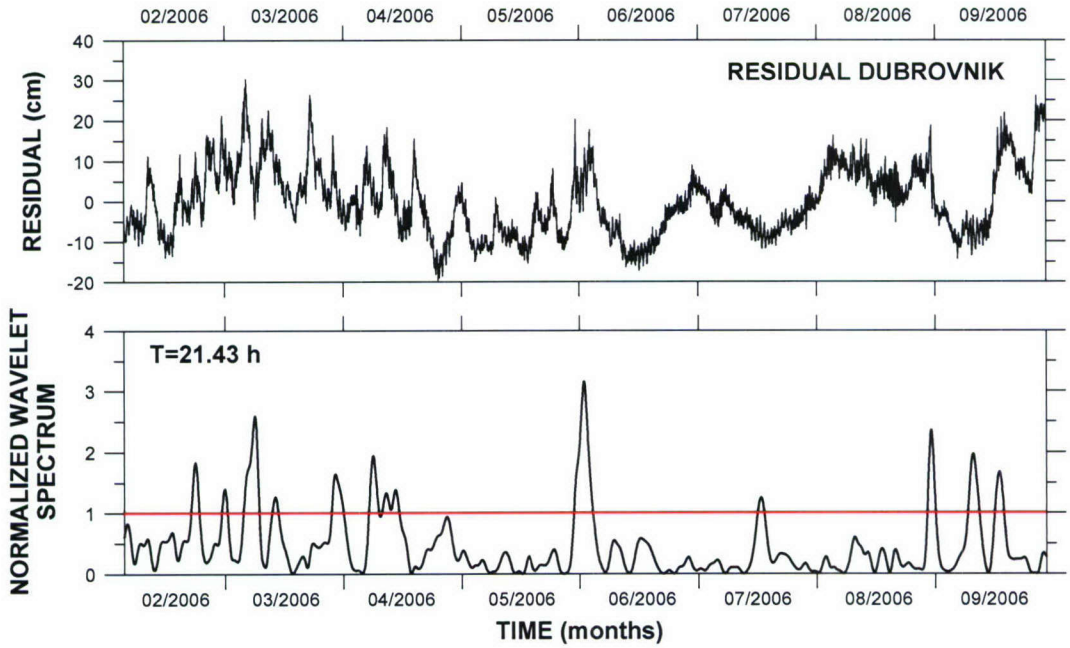

Figure 7.12 Residual sea level at Dubrovnik tide gauge and respective wavelet spectrum at the period of fundamental Adriatic seiche for the interval extending from 1 February to 30 September 2006. The spectrum is normalized by the respective variance and significance level, so that the confidence level at 95% equals 1.

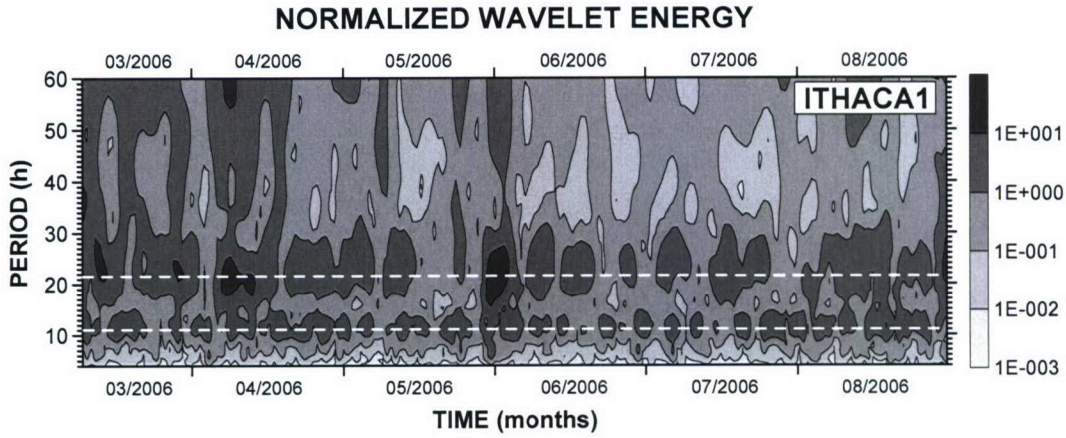

Figure 7.13 Wavelet spectrum of residual pressure at ITHACA 1 station, for the interval extending from 8 March to 1 September 2006. The spectrum is normalized by the respective variance. Dashed lines denote periods of the fundamental and second Adriatic mode.

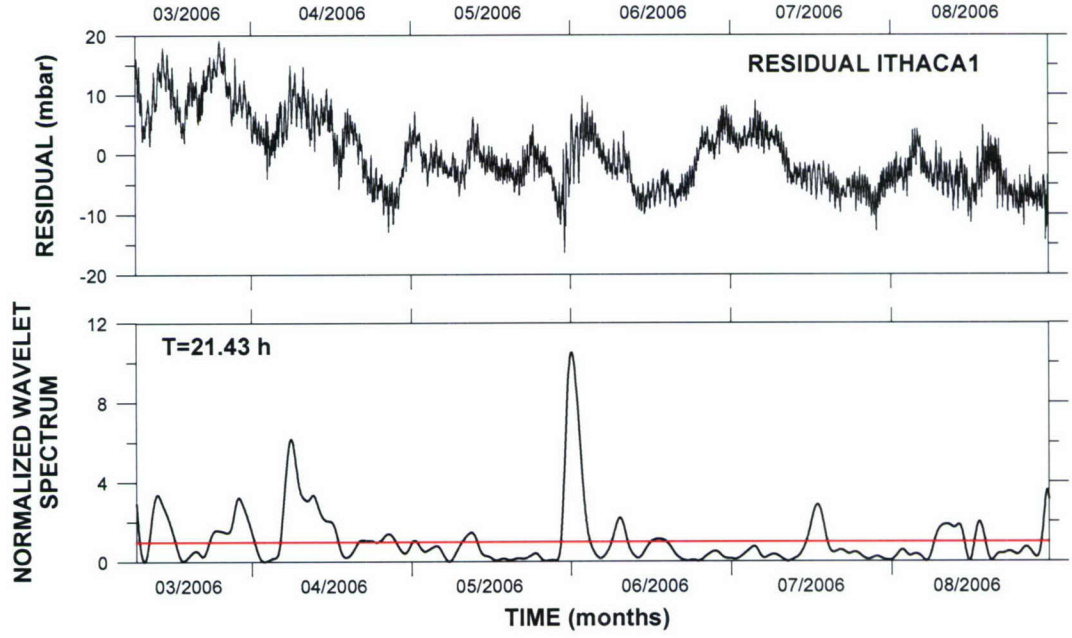

Figure 7.14 Residual pressure at ITHACA 1 station and respective wavelet spectrum at the period of fundamental Adriatic seiche for the interval extending from 8 March to 1 September 2006. The spectrum is normalized by the respective variance and significance level, so that the confidence level at 95% equals 1.

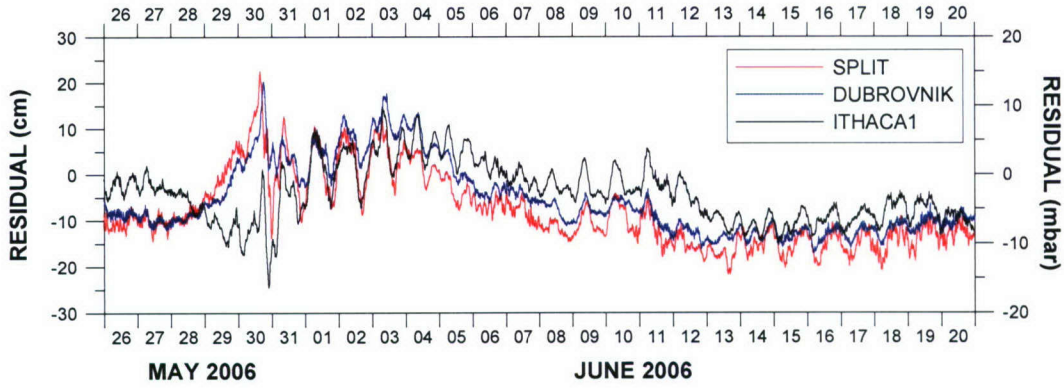

Figure 7.15 A strong seiche episode recorded at the end of May and the beginning of June 2006.

8. Summary and conclusion

The project focuses on the Adriatic shelf break area. Previously, it has been found that the along-basin flow there is oppositely directed in the winter and summer seasons, that seasonally dependent circulation contributes to a strong temporal variability of thermohaline properties, and that barotropic-like currents reverse on a few-day scale. More recently, it has been shown that during the stratified season diurnal internal tides are generated in the area by the interaction of diurnal barotropic tides with topography. As the previous detection of internal tides was based on a limited data set, the present project was initiated in order to provide a more complete information. The aim of the project was also to consider the way changes of background stratification and currents modify internal waves, and vice versa – to address a possible influence of internal waves on deductions based on measurements that are scattered in space and time.

The field phase of the project lasted from February to September 2006. During the experiment (1) meteorological conditions were documented by permanent stations in the area (Split-Marjan, Dubrovnik, Komiza, Hvar and Palagruza), (2) optical surveys were performed twice at stations Bisevo, Susac and Lastovo, (3) shipboard CTD surveys were carried out on four occasions at an along-basin transect comprising 13 closely spaced stations, (4) thermistor data were collected on the islands of Bisevo, Susac and Lastovo utilizing 3 x 10 sensors deployed on steep cliffs opened to the southeast, (5) ADCP measurements were performed at three stations using trawl-resistant bottom mounts (called barnys), and (6) surface tides were monitored at the permanent Split and Dubrovnik stations and at one of the ADCP stations.

The project was successful, as all the instruments were recovered except one of the thermistors. Preliminary analysis of the data collected has shown that diurnal temperature oscillations were particularly strong at one of the islands (Lastovo) and that corresponding baroclinic current variability was largest at a nearby ADCP station. Apparently, the diurnal signal was related not only to internal tides but also to periodic upwelling and downwelling events that were especially pronounced in July 2006. Inertial oscillations were also well visible in both the temperature and ADCP time series. Lower frequencies were dominated by the east-coast inflow to the Adriatic, which, however, underwent a summertime change – recorded in July 2006 at two of the ADCP stations, between May and July 2006 at one station.

It is planned that over the third project year the various data collected in the framework of the present project will be subjected to a further quality control and that they will be thoroughly analyzed and interpreted using the previously developed analytical model as well as a numerical model allowing for realistic topography and stratification. Particular attention will be paid to physical processes revealed by the preliminary data analysis – internal tides, periodic upwelling and downwelling events, and summertime changes of the current field. This should bring the project to a successful conclusion.

Acknowledgements

Drs. Michel Rixen (NURC, La Spezia, Italy) and Jeff Book (Naval Research Laboratory, Stennis Space Center, MS, USA) kindly organized measurements at stations TCH1-TCH4, carried out some CTD measurements on ITHACA polygon in the framework of DART cruises, and helped with deployment of ADCPs at stations ITHACA 1 and ITHACA 2. The ITHACA cruises were performed with *R/Vs Palagruza* and *Bios*. Andjelko and Maja Novosel led the team of divers who deployed and recovered thermistors on the islands of Bisevo, Susac and Lastovo. Satellite images were supplied by the Satellite Oceanography Group of the Institute of Atmospheric Sciences and Climate (Rome, Italy). Meteorological data were provided by the Meteorological and Hydrological Service of the Republic of Croatia (Zagreb, Croatia). The project was supported by the USA Office of Naval Research (award No. N00014-05-1-0698) and the Croatian Ministry of Science, Education and Sports (contract No. 3/2005).

References

Beg Paklar, G, Isakov, V., Koracin, D., Kourafalou, V., Orlic, M. (2001a): A case study of bora-driven flow and density changes on the Adriatic Shelf (January 1987). *Continental Shelf Research,* **21**, 1751–1783.

Beg Paklar G., Morovic M., Bone M. (2001b): The role of optical properties for the dynamics at the open sea station Stoncica. *Rapports et proces-verbaux des reunions CIESMM,* **36 (1)**, 52.

Bell, C., Vassie, J.M., Woodworth, P.L. (2000): *POL/PSMSL Tidal Analysis Software Kit 2000 (TASK-2000).* Permanent Service for Mean Sea Level, Proudman Oceanographic Laboratory, Bidston, 21 pp.

Belusic, D., Klaic, Z. B. (2004): Estimation of bora wind gusts using a limited area model. *Tellus*, **56A**, 296–307.

Belusic, D., Pasaric, M., Orlic, M. (2004): Quasiperiodic bora gusts related to the structure of the troposphere. *Quarterly Journal of the Royal Meteorological Society*, **130**, 1103–1121.

Belusic, D., Klaic, Z. B. (2006): Mesoscale dynamics, structure and predictability of a severe Adriatic bora case. *Meteorologische Zeitschrift*, **15**, 157–168.

Cerovecki, I., Orlic, M., Hendershott, M.C. (1997): Adriatic seiche decay and energy loss to the Mediterranean. *Deep-Sea Research I*, **44**, 2007-2029.

Cushman-Roisin, B. (1994): *Introduction to Geophysical Fluid Dynamics*. Prentice Hall, New Jersey, 318 pp.

Cushman-Roisin, B., Malacic, V., Gacic, M. (2001): Tides, seiches and low-frequency oscillations. In *"Physical Oceanography of the Adriatic Sea – Past, Present and Future"*, (Eds) Cushman-Roisin, B., Gacic, M., Poulain, P.M., and Artegiani, A., Kluwer Academic Publishers, Dordrecht, pp. 217-240.

Cushman-Roisin, B., Naimie, C. E. (2002): A 3-D finite-element model of the Adriatic tides. *Journal of Marine Systems*, **37**, 279-297.

Cvitan, L. (2003): Determining wind gusts using mean hourly wind speed. *Geofizika*, **20**, 63–74. (Also available at http://geofizika-journal.gfz.hr/vol20.htm.)

Emery, W.J., Thomson, R.E. (1997): *Data Analysis Methods in Physical Oceanography*. Pergamon, Oxford, 634 pp.

Foreman, M. G. G. (1978): *Manual for Tidal Current Analysis and Prediction*. Pacific Marine Science Report 78-6, Institute of Ocean Sciences, Patricia Bay, Sydney, BC, 57 pp.

Hydrographic Institute (1973): *Tide Tables, 1974 – Adriatic Sea – East Coast.* Split.

Jerlov, N. (1968): *Optical Oceanography.* Elsevier Publishing Company, Amsterdam, 194 pp.

Leder, N. (1988): Storm surges along the east coast of the Adriatic Sea. *Acta Adriatica,* **29**, 5-20.

Leder, N. (2004): *Adriatic Sea Pilot.* Hydrographic Institute of the Republic of Croatia, Split.

Leder, N., Orlic , M. (2004): Fundamental Adriatic seiche recorded by current meters. *Annales Geophysicae*, **22**, 1449–1464.

Makjanic, B. (1978): Bora, sirocco, etesian (in Croatian). *Prilozi poznavanju vremena i klime SFRJ*, **5**, 1-75.

MHS (2006): Meteorological and Hydrological Bulletins 2/2006 - 9/2006 (in Croatian).

Mihanovic, H. (2005): *Internal Tides in the Adriatic Sea* (in Croatian). M. Sc. Thesis, University of Zagreb, Zagreb, 118 pp.

Mihanovic, H., Orlic, M., Pasaric, Z. (2006): Diurnal internal tides detected in the Adriatic. *Annales Geophysicae*, **24**, 2773-2880.

Morovic M., Domijan N. (1991): Light attenuation in the Middle and Southern Adriatic Sea. *Acta Adriatica*, **32 (2)**, 621-635.

Morovic M., Bone M., Grbec B., Beg Paklar G. (2001): The role of optical properties in the Kastela Bay dynamics. *Rapports et proces-verbaux des reunions CIESMM,* **36 (1)**, 75.

Nitis, T., Kitsiou, D., Klaic, Z. B., Prtenjak, M.T, Moussiopoulos, N. (2005): The effects of basic flow and topography on the development of the sea breeze over a complex coastal environment. *Quarterly Journal of the Royal Meteorological Society*, **131**, 305–327.

Novosel, M., Pozar-Domac, A., Pasaric, M. (2004): Diversity and distribution of the bryozoa along underwater cliffs in the Adriatic Sea with special reference to thermal regime. *Marine Ecology*, **25(2)**, 155-170.

Orlic, M. (1987): Oscillations of the inertia period on the Adriatic Sea shelf. *Continental Shelf Research*, **7**, 577-598.

Orlic, M. (2001): Anatomy of sea level variability – an example from the Adriatic. In: El-Hawary, F. (Ed.), *The Ocean Engineering Handbook*, CRC Press, London, 1-13.

Orlic, M., Beg Paklar, G., Dadic, V., Leder, N., Grbec, B., Mihanovic, H., Pasaric, M., Pasaric, Z. (2005): *Internal Tidal Hydrodynamics and Ambient Characteristics of the Adriatic (ITHACA)*, Report on the first year of work, Zagreb, 56 pp.

Orlic, M., Dadic, V., Grbec, B., Leder, N., Marki, A., Matic, F., Mihanovic, H., Beg Paklar, G., Pasaric, M., Pasaric, Z., Vilibic, I. (2006): Wintertime buoyancy forcing,

changing seawater properties, and two different circulation systems produced in the Adriatic. *Journal of Geophysical Research - Oceans*, in press.

Orlic, M., Penzar, B., Penzar, I. (1988): Adriatic sea and land breezes: clockwise versus anticlockwise rotation. *Journal of Applied Meteorology*, **27**, 675-679.

Pasaric, M., Orlic, M. (2001): Long-term meteorological preconditioning of the North Adriatic coastal floods. *Continental Shelf Research*, **21**, 263-278.

Pasaric, M., Orlic, M. (2004): Meteorological forcing of the Adriatic: present vs. projected climate conditions. *Geofizika*, **21**, 69–86.

Pawlowicz, R., Beardsley, B., Lentz, S. (2002): Classical tidal harmonic analysis including error estimates in MATLAB using T_TIDE. *Computers and Geosciences*, **28**, 929-937.

Penzar, B., Penzar, I., and Orlic, M. (2001): *Weather and Climate of the Croatian Adriatic* (in Croatian). Feletar, Zagreb, 258 pp.

Petkovsek, Z. (1987): Main bora gusts - a model explanation. *Geofizika*, **4**, 41–50. (Also available at http://geofizika-journal.gfz.hr/vol04.htm.)

Polli, S. (1960): Le propagazione delle maree nell' Adriatico. *Atti del IX Convegno dell' Associazione Geofisica Italiana*, Roma, 1-11.

Poulos, S.E., Drakopoulos, P.G., Collins, M.B. (1997): Seasonal variability in sea surface oceanographic conditions in the Aegean Sea (Eastern Mediterranean): an overview. *Journal of Marine Systems*, **13**, 225-244.

Prtenjak, M.T. (2003): Main characteristics of sea/land breezes along the eastern coast of the Northern Adriatic. *Geofizika*, **20**, 75-92. (Also available at http://geofizika-journal.gfz.hr/vol20.htm.)

Prtenjak, M.T., Grisogono, B., Nitis, T. (2006): Shallow mesoscale flows at the north-eastern Adriatic coast. *Quarterly Journal of the Royal Meteorological Society,* **132**, 2191–2215.

Raicich, F., Orlic, M., Vilibic, I., Malacic, V. (1999): A case study of the Adriatic seiches (December 1997). *Il Nuovo Cimento C*, **22**, 715-726.

Torrence, C., Compo, G. P. (1998): A practical guide to wavelet analysis. *Bulletin of the American Meteorological Society*, **79(1)**, 61-78.

Vecenaj, Z. (2005): *Macro-scale Processes During Severe Winds over Dalmatia* (in Croatian). B. Sc. thesis, University of Zagreb, Zagreb, 59 pp.

Vilibic, I. (2006): The role of the fundamental seiche in the Adriatic coastal floods. *Continental Shelf Research*, **26**, 206-216.

Vilibic, I., Grbec, B., Supic, N. (2004): Dense water generation in the north Adriatic in 1999 and its recirculation along the Jabuka Pit. *Deep-Sea Research I*, **51**, 1457-1474.

Vilibic, I., Leder, N., Smircic, A. (1998): Forced and free response of the Adriatic sea level. *Il Nuovo Cimento C,* **21**, 439-451.

Vilibic, I., Orlic, M. (2001): Least-squares tracer analysis of water masses in the South Adriatic (1967-1990). *Deep-Sea Research I,* **48**, 2297-2330.

Vilibic, I., Orlic, M. (2002): Adriatic water masses, their rates of formation and transport through the Otranto Strait. *Deep-Sea Research I,* **49**, 1321-1340.

Vilibic, I., Orlic, M., Cupic, S., Domijan, N., Leder, N., Mihanovic, H., Pasaric, M., Pasaric. Z., Srdelic, M., Strinic, G. (2005): A new approach to sea level observations in Croatia. *Geofizika*, **22**, 21-57.

Welch, P. D. (1967): The use of Fast Fourier Transform for the estimation of power spectra: a method based on time averaging over short, modified periodograms. *IEEE Trans. Audio Electroacoustics,* **AU-15** (June 1967), 70-73.

REPORT DOCUMENTATION PAGE

Form Approved
OMB No. 0704-0188

1. REPORT DATE *(DD-MM-YYYY)*	2. REPORT TYPE	3. DATES COVERED *(From - To)*
31-12-2006	Performance / technical report	01-01-2006 - 31-12-2006

4. TITLE AND SUBTITLE
Internal Tidal Hydrodynamics and Ambient Characteristics of the Adriatic (ITHACA) - Report on the Second Year of Work

5a. CONTRACT NUMBER
/

5b. GRANT NUMBER
N00014-05-1-0698

5c. PROGRAM ELEMENT NUMBER
/

6. AUTHOR(S)
Orlic, Mirko; Beg Paklar, Gordana; Dadic, Vlado; Leder, Nenad; Bencetic Klaic, Zvjezdana; Grbec, Branka; Matic, Frano; Mihanovic, Hrvoje; Morovic, Mira; Pasaric, Miroslava; Pasaric, Zoran; Vilibic, Ivica.

5d. PROJECT NUMBER
05PR08927-00

5e. TASK NUMBER
/

5f. WORK UNIT NUMBER
/

7. PERFORMING ORGANIZATION NAME(S) AND ADDRESS(ES)
University of Zagreb, Horvatovac bb, 10000 Zagreb, Croatia

8. PERFORMING ORGANIZATION REPORT NUMBER
/

9. SPONSORING/MONITORING AGENCY NAME(S) AND ADDRESS(ES)
Office of Naval Research, 875 N. Randolph St., One Liberty Center, Arlington VA 22203-1995, USA

10. SPONSOR/MONITOR'S ACRONYM(S)
ONR

11. SPONSOR/MONITOR'S REPORT NUMBER(S)
/

12. DISTRIBUTION/AVAILABILITY STATEMENT
Approved for public release

13. SUPPLEMENTARY NOTES
/

14. ABSTRACT
Field phase of the ITHACA project has been carried out between February and September 2006. During the experiment (1) meteorological conditions were documented by permanent stations in the area (Split-Marjan, Dubrovnik, Komiza, Hvar and Palagruza), (2) optical surveys were performed twice at stations Bisevo, Susac and Lastovo, (3) shipboard CTD surveys were carried out on four occasions at an along-basin transect comprising 13 closely spaced stations, (4) thermistor data were collected on the islands of Bisevo, Susac and Lastovo utilizing 3 x 10 sensors deployed on steep cliffs opened to the southeast, (5) ADCP measurements were performed at three stations using trawl-resistant bottom mounts (called barnys), and (6) surface tides were monitored at the permanent Split and Dubrovnik stations and at one of the ADCP stations. The project was successful, as all the instruments were recovered except one of the thermistors. Preliminary analysis of the data collected has shown that diurnal temperature oscillations were particularly strong at one of the islands (Lastovo) and that corresponding baroclinic current variability was largest at a nearby ADCP station. Apparently, the diurnal signal was related not only to internal tides but also to periodic upwelling and downwelling events that were especially pronounced in July 2006. Inertial oscillations were also well visible in both the temperature and ADCP time series. Lower frequencies were dominated by the east-coast inflow to the Adriatic, which, however, underwent a summertime change – recorded in July 2006 at two of the ADCP stations, between May and July 2006 at one station.

15. SUBJECT TERMS
Internal tides, surface tides, thermohaline properties, meteorological conditions, Adriatic.

16. SECURITY CLASSIFICATION OF:			17. LIMITATION OF ABSTRACT	18. NUMBER OF PAGES	19a. NAME OF RESPONSIBLE PERSON
a. REPORT	b. ABSTRACT	c. THIS PAGE			Mirko Orlic
U	U	U	SAR	106	19b. TELEPHONE NUMBER *(Include area code)* +385-1-460-5900